MAGMATISM AND ORE DEPOSIT FORMATION IN SW PACIFIC ISLAND ARCS

By

GEORGE DIMITROV KAMENOV

A DISSERTATION PRESENTED TO THE GRADUATE SCHOOL
OF THE UNIVERSITY OF FLORIDA IN PARTIAL FULFILLMENT
OF THE REQUIREMENTS FOR THE DEGREE OF
DOCTOR OF PHILOSOPHY

UNIVERSITY OF FLORIDA

2004

ACKNOWLEDGMENTS

I wish to thank the members of my committee for their support, patience and guidance during the project. This dissertation would not be possible without the insights, expert guidance, and support of Drs. Michael Perfit and Paul Mueller. Dr. Ann Heatherington and Howard Scher provided invaluable help during the clean lab sample preparation and TIMS analyses. I am grateful to Drs. David Foster, Joseph Delfino, and Ian Jonasson for providing insights and reviewing this work.

I am grateful to Drs. Michael Perfit, Brent McInnes, Mark Hannington, and Peter Herzig, and the crew of the RV SONNE for obtaining the samples from the TLTF area. Dr. David Foster provided the biotite Ar-Ar data on Tubaf seamount. The accomplishment of this research would not be possible without the major and trace element analyses at the Canadian Geological Survey under the supervision of Dr. Ian Jonasson. I am grateful to Rahul Chopra for separating the xenolith samples from the Tubaf lavas. I am thankful to Tom Bisley for providing technical assistance with the microprobe analyses at the Florida International University. Field and laboratory investigations were supported by an NSF OCE-9403773 grant awarded to Dr. Michael Perfit and a GSA 7430-03 student grant. This study would not be possible without the NSF ARI grant 96-01872 for the purchase of the “Nu-plasma” MC-ICP-MS. Many thanks go to Dr. Jamie Williams for his invaluable assistance during the set up of the MC-ICP-MS lab. I am grateful for the financial support by the

University of Florida Alumni Fellowship during the course of this study. This work benefited from the expertise provided by Drs. Ray Russo, and Phil Neuhoff. Many thanks go to Ray Thomas and Kevin Hartl for their invaluable technical support. The staff of the geology department, Ron, Mary, and Jodie, have been very helpful during my study in the University of Florida. I would like to thank all of my friends in the Department of Geological Sciences for the friendship and support throughout the 4 years of graduate study. Finally, I would like to thank my wife, Katrin, for her love, patience, and encouragement during this study.

TABLE OF CONTENTS

LIST OF TABLES

LIST OF FIGURES

Abstract of Dissertation Presented to the Graduate School
of the University of Florida in Partial Fulfillment of the
Requirements for the Degree of Doctor of Philosophy

MAGMATISM AND ORE DEPOSIT FORMATION IN SW PACIFIC ISLAND ARCS

By

George Dimitrov Kamenov

December 2004

Chair: Michael R. Perfit
Major Department: Geological Sciences

Majority of the richest base and precious metal deposits on Earth are located in the Circum-Pacific region and are found either in a close proximity or within subduction-related volcano-magmatic complexes. It is not clear, however, why some of the volcanic centers contain ore deposits but others do not. This study utilizes a novel method for high-precision Pb isotopic measurements by multi-collector-ICP-MS and reveals a genetical connection between the ore-formation and magmatism in the Tabar-Lihir-Tanga-Feni (TLTF) island arc, SW Pacific. The developed model suggests that injection of a volatile-rich magma into an evolving magma body near the surface is the triggering event that ultimately results in the ore mineralization.

Isotope data for mantle xenoliths suggest that three possible end-members, including Pacific and Indian mantle, and Pacific sediments, can control the chemistry of the magmas in the region. Comparison between the isotopic compositions of lavas, and crustal and mantle xenoliths indicate that the incompatible elements in the TLTF

magmas, including a major part of the ore metals, were ultimately derived from a subducted oceanic slab with Pacific mantle affinity. Regional and local isotopic trends in the volcanic rocks in the region indicate that subducted oceanic slabs overall control the composition of the island-arc magmas. Once the contribution from the subducting slab decreases, incorporation of a mantle component with Indian affinity can be identified in the isotopic composition of the lavas in the region.

CHAPTER 1
INTRODUCTION

The most significant geological phenomena on Earth, such as powerful earthquakes, widespread volcanism, and island-arcs and continents growth, occur in the zones of subduction. In addition, these zones are of great economic importance because most of the world's richest base and precious metal deposits are associated with subduction-related volcanism. A number of subduction zones and back-arc basins are located in the western Pacific (Fig. 1-1) and a subject of this study is the Tabar-Lihir-Tanga-Feni (TLTF) island chain, part of the Bismarck Archipelago. The TLTF islands are part of the Western Pacific gold province (Fig. 1-1), which extends from Japan, through the Philippines, Papua New Guinea, Solomon Islands, and Fiji to New Zealand (Sillitoe 1989). The formation of the Bismarck Archipelago is related to the subduction of the Pacific plate under the Indo-Australian plate and most of the arcs are dominated by calc-alkaline volcanism, although the TLTF chain is dominated by alkaline volcanoes (Wallace et al. 1983).

It is generally believed that the widespread magmatic activity in the island arcs is due to lowering the mantle wedge peridotite melting point as a result of dehydration of the subducted slab (Tatsumi 1989). However, some fundamental geological processes, such as what controls the chemistry of the magmas and why there are ore deposits associated with some of the volcanic systems but none with others, remain unclear. The TLTF island chain provides an outstanding opportunity to investigate these processes in detail because a number of xenoliths were recovered from a submarine

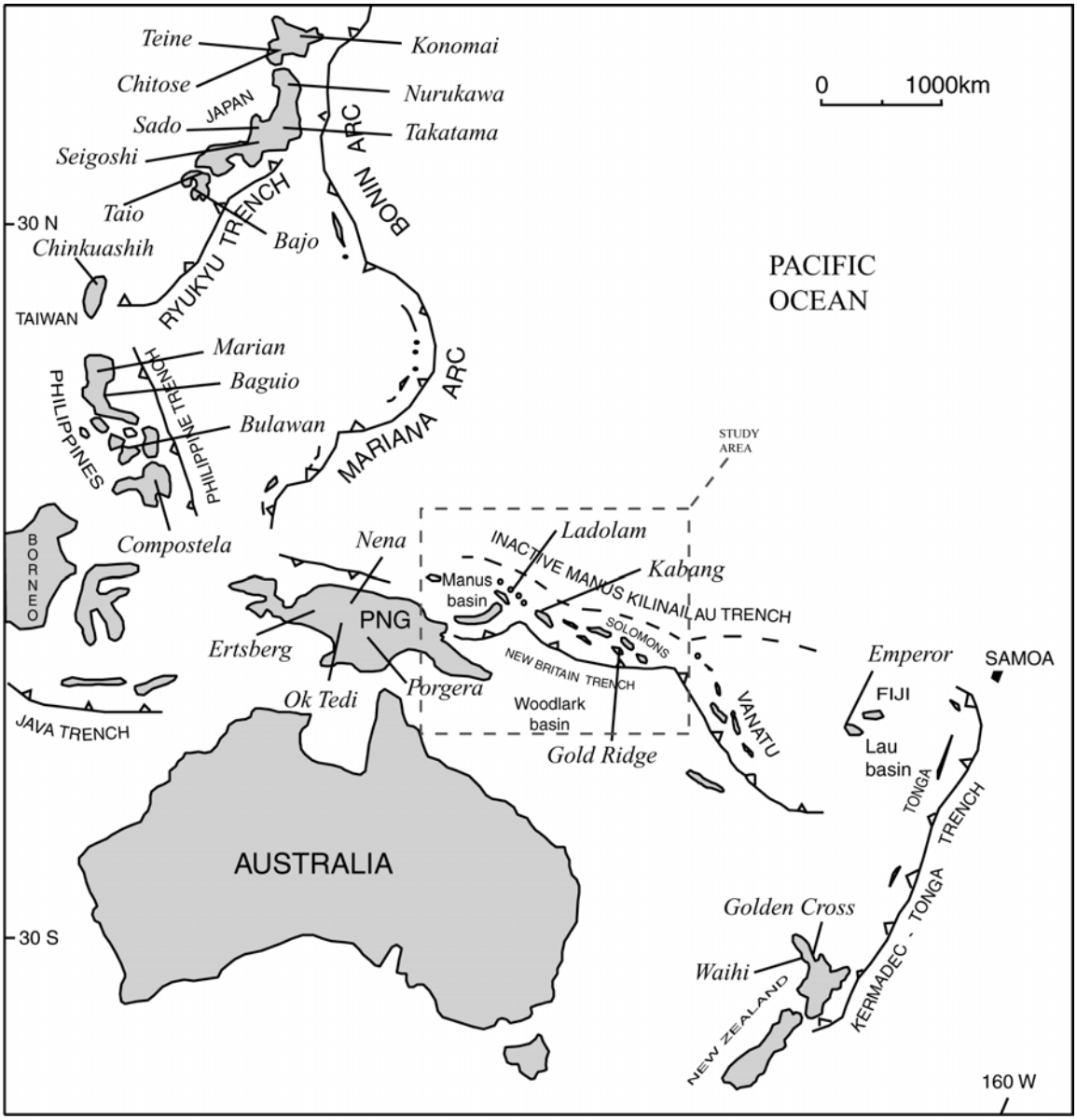

Figure 1-1. Regional map of the Western Pacific Ocean, showing some of the Western Pacific Gold Province deposits (in italic). Note that only about 1/3 of the known deposits are shown on the map for clarity purposes, for more details see Sillitoe (1989). Deposits are characterized by porphyry and epithermal gold mineralizations and are young, ranging from Middle Miocene to Quaternary (17-0 Ma). The study area (enclosed in the dashed field) includes Bismarck Archipelago (New Britain, New Ireland, TLTF, Bougainville), the Solomon Islands, and Manus and Woodlark back-arc basins, more detailed maps are available in Chapters 3 and 4.

volcano, located on the flanks of Lihir island, host of one of the richest gold deposits on Earth (Moyle et al. 1990). The xenoliths provide us with rare samples from the crust and mantle underlying the islands, and detailed geochemical and isotopic study of xenoliths, lavas, and ores will allow us to look at details of the processes responsible for the magmatism and ore deposit formation in the region.

A number of existing and novel techniques, such as petrographic observations, major and trace element analyses, Sr and Nd isotope data, and high-precision Pb isotope measurements, are utilized throughout this study. Comparison of existing data from the area (Wallace et al. 1983; Kennedy et al. 1990a,b; McInnes and Cameron 1994; Stracke and Hegner 1998; Müller et al. 2001, 2003) and new major and trace element analyses of lavas allow us to look in detail at the nature of the magmas in the area and processes that led to their formation. Previous studies indicate that the lavas erupted on the surface are not common for island arc settings because of their high alkalinity, and was hypothesized that they are products of adiabatic decompression melting of the subduction-modified mantle wedge (McInnes and Cameron 1994). The mantle wedge beneath TLTF islands is composed of depleted peridotites, probably a residue from a partial melting event at Mid-ocean ridge settings (McInnes et al. 2001, Gregoire et al. 2001, Franz et al. 2002). Visual and chemical evidences, however, indicated that the ultramafic xenoliths experienced strong metasomatism by fluids released probably from the subducted Pacific slab (McInnes et al. 2001, Gregoire et al. 2001, Franz et al. 2002). Detailed Sr, Nd, and Pb isotopic comparison between the metasomatized xenoliths and TLTF lavas, therefore, will provide evidence if the magmas in the region are a result of partial melting of the metasomatized mantle wedge.

Sr, Nd, and Pb isotopic comparison is a routine technique utilized in geochemical studies (Faure 1986) however, some recent studies indicate that significant analytical errors can be generated during the traditional thermal ionization mass-spectrometry (TIMS) measurements of Pb isotopes (Woodhead et al. 1995, Kamenov et al. 2003). The problems stem from uncompensated Pb isotopic fractionation behavior during the TIMS analyses. For example, during the Sr isotopic analyses a non-radiogenic pair ($^{86}Sr/^{88}Sr$) is used to correct for the fractionation behavior of Sr during the TIMS analyses. Such correction is not possible during the Pb analyses due to the existence of only one non-radiogenic lead isotope (^{204}Pb). A novel technique utilizing $^{205}Tl/^{203}Tl$ to serve as a "non-radiogenic pair" for mass-bias correction during Pb isotope measurements was adopted with the development of the multi-collector ICP-MS (Rehkämper and Halliday 1998). Although some studies have questioned the technique (Thirwall, 2002), our recent experiments demonstrated that highly precise Pb isotope measurements can be obtained by preventing the thallium photoxidation to 3+ state (Kamenov et al. 2004a,b).

In addition to deciphering the relationships between magmas and xenoliths, Pb isotopic measurements provide valuable information for the formation of the ore mineralizations in the area. Lead is the only ore metal other than Os which shows large natural isotopic variability and has similar geochemical behavior to other ore metals, such as zinc, copper, and silver. Therefore, comparison of ore lead isotope ratios with those of host rocks and other units in a particular mining district will suggest and/or rule out possible ore metal sources. Combining the high-precision Pb isotopic measurements with

petrographic and geochemical data will lead to development of a model integrating the magmatism and the ore-formation in the area.

On a larger scale, the observations and the wealth of data collected during the course of this study provide valuable information on the composition of the mantle in the area. Local and regional trends observed in the arc lavas from the region can be related to a particular source or sources, which can be either a subduction-derived oceanic crust and/or sediment component, or the local mantle. This will shed new light on the island arc petrogenesis in the region and will further contribute to our understanding of the subduction zone magmatism and associated ore deposit formation.

CHAPTER 2
OPTIMIZATION OF MIXED LEAD-THALLIUM SOLUTIONS FOR HIGH PRECISION ISOTOPIC ANALYSES BY MC-ICP-MS

Introduction

The introduction of the MC-ICP-MS has led to a novel technique for Pb isotope ratio measurements that utilizes $^{205}Tl/^{203}Tl$ as an internal standard to correct for mass-dependant fractionation in mixed Pb-Tl solutions (Belshaw et al. 1998, Rehkämper and Halliday 1999, Collerson et al. 2002). Conversely, precise Tl isotope measurements can be obtained by mixing a Tl-bearing solution with Pb of known isotopic composition (e.g., $^{208}Pb/^{206}Pb$) as an internal standard to correct for mass-dependant fractionation of Tl (Rehkämper and Halliday 1999). Thirwall (2002), however, suggested that the Pb-Tl isotope measurements determined by MC-ICP-MS are subject to large analytical uncertainties and that this technique is not suitable for obtaining highly precise data for Pb or Tl isotopes. Thirwall's contribution constituted part of an on-going debate concerning the reliability of Pb isotope analyses corrected by Tl-normalization (Rehkämper and Mezger 200,; White et al. 2000, Woodhead 2002). For example, Rehkämper and Mezger (2000) adjusted the $^{205}Tl/^{203}Tl$ normalization ratio on a daily basis to obtain results closest to the DS (double spike) TIMS SRM 981 values of Todt et al. (1996). The need for such adjustments implies inconsistent mass-fractionation of Pb and Tl during the analytical procedure. In addition, Thirwall (2002) and Collerson et al. (2002) observed that Tl intensity was lower than expected in some mixed Pb-Tl solutions and suggested that it resulted from unspecified and anomalous behavior of thallium in

solution. Rehkämper and Halliday (1998) also observed anomalous behavior of Tl in mixed Pb-Tl solutions and suggested that it resulted from variations in the complexation of Tl that could be avoided if the solutions were allowed to "age" for a period of several days.

In this chapter I report results of an investigation of the interaction between Pb and Tl in mixed, dilute nitric and hydrochloric acid solutions and its effects on the elemental and isotopic ratio measurements. I show that very precise MC-ICP-MS isotope analyses of lead and thallium can be obtained using this system by controlling the analyte conditions to minimize the formation of Tl^{3+}.

Analytical Procedures

Solutions were prepared in Teflon bottles or vials by mixing SRM 981 Pb standard solution with commercially available ICP Tl stock solutions (QCD Analysts, USA and Aldrich, USA). The mixed solutions were prepared with Pb-Tl elemental ratios ranging from 2 to 6 and were diluted to 100 to 150 ppb Pb and 25 to 35 Pb ppb for the wet and dry plasma experiments, respectively (Appendix A). Most of the experiments were conducted on mixed solutions diluted in either 0.6, 2, or 5% HNO3 (percent dilution of concentrated Optima-brand HNO3); several experiments were conducted in 2% HCl solutions and in 2% HNO3 solutions with traces of HCl. A Nu-Plasma MC-ICP-MS (Nu Instruments, UK) in the Department of Geological Sciences at the University of Florida was used for this study. The instrument description, typical operating conditions, and analytical protocol during Pb-Tl analysis are reported in Belshaw et al. (1998). Sample and standard solutions were aspirated either through a Nu Instruments desolvating nebulizer (DSN-100) ("dry plasma" mode) or directly into the plasma source through a Micromist nebulizer with GE spray chamber ("wet plasma" mode). Measured uptake rate

for both sample introduction methods was about 100 μL min-1. The instrument settings were carefully tuned to maximize the signal intensities on a daily basis. Preamplifier gain calibrations were run before the beginning of each analytical session. Typical sensitivities for Pb were about 300 V ppm-1 and about 40 V ppm-1 for dry and wet plasma modes, respectively. Sampler and skimmer cones (Ni) were thoroughly cleaned after 3 or 4 analytical sessions. All analyses reported in this paper were conducted in static mode by directing 202Hg on low-2, 203Tl on low-1, 204Pb on Axial, 205Tl on high-1, 206Pb on high-2, 207Pb on high-3, and 208Pb on high-4 (all Faraday detectors). The measured 204Pb beam was corrected for isobaric interference from 204Hg using 204Hg/202Hg=0.2290 (before mass-bias correction), although always negligible. Data were acquired in blocks of 20 ratios with 10 s integration times. Background measurements of 30 s durations preceded each block. All of the reported SRM 981 ratios were normalized using the exponential law for mass-bias correction and 205Tl/203Tl=2.3875 after Belshaw et al. (1998). All Tl isotope analyses were normalized using the exponential law and SRM 981 208Pb/206Pb=2.1664. This ratio represents the average of all fresh SRM 981 runs conducted during this study and is identical to the average of all MC-ICP-MS SRM 981 208Pb/206Pb analyses reported by Reuer et al. (2003). Tl ε-notation values are calculated relative to NIST 997 205Tl/203Tl=2.3871, following Rehkämper et al. (2002). Note that the 205Tl/203Tl (2.3875) used throughout these experiments is 1.68 epsilon units greater than the value of NIST 997 (205Tl/203Tl=2.3871), which is why our average ε205Tl results for QCD are greater than zero (Table 2-1).

Results

Wet Plasma Experiments

Forty two wet plasma analyses of SRM 981 mixed with QCD Tl were conducted between April and June, 2003 and gave the following results: $^{206}Pb/^{204}Pb$=16.9369 (+/-0.0039, 2σ), $^{207}Pb/^{204}Pb$=15.4904 (+/-0.0034, 2σ), and $^{208}Pb/^{204}Pb$=36.6949 (+/-0.0087, 2σ) (Table 2-1). The reported 2-sigma error (2σ) is the external precision, calculated on the basis of these 42 runs. The internal precision obtained during a single analysis is usually lower, on the order of +/- 0.001 to 0.002 (2σ). Measured $\varepsilon^{205}Tl$ in the QCD standard during the wet plasma experiments was 0.9 (+/-1.2, 2σ) (Table 2-1). Measured Pb and Tl beam intensities for these solutions showed intensity ratios similar to the elemental ratios in the original mixtures (Table 2-1, Appendix A).

Table 2-1. Measured SRM 981 Pb, QCD Tl isotopic compositions, Pb/Tl intensity ratios

experiment	Pb/Tl (mixed)	Pb/Tl (measured)	$^{206}Pb/^{204}Pb$	$^{207}Pb/^{204}Pb$	$^{208}Pb/^{204}Pb$	$\varepsilon^{205}Tl$ (QCD)
wet plasma (fresh and Tl^{3+} solutions) n=42	2 to 6	2 to 6	16.9369 (+/-0.0039, 2σ)	15.4904 (+/-0.0034, 2σ)	36.6949 (+/-0.0087, 2σ)	0.9 (+/-1.2, 2σ)
dry plasma (only fresh mixtures) n=29	2 to 6	2 to 6	16.9373 (+/-0.0011, 2σ)	15.4907 (+/-0.0012, 2σ)	36.6935 (+/-0.0039, 2σ)	1.5 (+/-0.8, 2σ)
dry plasma (only Tl^{3+} solutions) n=39	2 to 6	variable up to 36	16.921 (+/-0.039 2σ)	15.469 (+/-0.052 2σ)	36.630 (+/-0.160 2σ)	from –3.9 to +30.1
dry plasma (fresh mix)	20	20	16.9375 (+/-0.0018, 2σ)	15.4910 (+/-0.0018, 2σ)	36.6979 (+/-0.0052, 2σ)	0.4 (+/-1.0, 2σ)
dry plasma (fresh mix)	40	40	16.9359 (+/-0.0020, 2σ)	15.4886 (+/-0.0020, 2σ)	36.6908 (+/-0.0062, 2σ)	1.4 (+/-1.0, 2σ)

Dry Plasma Experiments

Experiments using the DSN-100 were also conducted between April 2003 and January 2004. During the initial experiments, Pb and Tl from single stock solutions were mixed in 2% HNO_3. Solutions were then measured from 48 hours to 60 days after preparation (mixing), as suggested by Rehkämper and Halliday (1999). Contrary to the

results of Rehkämper and Halliday (1999), however, our initial results with these solutions revealed poor overall precision and accuracy with $^{206}Pb/^{204}Pb$=16.921 (+/-0.039 2σ), $^{207}Pb/^{204}Pb$=15.469 (+/-0.052 2σ), and $^{208}Pb/^{204}Pb$=36.630 (+/-0.160 2σ) (Table 2-1, Fig. 2-1A). Similarly, using SRM 981 as a fixed Pb isotopic composition for mass bias corrections of the Tl isotopes yielded relatively large $\varepsilon^{205}Tl$ variations (i.e., from –3.9 to +30.1) for our QCD standard (Table 2-1, Fig. 2-1B).

Comparison of measured Pb and Tl beam intensities for these solutions over this period showed essentially constant Pb ion beam intensities, but lower Tl intensities (i.e., higher Pb:Tl intensity ratios compared to the known elemental ratios in the original mixtures) (Fig. 2-2A). Measured intensities in Pb-only (30 ppb) and Tl-only (5 ppb) control solutions did not show changes in intensity during the experiments, indicating that the decrease in the Tl signal intensity occurred only in aged, mixed solutions. In addition, the wash out times were consistently longer for the aged compared to the fresh mixtures. Condensate (i.e., waste solution) from the DSN collected during analyses of the aged solutions showed lower Pb-Tl intensity ratios, from 0.6 to 1, indicating a net increase in Tl over Pb in the waste (i.e., during the combined desolvation and washout processes). Overall, it appeared that extending the interval between mixing the Pb and Tl solutions and analysis produced significant, but irregular, Pb-Tl elemental decoupling along with poorer precision and accuracy in the isotope ratio measurements for both Pb and Tl.

To address this problem, we prepared new mixed solutions (also in 2% HNO_3) and analyzed them immediately (<1 h) after mixing. Analyses of these mixed solutions (n=29) yielded consistent and highly precise results with $^{206}Pb/^{204}Pb$=16.9373 (+/-0.0011,

2σ), $^{207}Pb/^{204}Pb$=15.4907 (+/-0.0012, 2σ), and $^{208}Pb/^{204}Pb$=36.6935 (+/-0.0039, 2σ) (Table 2-1, Fig. 2-1A). The average of the measured $\varepsilon^{205}Tl$ in these "fresh" solutions

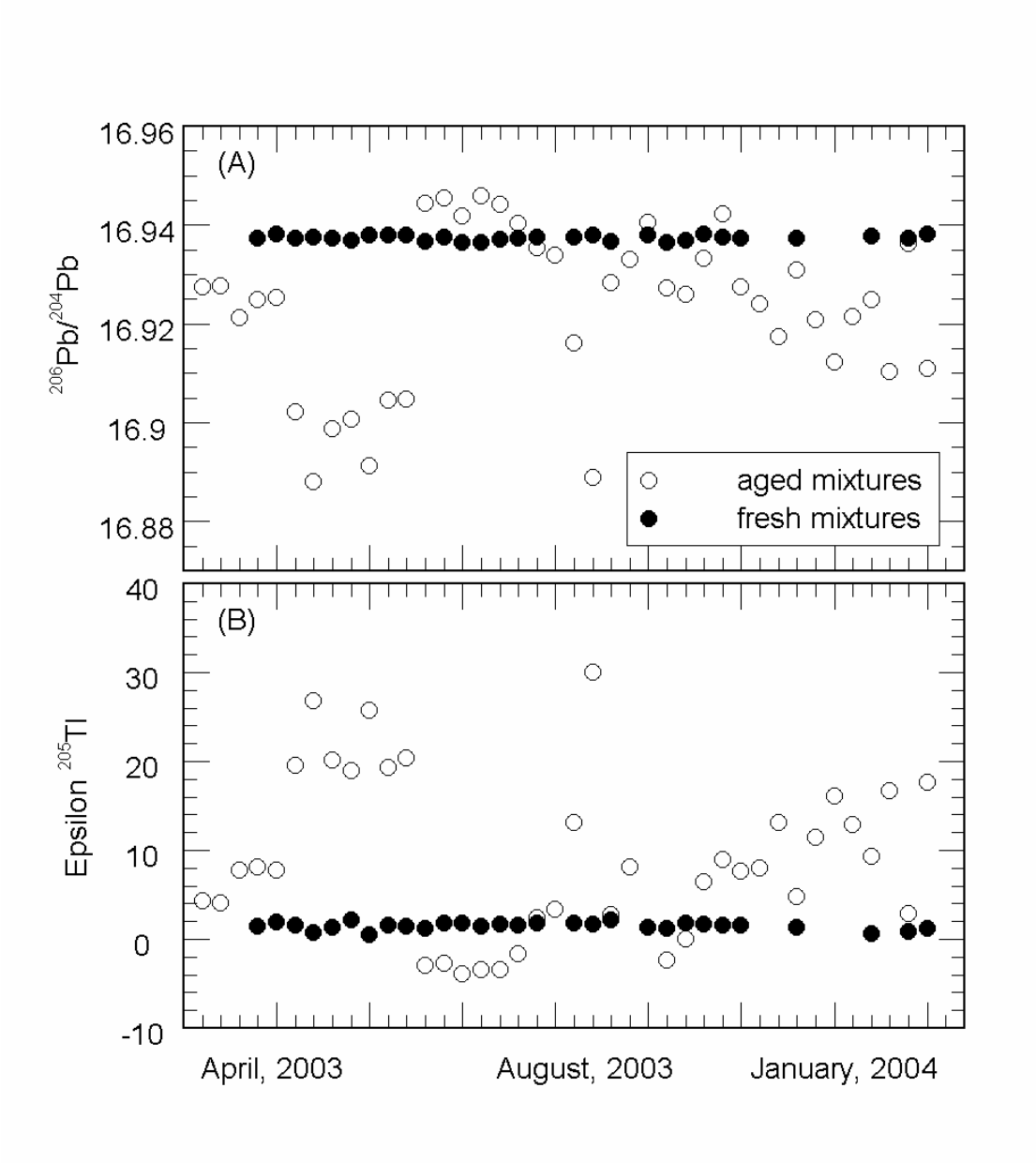

Figure 2-1. (A) SRM 981 206Pb/204Pb DSN measurements of fresh and aged, exposed to sunlight mixtures. (B) QCD ε205Tl DSN measurements of fresh and aged, exposed to sunlight mixtures (for more details see the text, Table 2-1, and Appendix A).

prepared with the QCD standard and SRM 981 was 1.5 (+/-0.8, 2σ) (Table 2-1, Fig. 2-1B). In addition, measured Pb and Tl ion beam intensities always reflected those calculated for the mixtures. Analyses of fresh 2%HNO_3 mixtures prepared with high Pb/Tl ratios yielded Pb and Tl isotopic values within error with the rest of the fresh mixtures, suggesting that the observed discrepancies during the analyses of the aged mixtures is not a result of the decrease in the Tl signal (i.e., high Pb/Tl, Table 2-1). Several experiments were also conducted with 2%HCl and a range of HNO_3 concentrations. Aging of mixed Pb:Tl solutions in 2%HCl, 5%HNO_3, and 2%HNO_3+0.05%HCl showed similar behavior to the 2%HNO_3 experiments, i.e., decoupling of the Pb-Tl elemental abundances and imprecise and inaccurate isotope ratios (Fig. 2-2A and B). Using solutions with a lower HNO_3 concentration (0.6%) showed less Pb-Tl elemental decoupling and more precise reproducibility of isotope ratios over time compared to the solutions with higher HNO_3 concentrations (Fig. 2-2A and B).

Subsequent testing of the same mixed solutions noted above (0.6 to 5% HNO_3) after several months of storage, however, showed that the solutions reverted to behave as fresh mixtures; that is, they did not show the Pb-Tl elemental decoupling and poor precision of Tl and Pb isotope ratio measurements that had characterized them previously (Fig. 2-2A and B). The source of the "freshening" of the solutions was ultimately traced to the fact that the solutions were stored in cabinets and were not exposed to sunlight, suggesting a photochemical effect. To test this hypothesis, the solutions were again moved to their initial storage location, which allowed exposure to direct sunlight. The subsequent analyses showed the strong decoupling in the Pb/Tl ratios and the relatively imprecise Pb

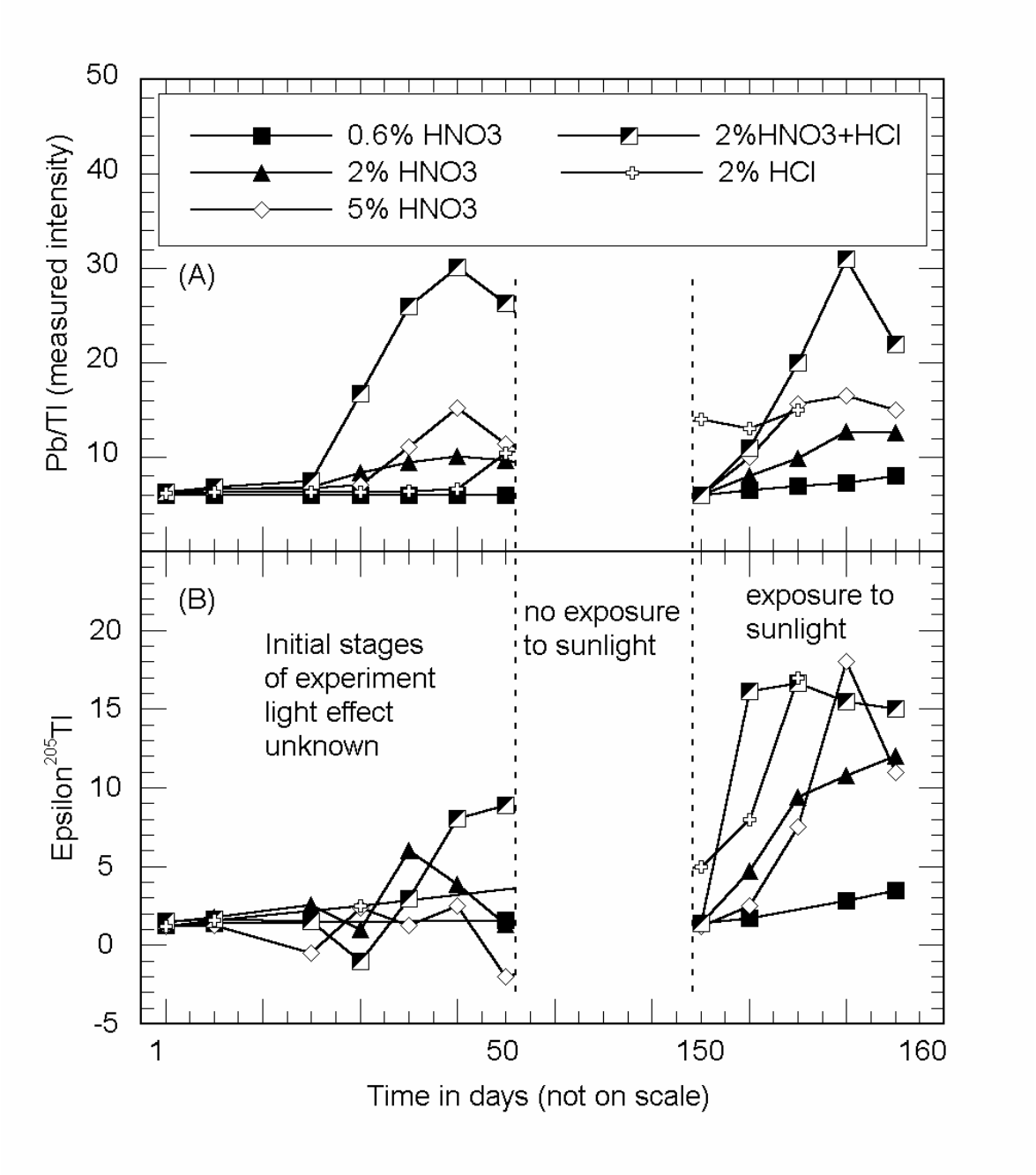

Figure 2-2. (A) Changes in measured Pb/Tl intensity ratios in mixed solutions with time and exposure to sunlight. All solutions prepared with Pb/Tl=6 (B) Changes in measured ε^{205}Tl in mixed solutions with time and exposure to sunlight. Note that all (with the exception of 2%HCl) solutions revert to behave as fresh mixtures after prolonged storage without exposure to sunlight.

and Tl isotope ratio measurements again characterized these solutions. Repeated experiments confirmed that exposure to sunlight plays a major role in the interaction of Pb and Tl in the solutions (Fig. 2-2A and B).

The nature of this reaction was constrained using chromatographic columns (Chelex-100 resin) designed (Lin and Nriagu, 1999) to separate Tl^{+} from Tl^{3+}. The Tl from the fresh mixtures and Pb from both fresh and aged, exposed to sunlight mixtures elute similarly in 2% HNO_3. Tl from solutions containing Pb and exposed to sunlight, however, eluted much later, and ultimately required the use of 10% and 20% HNO_3 for complete elution (Fig. 2-3). These results strongly suggest that Tl^{+} is oxidized to Tl^{3+} in solutions containing Pb when exposed to sunlight. The reaction is reversible when the solutions are stored without exposure to sunlight.

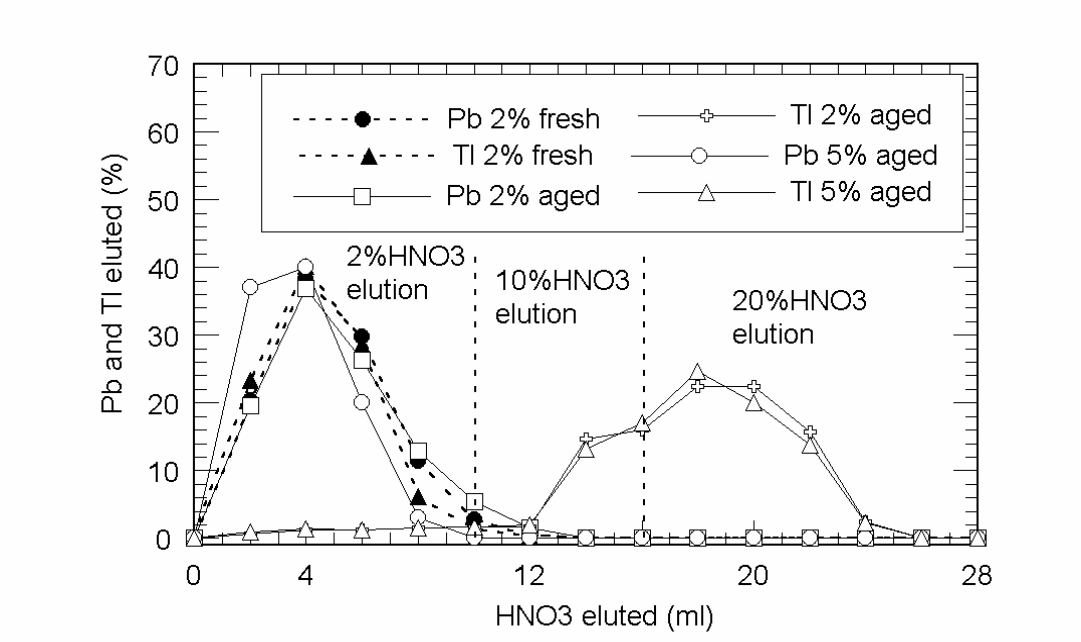

Figure 2-3. Chelex-100 resin elution behavior of Pb and Tl in fresh and aged, exposed to sunlight mixed solutions, for more details see the text.

Discussion

Accuracy and Precision of the Pb and Tl Isotope Measurements

Data for SRM 981 "wet plasma" experiments provide a significant improvement over unspiked Pb isotopic analyses by TIMS, but are not generally as precise as double spike results. Analyses, however, completed using the DSN and fresh Pb-Tl mixtures revealed excellent precision, equivalent or even better than commonly reported for double spike methods via TIMS (Todt et al. 1996, Thirwall 2000). The generally lower precision of wet plasma vs dry plasma experiments is probably related to less stable plasma conditions during wet plasma mode. The absolute value of the SRM 981, however, is dependant on the $^{205}Tl/^{203}Tl$ ratio used for normalization (Belshaw et al. 1998, Collerson et al. 2002). All of the reported SRM 981 data in this paper, summarized in Table 2-1, were normalized using $^{205}Tl/^{203}Tl=2.3875$, adapted from Belshaw et al. (1998). The values observed during wet plasma and DSN fresh mixtures analyses (Table 2-1) are in excellent agreement with the DS TIMS data of Todt et al. (1996).

In terms of Tl isotopes, Rehkämper and Halliday (1999) measured the $^{205}Tl/^{203}Tl$ ratios in commercially available Alfa/AESAR, Aldrich, and NBS 997 Tl solutions and concluded that they all have indistinguishable isotopic compositions. They reported $\varepsilon^{205}Tl=-1.38$ (+/-1.48 3σ) for Aldrich and $\varepsilon^{205}Tl=0.19$ (+/-1.28 3σ) for Alfa/AESAR solutions, relative to NIST 997 $^{205}Tl/^{203}Tl=2.3871$. Fresh mixture measurements of our aliquots of commercially available QCD and Aldrich Tl solutions yielded $\varepsilon^{205}Tl=1.5$ (+/-0.8 2σ) and $\varepsilon^{205}Tl=0.1$ (+/-0.8 2σ) respectively, values that are within error of the values measured by Rehkamper and Halliday (1999). Conversely, the measured Tl and Pb

isotopic compositions in the aged Pb-Tl mixtures reveal large discrepancies (Fig. 2-1A and 2-1B) that I attribute to the presence of Tl^{3+} in these solutions.

Production of Tl^{3+}

Thermodynamic considerations indicate that only monovalent thallium is stable in the solutions measured for this study (Lin and Nriagu 1999), and this expectation was confirmed by our experiments on the elution behavior of fresh mixtures with the Chelex-100 resin (Fig. 2-3). The observed change in the thallium elution behavior for the mixed solutions exposed to sunlight in the laboratory, however, indicates that Tl^{+} was oxidized to Tl^{3+} (Fig. 2-3). The fact that measured ion beam intensities in unmixed Pb and Tl control solutions did not exhibit this behavior suggests that the photo-oxidation of Tl was catalyzed by the presence of Pb. Photoelectrochemical reactions can be driven in an "uphill" direction by exposure to ultraviolet radiation (Bard 1980). In particular, Switzer et al. (1982) demonstrated that Tl^{+} can be oxidized to Tl^{3+} in a liquid photovoltaic cell by exposure to UV light in the presence of semiconductors such as TiO_2, WO_3, and ZnO. It has been proposed that ultraviolet irradiation induces a $Tl^{+} \leftrightarrow Tl^{3+}$ electron transfer by production of a short-lived Tl^{2+} chain carrier (Stranks and Yandell 1969). Because Tl^{+} was converted to Tl^{3+} upon exposure to solar UV radiation and only in the presence of Pb^{2+} during our experiments, it may be that Pb^{2+} acts as a short-lived electron carrier in a possible one or two stage reaction, e.g.:

$$Tl^{+}+Pb^{2+} \leftrightarrow Tl^{3+}+Pb^{\circ} \text{ or } Tl^{+}+2Pb^{2+} \leftrightarrow Tl^{3+}+2Pb^{+}$$

It is difficult to confirm the formation of either of the two lead species noted above due to the very low concentrations and the fact that Pb° and Pb^{+} are not stable in nitric acid and should be rapidly oxidized to Pb^{2+}. Consequently, the ultimate storage of

the electrons liberated during the oxidation is likely to be accommodated by small changes in the NO_2^-/NO_3^- ratio (i.e., amount of nitric acid reduction). This hypothesis is supported by the observation that after storage without exposure to sunlight, all of the solutions returned to their initial state (Fig. 2-2A and B); that is, they behave as Tl^+-bearing mixtures. The exception is the 2%HCl solution, probably because Tl^{3+} is stabilized in presence of Cl (Cotton et al. 1999). In addition, it appears that after aging and exposure to sunlight, HNO_3 solutions with added traces of Cl tend to produce less variable $^{205}Tl/^{203}Tl$ isotopic compositions, although very different than the $\varepsilon^{205}Tl$ defined by the "fresh" and wet plasma experiments (Fig. 2-2B and 2-4B).

The association between Tl^{3+} and the generation of increased Pb/Tl ratios, increased wash-out time for Tl, and imprecise isotopic ratios in the post-desolvation fraction of the analyte suggests that Tl^{3+} does not behave in the same manner as Tl^+ or Pb^{2+} during the desolvation. The differential behavior of these two Tl species may be related to more than one factor or process. For example, Tl^+ is much more soluble than Tl^{3+} and Tl^{3+} (or complex ions/molecules containing Tl^{3+}) may precipitate or adsorb onto surfaces inside the DSN more readily than Tl^+ during the concentration that occurs as the sample is evaporated. Tl^{3+} is more likely to be hydrolyzed and form colloids than Tl^+, even at pH 1 to 2.5 (Cotton et al. 1999). If formed, these colloidal particles would be small enough to be transported downstream from the spray chamber and may adhere, therefore, to a variety of surfaces inside the DSN, including the membrane. Similarly, Tl^{3+} (or a complex ion containing Tl^{3+}) may interact differently with the desolvation membrane. Although composed of relatively inert fluorocarbon, the membrane has a

relatively large surface area compared to the other components of the DSN and is, therefore, a likely zone of retention.

Mass Discrimination Behavior of Pb and Tl

The observed elemental fractionation that occurs during desolvation of Tl^{3+}-bearing solutions appears to be accompanied by fractionation of Tl isotopes. Figure 2-4 shows the fractionation factors derived for Tl and Pb for the experiments reported here. The calculated Pb and Tl fractionation factors for fresh mixtures and wet plasma show very similar behavior and define a common line (indistinguishable slopes) indicating identical mass fractionation behavior for the Pb and Tl isotopes (Fig. 2-4A). Data from the wet plasma experiments include data generated from both Tl^{+} and Tl^{3+}-bearing solutions (Table 2-1), which also lie on this common fractionation line. This suggests that even though thallium is oxidized to Tl^{3+}, it does not experience differential mass-bias behavior in the plasma compared to Pb nor does the oxidation process itself appear to cause isotopic fractionation. No decoupling in the Pb/Tl ratios was observed in wet plasma mode (Table 2-1) and furthermore, scanning at lower masses (68.3, 102.5, etc.) failed to detect any peaks where Tl^{3+} or Tl^{2+} would be present, suggesting that Tl^{3+} is efficiently transformed to Tl^{+} in the plasma.

Fractionation factors for the Tl^{3+}-bearing solutions analyzed by DSN, however, deviate from the factors calculated for the Tl^{+}-bearing solutions and wet plasma experiments, which suggests mass-dependant fractionation of Tl during desolvation. The variations in the isotopic composition of Tl produced during desolvation can be represented by fractionation lines offset from, but parallel to, the fractionation line defined by the “fresh” and wet plasma experiments (Fig. 2-4B). These results indicate

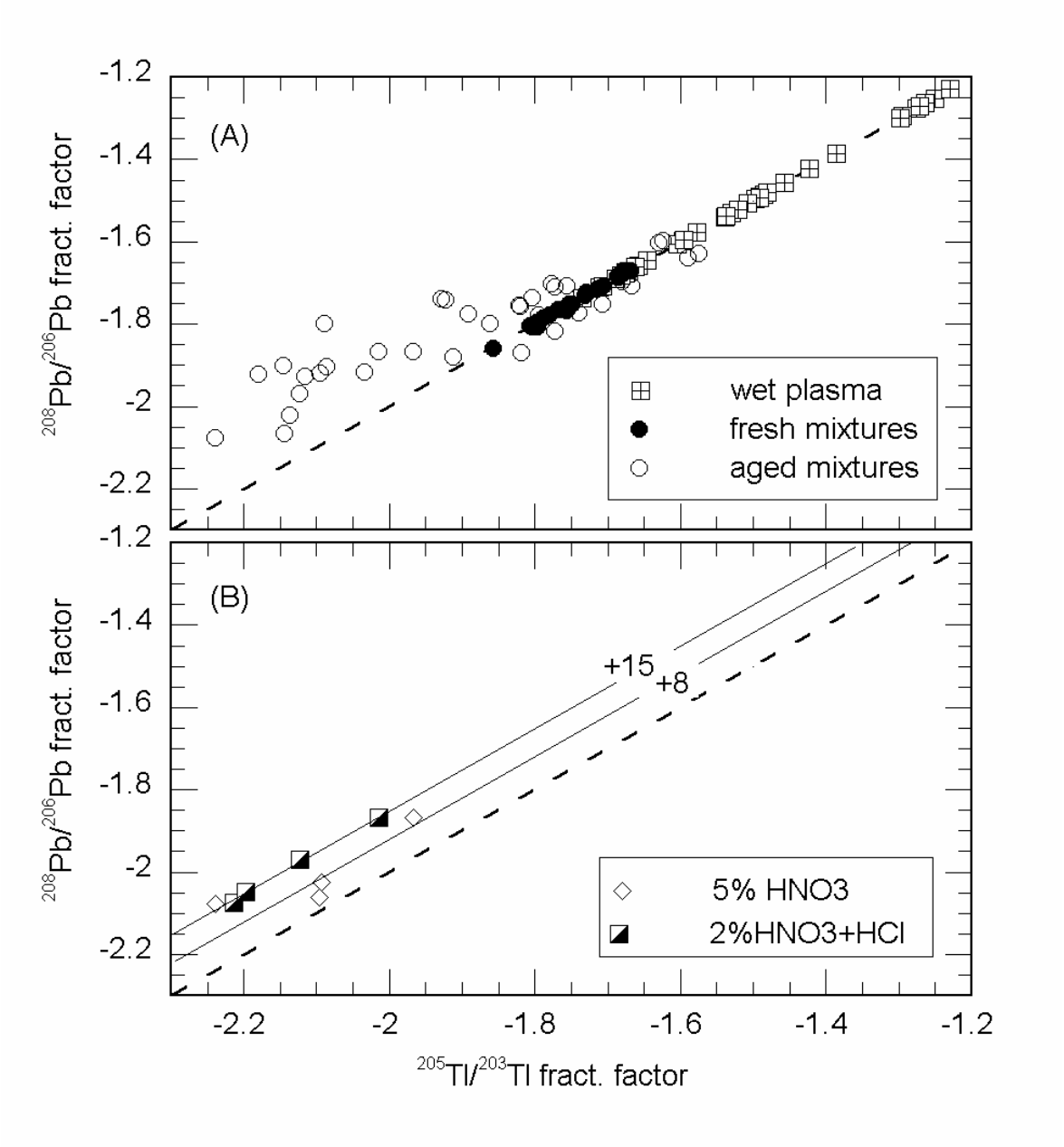

Figure 2-4. (A) Fractionation factors obtained for lead and thallium in Tl^{3+}-bearing solutions, fresh mixtures, and wet plasma experiments. The data for wet and DSN fresh mixtures show very similar behavior and lie on a line expected for identical mass-bias behavior experienced by Pb and Tl (dashed line). (B) Comparison of fractionation factors for several Tl^{3+}-solutions analyses collected within a few days with the true Pb and Tl fractionation factor line (dashed line). Solid lines represent calculated fractionation factors using different Tl isotopic compositions (the offset from the wet and fresh analyses is shown in epsilon notation).

that Pb and Tl continue to experience similar mass-bias behavior, but that a net change in the isotopic composition of thallium in the desolvated Tl^{3+}-bearing solutions occurred.

Changes in the isotopic composition of Tl are not, however, consistent. For example, a 0.6% HNO_3 Pb-Tl solution exhibited relatively small changes in $\varepsilon^{205}Tl$, but at the same time, a 5%HNO_3 Pb-Tl solution exhibited a range of almost 10 $\varepsilon^{205}Tl$ units over a several days time period (Fig. 2-2B and 2-4B). Over the same period a 2%HNO_3+traces of HCl Pb-Tl solution showed relatively stable $\varepsilon^{205}Tl$, although the values were very different than the value obtained for the fresh mixtures (Fig. 2-4B). These observations suggest that the measured $\varepsilon^{205}Tl$ in the Tl^{3+}-bearing solutions is influenced by several factors, including the acid matrix, the conditions during desolvation, and the dose of UV (sunlight) received (Fig. 2-2 and 2-4).

The exact process or processes which produce differential mass fractionation of Tl^{+3}-bearing solutions during desolvation is not clear. Mass-dependant isotopic fractionation during redox reactions involving Fe has been suggested by Zhu et al. (2002). Nielsen et al. (2004), however, demonstrated that mass-fractionation of Tl does not occur during laboratory handling that includes ion exchange chromatography and oxidation of Tl^{+} to Tl^{3+}. Our experiments also show no evidence for mass fractionation during photo-oxidation reaction. It seems most likely, therefore, that the observed isotopic fractionation (enrichment in ^{205}Tl) occurs during desolvation. The fact that the analyte is enriched in the heavier isotope suggests that adsorption (Rehkämper et al. 2002) is not the controlling process, though we cannot rule out its occurrence. A more likely process that must be considered for the preferential removal of ^{203}Tl from the analyte during desolvation is diffusion related mass-dependant fractionation. During the

diffusion process the lighter isotopes have higher average velocities and so diffuse proportionally faster than the heavier isotopes through a porous membrane (Chopin et al. 2002). This process, known for almost a century, is commercially utilized in uranium enrichment plants using UF_6. The isotope enrichment is accomplished in a series of diffusion devises consisting of cells divided by a porous membrane (commonly made of fluorocarbon), which can maintain differential gas pressure (Chopin et al. 2002). The basic construction of gaseous diffusion devices, therefore, is similar to the desolvators utilized in this and other studies referred to herein. By analogy with the enrichment of uranium, it may be that the $^{203}Tl^{3+}$ ions, molecules, or complex ions (e.g., hydrated Tl^{3+}) pass through the membrane at a greater rate than the $^{205}Tl^{3+}$ species as they pass along the length of the desolvating membrane, which results in an enrichment in ^{205}Tl in the desolvated analyte. The greater rate of transfer of Tl under these conditions may also lead to greater interaction with the membrane to the point that more Tl is ultimately held on the membrane, which results in the longer washout times observed. The net effect of these two processes (adsorption and diffusive fractionation) appears to favor diffusion as the primary process that determines the isotopic composition of the analyte.

Fractionation during diffusion, however, should affect all species in the analyte stream to some degree, including Pb. If, however, the fractionation behavior of the elements of interest is governed by a common fractionation law during the passage through the DSN and in the plasma, then precise isotopic ratios can be obtained by applying a single correction factor (e.g., exponential law), as is the case for our fresh Pb-Tl mixtures. If the fractionation behavior of the elements of interest does not result from processes adequately described by a single fractionation law, then such a correction will

not result in precise isotopic measurements, as is observed in our aged, exposed to sunlight mixtures. At this stage, however, it is not clear why Tl^{3+} species experience different fractionation behavior than Tl^{+} and Pb^{2+}. Possible explanations include 1) Tl^{3+} ions have lower hydration enthalphy (-4184) compared to Tl^{+} (-326) and Pb^{2+}(-1480) (Burgess 1978) and, therefore, form stronger bonds with water molecules (or with Ar, N) that may persist through the desolvation process and interact with the membrane to a greater extend; 2) by analogy with the use of the volatile UF_6 for U-enrichment, it may be that the formed Tl^{3+} species are more volatile than Tl^{+} species and, therefore, are more susceptible to gaseous diffusion enrichment; and 3) it is also possible that the emerging from the DSN Tl^{3+}-bearing dry aerosols experience different mass-bias than the Tl^{+}-bearing dry aerosols in the plasma, although the wet plasma experiments argue against such possibility. Fractionation may occur also during the vaporization of solvent, which leads to the formation of compounds and/or complex molecules that may preferentially incorporate heavier isotopes. In addition, the so formed compounds, molecules, and/or hydrous ions may have different vapor pressures, and consequently, one species (e.g., Tl) may be lost preferentially to another (e.g., Pb) and also isotopically fractionated. Further experiments are required to test these hypotheses.

Conclusions

High-precision Pb isotopic measurements provide valuable geochemical information, however, significant analytical errors can be introduced during MC-ICP-MS isotopic analyses of desolvated Pb and Tl-bearing solutions because different species appear to exhibit different behavior during the liquid-vapor transition and subsequent desolvation process inside the DSN. My experiments demonstrate that significant Tl

isotopic variations, equivalent to the range observed in natural samples by Rehkämper et al. (2002) can be generated by varying experimental conditions, as reported here.

The interaction of Pb and Tl is thermodynamically unexpected and appears to result from photoelectric driven oxidation of Tl^{+} to Tl^{3+}. The reaction occurs only after the addition of Pb, which appears to act as an intermediate (short-lived) electron acceptor. Although no detailed experiments were conducted to constrain the kinetics of the reaction in detail, this phenomenon was observed in mixed solutions exposed to sunlight for more than several hours. The demonstrated production of Tl^{3+} in solution, which is related to a complex combination of factors (e.g., differences in the acid matrix and molarity, desolvation conditions, and duration of UV light exposure), greatly affects the precision and accuracy of Pb and Tl isotopic measurements. Spiking samples intended for Pb isotope measurements with Tl just before the analysis and/or preventing the mixed Pb-Tl solutions from being exposed to sunlight (UV light) are critical for achieving the most precise Pb isotope ratio measurements from desolvated nitric acid solutions.

CHAPTER 3
HIGH-PRECISION PB ISOTOPE MEASUREMENTS REVEAL MAGMA RECHARGE AS A MECHANISM FOR ORE DEPOSIT FORMATION: EXAMPLES FROM LIHIR ISLAND AND CONICAL SEAMOUNT, PAPUA NEW GUINEA.

Introduction

Ore deposits associated with subduction-related volcanism are among the most important sources of base and precious metals in the world. Although many of these deposits have received extensive study, several major questions regarding their genesis remain unanswered. Such major questions include why base metal mineralization is associated with some magmatic systems, but not with others? What is the mechanism of incorporation of ore metals into hydrothermal fluids, have these components been derived from active sub-volcanic melts as a result of magma degassing, or have they been extracted from the host rocks via meteoric or seawater hydrothermal leaching driven by thermal energy from magmas? If the latter is the case, magmatic heat will drive the hydrothermal circulation and, consequently, is the most critical factor for the formation of an ore deposit. Relatively few magmatic complexes, however, contain world-class deposits, suggesting that other mechanisms must also play important roles in the formation of ore deposits associated with magmatic systems. Such mechanisms include efficient release of metal-bearing fluids from solidifying magmas (Hedenquist and Lowenstern 1994). Suitable conditions for magmatic fluid saturation and release can be reached during magma cooling accompanied by crystallization or during recharge by volatile-rich magma (Sillitoe 1997). Studies suggest that during degassing, magma chambers maintain relatively oxidizing conditions that inhibit formation of immiscible

sulfide liquids that can sequester ore metals (McInnes and Evans 1996) and thereby enhance the ore formation potential of the exsolving fluids. Providing clear evidence that the exsolution of ore-bearing fluids from magmas is a major mechanism for ore formation remains elusive. Studies utilizing stable isotope tracers, such as oxygen and sulfur, have shown that the magmatic signature in the ore-forming fluid is often obscured due to mixing with meteoric fluids in the near surface environment and so considerable disagreement exists concerning which of the fluids (i.e., magmatic or meteoric) transport and deposit ore metals (Bodnar 1995).

Another important isotopic tracer that can be directly related to the ore metal sources are the lead isotopes. Lead is a common ore metal and shares similar geochemical behavior with other ore metals such as Ag, Cu, and Zn. Numerous studies have utilized Pb isotopes to investigate the relationship between ores and their possible sources (Doe and Delevaux 1972, Tilton et al. 1981, Macfarlane et al. 1990, Richards et al. 1991, Kamenov et al. 2002). Historically, the use of Pb isotopes suffered from the fact that due to isotopic fractionation, lead isotopic data obtained by thermal ionization mass spectrometry (TIMS) lack the precision and accuracy readily obtained for Sr, Nd, Hf, and Os isotopic analyses. For example, for Sr a non-radiogenic isotope pair, usually ^{86}Sr and ^{88}Sr, is used to correct for the observed isotopic fractionation and thus highly precise data can be obtained. A similar correction is not possible for lead because there is only one non-radiogenic isotope (^{204}Pb). So, in the conventional TIMS analysis, a set of samples is corrected using the fractionation measured in a well-characterized standard, usually NBS 981, by assuming similar mass-bias behavior in the standard and the unknowns. It has been shown, however, that samples may exhibit different

fractionation behavior than the pure standards due to the presence of other metals and varying amounts of sample loaded and the extent of evaporation for individual samples (Woodhead et al. 1995, Kamenov et al. 2003). In order to deal with this problem some studies have adopted double (DS) and triple (TS) spike methods to correct for instrumental mass bias and have successfully produced high-precision Pb isotopic data (Todt et al. 1996, Abouchami et al. 2000, Thirwall 2000). Recent studies have demonstrated that important geochemical correlations and trends among Pb isotopes, not readily observable in the traditional TIMS-derived data, can be revealed by utilizing high-precision Pb isotopic analyses (Abouchami et al. 2000, Woodhead 2002).

With the development of the MC-ICP-MS a novel technique for Pb isotopic measurements was adopted that uses $^{205}Tl/^{203}Tl$ as an internal standard to correct for mass-dependant fractionation of Pb (Rehkämper and Halliday 1998, Collerson et al. 2002, Woodhead 2002). Although some studies have questioned the applicability of Tl isotopes for instrumental mass fractionation corrections of Pb isotopes (Thirwall 2002, Baker et al. 2004), our recent experiments have shown that highly precise Pb isotopic ratios, equivalent to the DS and TS TIMS Pb isotope measurements, can be obtained using MC-ICP-MS. The key issue in this application is to control the interaction of Pb and Tl in solution so that thallium does not oxidize to the 3+ state (Kamenov et al. 2004).

Here I present high-precision Pb isotopic data (measured by MC-ICP-MS) from subaerial and submarine alkaline lavas and gold-bearing ores from Papua-New Guinea to address the origin of these valuable mineral deposits. A number of large epithermal gold and copper deposits genetically associated with alkaline rocks have recently attracted

considerable interest (Sillitoe, 2002), including the giant Ladolam gold deposit in the Luise caldera, located on Lihir Island, Papua-New Guinea (Moyle et al. 1990; Rytuba et al. 1993; Müller et al. 2001, 2003). A group of seamounts (Edi's Daughter, Edison, Tubaf, and Conical) were recently discovered on the flanks of Lihir Island and the presence of gold mineralization was discovered at the summit of Conical seamount in 1998 (Herzig et al. 1999). In this Chapter, I investigate the sources and processes that may have led to the development of the deposits at both Lihir Island and Conical seamount.

Geological Settings

Lihir island is one of a group of islands in Papua-New Guinea that lie northeast of the islands of New Britain and New Ireland in the Southwest Pacific. The Tabar, Lihir, Tanga, and Feni (TLTF) island chain is located in the former fore-arc region of New Ireland, part of the Bismarck archipelago (Fig. 3-1). Volcanism on New Ireland and on most of the islands in the archipelago is dominantly calc-alkaline to high K/calcalkaline, and was generated as a result of subduction of the Pacific plate under the Indo-Australian plate along the Manus-Kilinailau trench (Johnson 1979). Subduction ceased about 10 Ma ago, when the thick and relatively buoyant Ontong-Java plateau collided with the subduction zone (Coleman and Kroenke 1981). Subsequent to the collision, regional relocation of stress caused reversal of the subduction direction, formation of the north-norhtwest facing New Britain-San Cristobal trench, initiation of back-arc spreading in the Manus Basin at about 3.5 Ma, and development of several microplates (Taylor 1979).

The TLTF island chain extends for about 250 km parallel to the presently inactive Manus-Kilinailau trench (Fig. 3-1). The islands are equally spaced at about 75 km, and

seismic reflection surveys have delineated horst and sediment-filled grabens bounding the chain, suggesting extension and crustal thinning (Exon et al. 1986). Volcanism in the

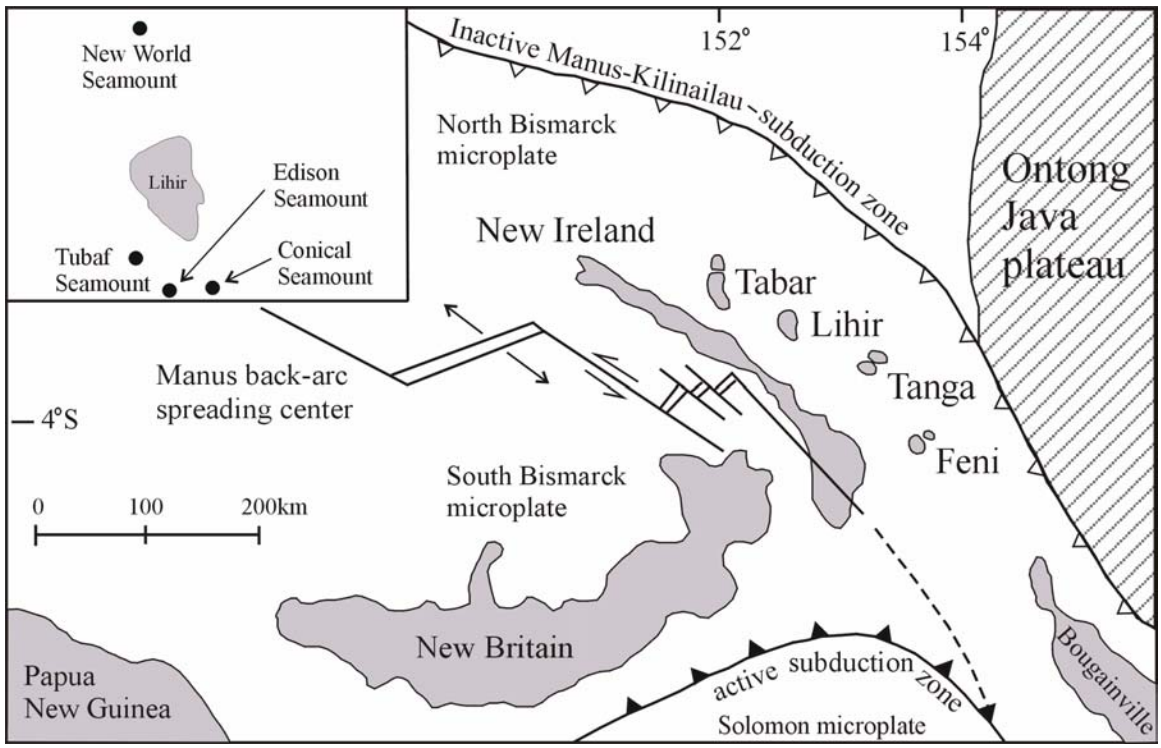

Figure 3-1. Regional map of Northwest Papaua New Guinea showing the Tabar-Lihir-Tanga-Feni island chain, modified after Taylor, 1979. The inset shows the location of Lihir Island and the seamounts, where samples for this study were recovered.

TLTF area began on Simberi island, about 3.7 Ma ago (Johnson et al., 1976, McInnes, 1992), coeval with the initiation of back-arc spreading in the Manus Basin, and migrated southward to Feni island (2300 y), as the island of New Britain was transported to the southeast. Taylor (1979) suggests that the local extension and volcanism are related to the opening of the Manus back-arc spreading center. TLTF islands are characterized mainly by high-K calc-alkaline rocks with similar to arc lavas trace element and isotopic characteristics (Wallace et al. 1983; Kennedy et al. 1990a,b; Stracke and Hegner 1998). These lavas were probably derived from a number of different parental magmas

generated in a mantle source enriched in incompatible elements during earlier periods of subduction of the Pacific plate (McInnes and Cameron 1994, Stracke and Hegner 1998).

During a cruise of the RV SONNE in 1994 (SONNE 94) Edi's Daughter, Edison, TUBAF, and Conical volcanic seamounts were discovered on the flanks of Lihir Island (Fig. 3-1, Herzig et al. 1994). Sampling (dredge and TV-assisted grab) and observations using a remote camera indicated the seamounts were volcanically active in the recent past and that Conical seamount had recently been hydrothermally active (Herzig et al. 1994). Ultramafic, gabbroic, basaltic, and sedimentary xenoliths were recovered in submarine lavas from Tubaf and Edison seamounts. The abundance of xenoliths in Tubaf lavas is remarkable; one TV-grab sample weighing 200 kg contained more than 70 cm-sized xenoliths (McInnes et al. 2001). During a cruise of the RV SONNE in 1998 (SO-133) the existence of epithermal-style gold mineralization at Conical seamount was confirmed by extensive sampling (Herzig et al. 1998). The seamount is a submarine volcanic cone underlain by a thick (about 5 km) layer of Miocene to Recent sediments (McInnes et al. 2001). The recovered lavas are porphyritic vesicular trachybasalts to basaltic trachyandesites (Müller et al. 2003). The mineralization is confined to the top of the seamount along a main eruptive fissure and shows zonal distribution (Herzig et al., 1999). Three styles of mineralization can be identified (Petersen et al. 2002): (a) intensely altered clay-silica rich zone containing semi-massive and stockwork-like pyrite, (b) gold-rich, disseminated, polymetallic sulfides in feldspathic and siliceous veins, and (c) low-temperature, late-stage, fracture-hosted As-Sb mineralization. Here I have divided the mineralized samples analyzed in this study into two groups: 1) high-temperature gold-rich samples (including (a) and (b)) and 2) low-temperature samples (c) (Table 3-1).

Samples and Analytical Methods

General descriptions and locations of samples analyzed in the study are presented in Table 3-1. Fresh volcanic rocks and altered volcanic rock samples exhibiting various degrees of mineralization were recovered from the seamounts during the 1998 R/V Sonne cruise. Conical seamount trachybasalts are composed of about 20 to 25% clinopyroxene (Cpx), 5% plagioclase (Plag), and rare olivine and phlogopite phenocrysts embedded in a slightly vesicular, fine-grained groundmass which consists of glass, plagioclase, clinopyroxene, spinel, and apatite microcrysts (Müller et al. 2003). The clinopyroxene phenocrysts are large (up to about 6mm), euhedral to subhedral, and exhibit distinct zoning. Plagioclase phenocrysts are much smaller, up to about 1mm long. Tubaf and Edison seamounts' lavas are also trachybasalts and contain phenocrysts of clinopyroxene, as well as phlogopite and amphibole embedded in a groundmass containing about 20% vesicles and glass (McInnes et al. 2001). Clinopyroxenes in these samples are smaller (up to 1mm) and more homogeneous than those from Conical lavas.

Mineralized samples were collected from the Ladolam mine. Two unaltered monzonite samples were obtained from a drill core taken from different depths in the Ladolam mine. Sedimentary (limestones and carbonaceous mudstones) and mafic (gabbro and basaltic) xenoliths were extracted from Tubaf seamount lavas using a microdrill (Table 3-1).

Mineral analyses in seamount lavas were conducted at the Florida Center for Analytical Electron Microscopy (Florida International University) using a JEOL EPMA JXA-8900-R equipped with 5 wavelength dispersive spectrometers. Mineralized samples

Table 3-1. Location, general description, and strontium and lead isotopic compositions of samples in the study area. Table includes also Pb isotope data for USGS rock standards prepared and analyzed together with the samples.

Sample #	Location	Description	Sr	$^{87}Sr/^{86}Sr$	Pb	$^{206}Pb/^{204}Pb$	$^{207}Pb/^{204}Pb$	$^{208}Pb/^{204}Pb$
15GTVA 2DSp	Conical	High temperature mineralization (Gn*, Sp)	25	0.70401	29300	18.764	15.546	38.372
15GTVA 2DSp	-	Duplicate	-	-	-	18.765	15.549	38.374
23GTVA Sp	Conical	High temperature mineralization (Sp)	-	-	-	18.768	15.548	38.382
25GTVA 6BSp	Conical	High temperature mineralization (Cp, Sp, Stbn, Plag, Kfs)	490	0.70411	13500	18.763	15.549	38.380
25GTVA 6BSp	-	Duplicate	-	-	-	18.761	15.547	38.371
25GTVA 8C2	Conical	High temperature mineralization (Gn, Sp, Cp, Chd, Plag)	172	0.70457	34100	18.767	15.551	38.379
53GTVA 2AGn	Conical	High temperature mineralization (Gn, Py, Cp, Kfs, Qtz)	212	0.70575	25700	18.764	15.546	39.372
53GTVA 2Agn	-	Duplicate	-	-	-	18.766	15.547	38.371
39GTVA 2Xpy	Conical	Low temperature mineralization (Py, Mrc, Qtz, Kfs, Rlg, Jar)	846	0.70745	298	18.756	15.554	38.377
40GTVA 2Py2	Conical	Low temperature mineralization (Chl, Am-Si, Py, Anat)	66	0.70493	563	18.742	15.543	38.350
42GTVA 2Py	Conical	Low temperature mineralization (Qtz, Chd, Py, Hm, Plag)	928	0.70421	286	18.764	15.546	38.366
53GTVA 1Bpy	Conical	Low temperature mineralization (Py, Hm, Qtz, Plag, Smec)	411	0.70863	33	18.754	15.547	38.359
7DR	Conical	Fresh lava	-	-	4	18.742	15.542	38.341
12DR2A	Conical	Fresh lava	-	-	4	18.733	15.551	39.351
12DR2A	-	Duplicate	-	-	-	18.732	15.549	38.344
13DR4	Conical	Fresh lava	-	-	6	18.734	15.539	38.335
36GTVA 1	Conical	Fresh lava	-	-	5	18.737	15.548	38.364
50DR1C	Conical	Fresh lava	-	-	4	18.746	15.548	38.360
52GTVA 1	Conical	Fresh lava	-	-	5	18.721	15.547	38.332
52GTVA 1	-	Duplicate	-	-	-	18.720	15.544	38.327
54GTVA 4-2	Tubaf	Fresh lava	1504	0.70397	10	18.759	15.554	38.391
56GTVA 2C	Tubaf	Fresh lava	1698	0.70397	10	18.756	15.550	38.377
56GTVA 2M	Tubaf	Fresh lava	-	-	11	18.766	15.550	38.366
10GTVA 5A2	Edison	Fresh lava	-	-	5	18.761	15.547	38.371
11GTVA 2A1	Edison	Fresh lava	-	-	4	18.762	15.546	38.373
33GTVA 2J1	Edison	Fresh lava	-	-	5	18.766	15.550	38.384
34GTVA 3-1	Edison	Fresh lava	-	-	5	18.765	15.549	38.378
LH98-3	Lihir, Ladolam	Mineralization (Kfs, Py, Cp)	-	0.70395	-	18.718	15.545	38.339

Table 3-1. Continued

LH98-6	Lihir, Ladolam	Mineralization (Qtz, Py, Cp, Gn)	-	0.70405	-	18.715	15.544	38.337
LH98-7	Lihir, Ladolam	Mineralization (Qtz, Py)	-	0.70409	-	18.726	15.543	38.342
LH98-7	-	Duplicate	-	-	-	18.726	15.542	38.336
LH98-8	Lihir, Ladolam	Mineralization (Qtz, Py)	-	-	-	18.727	15.543	38.340
LH98-9	Lihir, Ladolam	Mineralization (Qtz, Py, Cp, Gn)	-	-	-	18.720	15.539	38.331
LIH-10	Lihir, Londolovit	Fresh lava	-	-	-	18.765	15.546	38.357
LIH-11	Lihir, Londolovit	Fresh lava	-	-	-	18.766	15.554	38.377
LIH-18	Lihir, Luise	Fresh lava	-	-	-	18.759	15.549	38.368
LIH-21	Lihir, Luise	Fresh lava	-	-	-	18.762	15.548	38.367
LIH-23	Lihir, Luise	Fresh lava	-	-	-	18.757	15.549	38.368
LIH-25	Lihir, Luise	Fresh lava	-	-	-	18.747	15.553	38.366
LIH98-1	Lihir, Luise	Fresh lava	-	-	-	18.748	15.543	38.347
LIH98-2	Lihir, Luise	Fresh lava	-	-	-	18.745	15.541	38.341
471-265	Lihir, Luise	Monzonite	-	-	-	18.737	15.553	38.369
471-339[50]	Lihir, Luise	Monzonite	795	0.70396	-	18.727	15.544	38.342
471-339[50]	-	Duplicate	-	-	-	18.728	15.544	38.344
56GTVA 3O	Tubaf	Basaltic xenolith	144	0.70297	0.33	18.692	15.509	38.163
54GTVA 3E	Tubaf	Gabbro xenolith	120	0.70302	-	18.747	15.509	38.196
55GTVA 2E	Tubaf	Gabbro xenolith	-	-	-	18.722	15.533	38.280
56GTVA 3I	Tubaf	Gabbro xenolith	130	0.70293	0.26	18.647	15.529	38.191
54GTVA 6B	Tubaf	Sedimentary xenolith	892	0.70751	2	18.627	15.557	38.302
54GTVA 6G	Tubaf	Sedimentary xenolith	820	0.70828	6	18.640	15.568	38.325
54GTVA 6E	Tubaf	Sedimentary xenolith	818	0.70759	2	18.901	15.560	38.495
54GTVA 6F	Tubaf	Sedimentary xenolith	456	0.70669	4	18.771	15.567	38.441
56GTVA 4D	Tubaf	Sedimentary xenolith	1221	0.70791	5	18.712	15.528	38.307
56GTVA 4F	Tubaf	Sedimentary xenolith	-	-	2	18.770	15.583	38.495
72GTVA	Near Conical	Surface sediment	-	-	-	18.743	15.585	38.512
BCR-2	-	USGS rock standard	-	-	-	18.767	15.624	38.728
BCR-2	-	Duplicate	-	-	-	18.765	15.622	38.721
BCR-2	-	Duplicate	-	-	-	18.767	15.618	38.738
BCR-2	-	Duplicate	-	-	-	18.763	15.620	38.729
BCR-2	-	Duplicate	-	-	-	18.762	15.620	38.730
AGV-1	-	USGS rock standard	-	-	-	18.942	15.653	38.548
AGV-1	-	Duplicate	-	-	-	18.944	15.655	38.549
AGV-1	-	Duplicate	-	-	-	18.940	15.652	38.541
AGV-1	-	Duplicate	-	-	-	18.944	15.655	38.550
AGV-1	-	Duplicate	-	-	-	18.940	15.652	38.545

*Gn-galena; Sp-sphalerite; Stbn-stibnite; Cp-chalcopyrite; Chd-chalcedony; Rlg-realgar; Jar-jarosite;

from Conical Seamount were carefully micro-drilled and the mineral phases (Table 3-1) were determined by XRD at the Geological Survey of Canada in Ottawa. Trace element concentrations were determined by ICP-MS at the Geological Survey of Canada (http://www.nrcan.gc.ca/gsc/mrd/labs/chem-e.html).

Whole-rock powders (free of xenoliths and alteration) were leached in Optima grade 2N HCl at about 70°C for several hours, then rinsed several times with 4x distilled H_2O to remove leachate residue, and then dissolved in a mixture of $HF+HNO_3$. Micro-drilled sample powders from the mineralized zones were dissolved (but not leached) similarly to the whole rock powders. Sr and Pb for isotopic analyses were separated using standard chromatographic methods under clean lab environment (Chapter 4 and Appendix B). Sr isotopic analyses were performed on a Micromass Sector 54 Thermal Ionization Mass Spectrometer equipped with seven Faraday collectors and one Daly detector at the University of Florida. The Sr was loaded on oxidized W single filaments and run in triple collector dynamic mode. Data were acquired at a beam intensity of about 1.5V for ^{88}Sr, with corrections for instrumental discrimination made assuming $^{86}Sr/^{88}Sr=0.1194$. Errors in measured $^{87}Sr/^{86}Sr$ are better than +/- 0.00002 (2σ) based on long-term reproducibility of NBS 987 ($^{87}Sr/^{86}Sr=0.71024$).

Pb isotopic analyses were conducted on a Nu Plasma multi-collector ICP-MS (Nu Instruments, UK), in the Department of Geological Sciences, University of Florida, using the Tl normalization technique (Chapter 1). Sample and standard solutions were aspirated into the plasma source through a Micromist nebulizer with a GE spray chamber. The instrument settings were carefully tuned to maximize the signal intensities on a daily basis. Preamplifier gain calibrations were determined before each analytical session. All

analyses reported in this paper were conducted in static mode acquiring simultaneously ^{202}Hg on low-1, ^{203}Tl on low-2, ^{204}Pb on Axial, ^{205}Tl on high-1, ^{206}Pb on high-2, ^{207}Pb on high-3, and ^{208}Pb on high-4 Faraday detectors. 42 analyses of NBS 981 conducted with the sample analyses in the period between April and June, 2003 gave the following results $^{206}Pb/^{204}Pb$=16.9369 (+/-0.0039 2σ), $^{207}Pb/^{204}Pb$=15.4904 (+/-0.0034 2σ), and $^{208}Pb/^{204}Pb$=36.6949 (+/-0.0087 2σ). All standard and sample Pb data were normalized with $^{205}Tl/^{203}Tl$=3-38750 (for more details see Chapter 2). Several samples were prepared and analyzed for Pb isotopes as duplicates to evaluate the reproducibility of the results (Table 3-1). In addition, 10 separate dissolutions of USGS rock standards (BCR-2 and AGV-1, Woodhead and Hergt, 2000) were prepared and analyzed together with the samples to further verify the precision and accuracy of the analytical protocol (Table 3-1).

Results

Isotopic analyses of rocks, xenoliths, and mineralized samples from the study area are presented in Table 3-1. Sr isotopic compositions of fresh lavas from the area show relatively small variations with $^{87}Sr/^{86}Sr$, close to 0.704, within the range of 0.7037 to 0.7044 observed in previous studies of TLTF islands and seamounts (Wallace et al. 1983, Kennedy et al. 1990b, Stracke and Hagner 1998). Measured $^{87}Sr/^{86}Sr$ in sedimentary xenoliths recovered from Tubaf seamount lavas exhibit much more radiogenic values than the lavas in the area (Fig.3-2). Sr isotopic compositions of the Conical seamount mineralized samples have values either similar to or more radiogenic than the host lavas (Fig. 3-2). Lihir mineralized samples also have $^{87}Sr/^{86}Sr$ values very similar to the host lavas (Table 3-1).

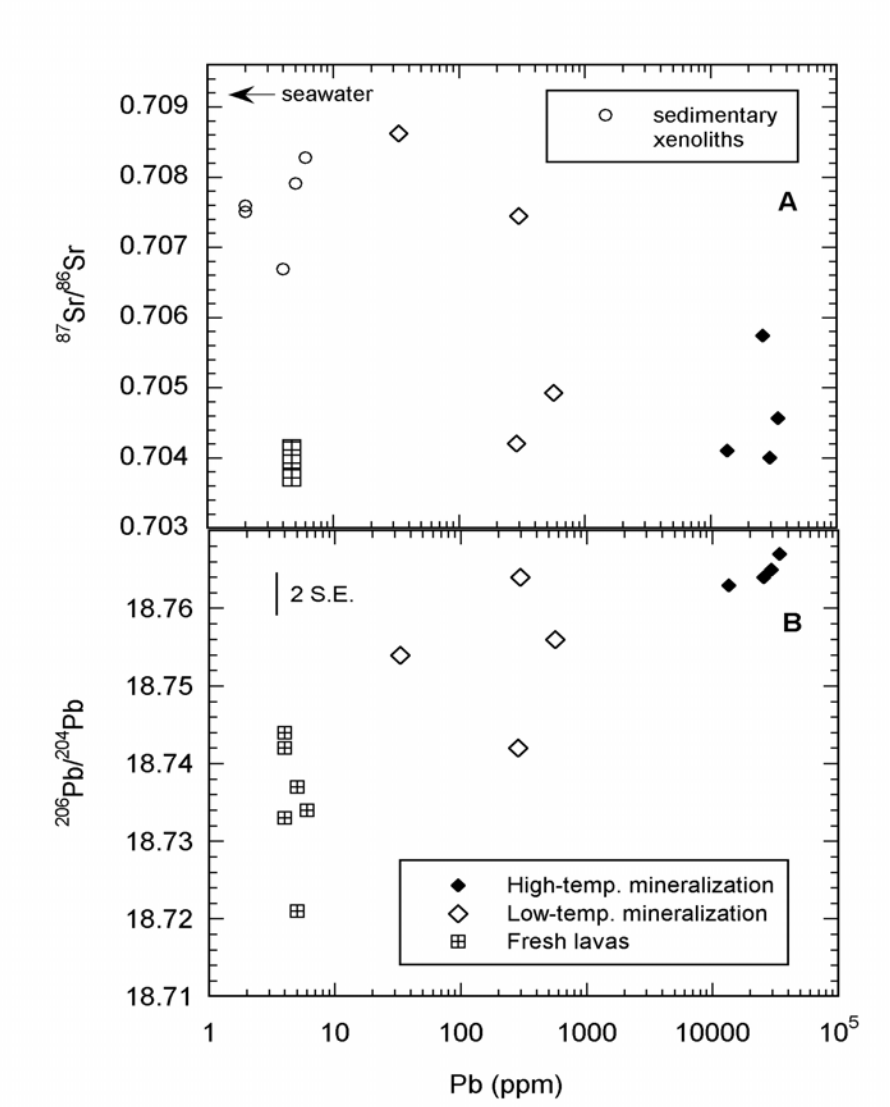

Figure 3-2. (A) $^{206}Pb/^{204}Pb$ vs Pb concentrations of Conical seamount lavas and high- and low-temperature mineralized zones (based on data from Table 3-1). Note that the high-temperature mineralized samples exhibit less variations in their Pb isotopic compositions compared to the lavas and the low-temperature mineralized samples. (B) $^{87}Sr/^{86}Sr$ vs Pb concentrations of Conical seamount lavas, high- and low-temperature mineralized zones, and sedimentary xenoliths (for discussion see the text). Sr data for fresh lavas from this study and Stracke and Hagner (1998).

Fresh volcanic rocks exhibit small, but distinguishable variations in their Pb isotopic compositions, with Conical seamount lavas having the least radiogenic ratios with $^{206}Pb/^{204}Pb$=18.721 to 18.746, $^{207}Pb/^{204}Pb$=15.539 to 15.551, and $^{208}Pb/^{204}Pb$=38.332 to 38.364. Tubaf and Edison seamount lavas are slightly more radiogenic than Conical with $^{206}Pb/^{204}Pb$=18.756 to 18.766, $^{207}Pb/^{204}Pb$=15.546 to 15.550, and $^{208}Pb/^{204}Pb$=38.366 to 38.391 (Fig. 3-3). Most of the analyzed Lihir Island lavas exhibit lead isotopic signatures indistinguishable from Edison and Tubaf lavas with several samples having slightly less radiogenic values, notably the two monzonite drill core samples from the Ladolam mine, with $^{206}Pb/^{204}Pb$=18.727 and 18.737, $^{207}Pb/^{204}Pb$=15.544 and 15.553, and $^{208}Pb/^{204}Pb$=38.342 and 38.369 (Table 3-1). Nine low- and high-temperature mineralized samples from the Conical seamount mineralized zones show slightly more radiogenic ratios than the fresh host lavas, ranging from $^{206}Pb/^{204}Pb$=18.742 to 18.768, $^{207}Pb/^{204}Pb$=15.543 to 15.554, and $^{208}Pb/^{204}Pb$=38.350 to 38.382. The measured lead isotopic compositions in the mineralized Conical seamount samples exhibit a positive correlation between Pb content and $^{206}Pb/^{204}Pb$ ratios (Fig. 3-2A). Mineralized samples from Lihir also show slightly different Pb isotopic ratios from the host fresh lavas exposed on the surface with $^{206}Pb/^{204}Pb$=18.711 to 18.727, $^{207}Pb/^{204}Pb$=15.539 to 15.545, and $^{208}Pb/^{204}Pb$=38.331 to 38.340. A surface sediment sample from New Ireland basin and several sedimentary and mafic xenoliths recovered from the Tubaf seamount lavas were also analyzed for Pb isotopes (Table 3-1). They exhibit larger range in their lead isotopic compositions compared to the fresh volcanic rocks in the area with values ranging from $^{206}Pb/^{204}Pb$=18.627 to 18.901, $^{207}Pb/^{204}Pb$=15.509 to 15.585, and $^{208}Pb/^{204}Pb$=38.163 to 38.512 (Fig. 3-4).

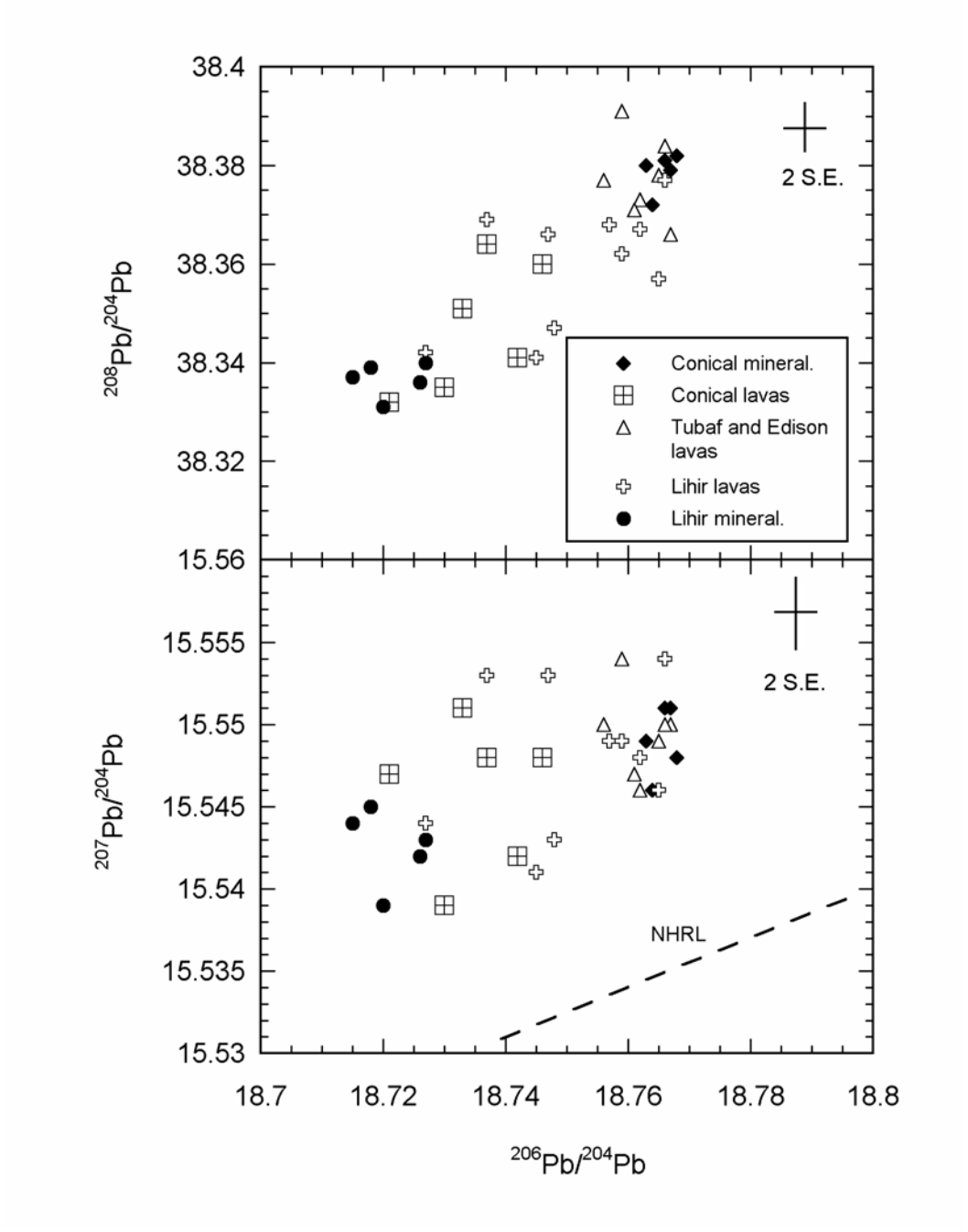

Figure 3-3. MC-ICP-MS Pb isotopic data for lavas and mineralized samples. Note the similarity between the Tubaf and Edison lavas and Conical high-temperature mineralization, suggesting magma with similar Pb isotopic composition as a source for the ore metals. Similarly, Lihir mineralized samples plot at the non-radiogenic end of the array, suggesting Pb source similar to the least radiogenic Conical lavas or the monzonite intrusion. Note that the ores and lavas from a trend parallel to the NHRL (for more discussion see the text).

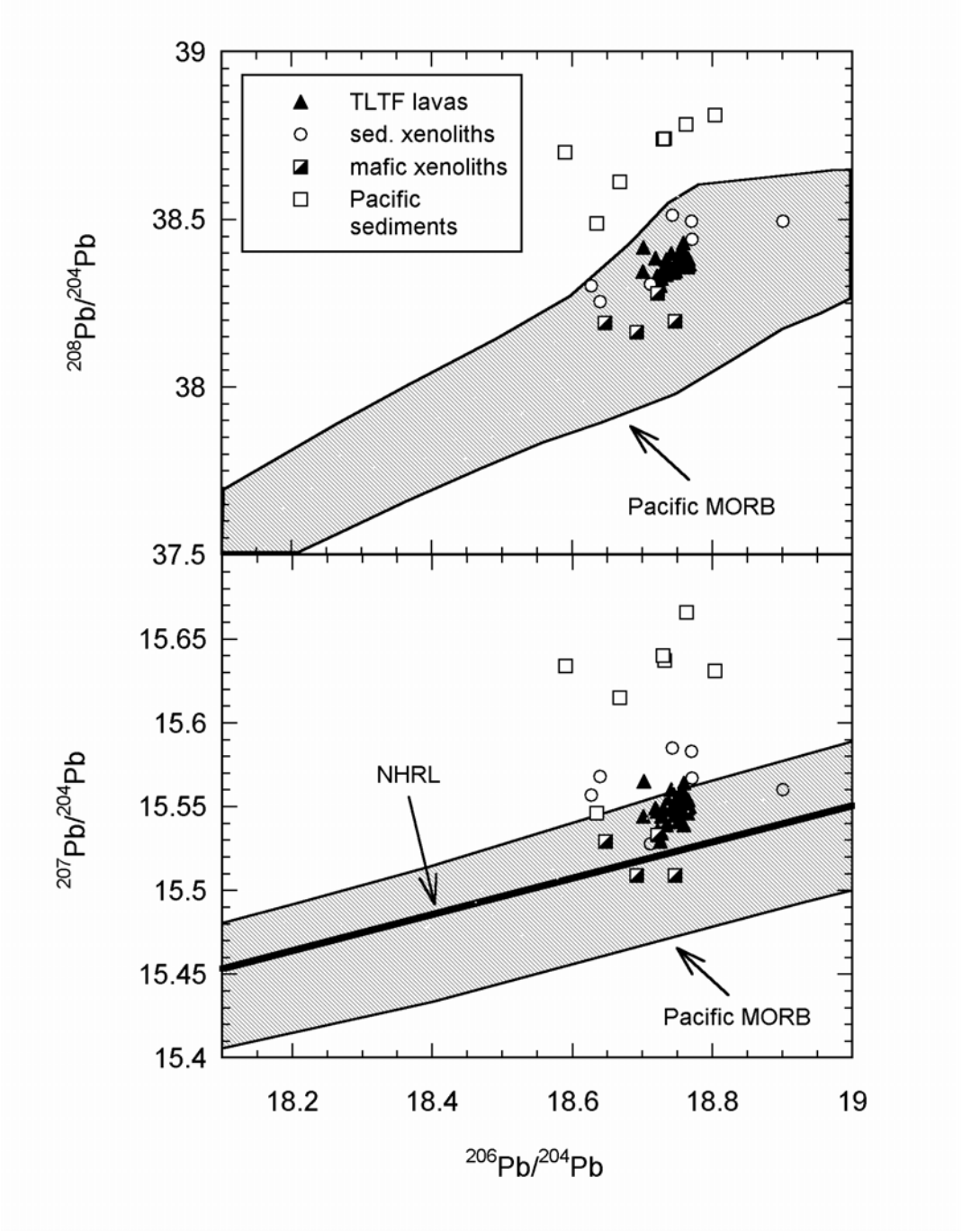

Figure 3-4. Comparison of Pb isotopic compositions of TLTF volcanic rocks with sedimentary and mafic xenoliths, and Pacific MORB and sediments. Note the homogeneous isotopic character of the TLTF samples compared to the possible sources in the area. TLTF volcanic rocks field is based on MC-ICP-MS data from this study and TIMS data from Stracke and Hagner (1998), Pacific MORB after White et al. (1987), and Pacific sediments after Othman et al. (1989).

Analyses of clinopyroxene phenocrysts from Conical, Tubaf, and Edison seamounts, completed by electron microprobe, provide more constraints on changing magmatic conditions (Table 3-2). Typically, Conical clinopyroxenes are larger compared to the clinopyroxenes in the other two seamounts and show concentric zoning with oscillatory chemical variations. The analyzed clinopyroxenes from Tubaf and Edison seamounts are smaller, homogeneous, and do not exhibit significant chemical variations.

Discussion

Physical Constraints on Magmatism and Pb Isotopic Variations in the Volcanic Rocks

Seamount volcanism is younger than volcanism associated with TLTF island formation. Tubaf seamount probably records the youngest volcanic event in the area (222 +/-34 Ka, one biotite Ar-Ar age determination). Conical seamount yielded slightly older age: 287 (+/-20) Ka (M. Hannington, personal communication). Edison seamount may be older than the other two seamounts, based on field observations (Herzig et al. 1998). Lihir Island is a Pliocene to Holocene volcanic complex built from several coalescent volcanoes (Wallace et al., 1983). Volcanism and hydrothermal activity in the area of the Ladolam deposit have been active during the last 1 Ma with biotite samples yielding K-Ar ages from 900 (+/-100) to 340 (+/-40) Ka in altered intrusions, and 610 (+/-250) to 150 (+/-20) Ka for hydrothermal adularia and alunite samples (Carman 2003 and references therein). The northernmost part of Lihir (Londolovit block) was formed during the oldest volcanic event on the island and shows slightly elevated $^{206}Pb/^{204}Pb$ ratios compared to the younger Luise volcano, which hosts the Ladolam deposit (Table 3-1).

Conical seamount has Pb isotopic ratios similar to, but extending to lower $^{206}Pb/^{204}Pb$ ratios compared to Luise volcano (Fig. 3-3, Table 3-1).

Table 3-2. Microprobe analyses on seamounts' clinopyroxene phenocrysts. Conical seamount data are for the CPx shown on figure 3-6, numbers correspond to the analysis points.

	Conical	Conical	Conical	Conical	Conical	Conical	Tubaf	Tubaf	Edison	Edison
Smpl#	50DR1C.1	50DR1C.2	50DR1C.3	50DR1C.4	50DR1C.5	50DR1C.6	21DR1A	21DR1B	11GTVA2A	11GTVA2B
SiO_2	51.20	48.30	49.91	52.02	48.20	49.90	52.01	51.9	53.32	53-1
TiO_2	0.25	0.53	0.38	0.2	0.44	0.52	0.15	0.19	0.15	0.14
Al_2O_3	3-76	5.74	4.14	3-13	4.06	3.89	1.99	3-1	1.91	3-1
Cr_2O_3	0.25	0.03	0.14	0.36	-	0.04	0.18	0.2	0.29	0.27
FeO	5.16	9.10	8.80	5.51	9.51	9.37	5.44	5.21	4.12	5.8
MnO	0.25	0.32	0.29	0.10	0.26	0.44	0.25	0.25	0.20	0.2
MgO	15.66	13.85	13.88	15.57	14.37	14.31	15.91	15.85	17.59	16.8
CaO	23.31	21.89	23.48	23.92	21.91	23.15	23.11	23.0	23.78	23.9
Na_2O	0.23	0.57	0.32	0.19	0.30	0.38	0.32	0.33	0.25	0.25
K_2O	0.05	-	0.03	0.01	-	-	0.02	0.01	-	0.03
Total	99.12	100.3	100.3	100.0	99.05	101.0	99.3	99.1	100.6	100.5

The two other seamounts, Tubaf and Edison have elevated lead isotopic ratios compared to Conical, but similar to the northernmost Londolovit block (Fig. 3-3, Table 3-1). Overall, there appears to be no correlation between the relative ages and the Pb isotopic compositions of the volcanic rocks. The variations can be either a result of small Pb isotopic variations in the magma sources or a result of magma modification processes during ascent. The presence of a large number of sedimentary, mafic, and ultramafic xenoliths in Tubaf and Edison seamount lavas allows me to address this possibility. The common occurrence of xenoliths in alkaline rocks is attributed to the high ascent velocities of the magmas, on the order of several kilometers per hour (Spera 1984, Morin and Corriveau 1996). Calculated minimum ascent velocity (after Spera 1984) for Tubaf magma required to lift an ultramafic xenolith (3.3 g/cm^3, 15 cm diameter) to the surface is on the order of 2 to 3 km/h. McInnes et al., (2001) argue on the basis of the observed

mineral assemblages that some of the ultramafic xenoliths come from about 60 to 70 km depth. Assuming an ascent velocity of 3 km/h, the Tubaf and Edison magmas must have ascended to the surface in about 20 to 24 h from their mantle source region. Rapid ascent rates calculated for the two seamounts' magmas suggest that existence of a magma chamber and/or upper crustal modification of the magmas close to the surface is highly unlikely. In addition, sharp contacts between the sedimentary and mafic xenoliths and host lavas provide no evidence for melting or resorption of the xenoliths, suggesting that no significant assimilation of sedimentary or basaltic/gabbro material occurred. This suggests that the lead isotopic compositions of the two seamounts are probably inherited from their source region.

The mantle wedge beneath the TLTF island chain has been metasomatically modified by fluids released during earlier subduction of the Pacific plate beneath the Indo-Australian plate (McInnes et al. 2001, Grégoire et al. 2001) and geochemical studies of fresh lavas suggest multiple parental melts (Kennedy et al. 1990a,b). Lead isotopic compositions of volcanic rocks from TLTF islands show relatively uniform $^{206}Pb/^{204}Pb$ ratios, ranging from 18.7 to 18.8 and slightly elevated $^{207}Pb/^{204}Pb$ ratios relative to Pacific MORB (Fig. 3-4) and were interpreted to be a result of a small contribution (ca. 1 to 2%) of subducted sediment to the mantle source region (Stracke and Hagner 1998). The fresh lavas shown on Figure 3-4 fall within the field defined by the sediment and oceanic crust samples, but overall are confined to the Pacific MORB field, which suggests that the Pb budget of the lavas is probably controlled mainly by oceanic crustal lead (Chapter 4).

Phase Chemical Constraints on Petrogenesis

The paucity of xenoliths in the lavas from Lihir Island and Conical seamount and the more fractionated chemistry of the lavas (Chapter 4) are consistent with slower magma ascent and evolution in a magma chamber close to the surface. Müller et al.

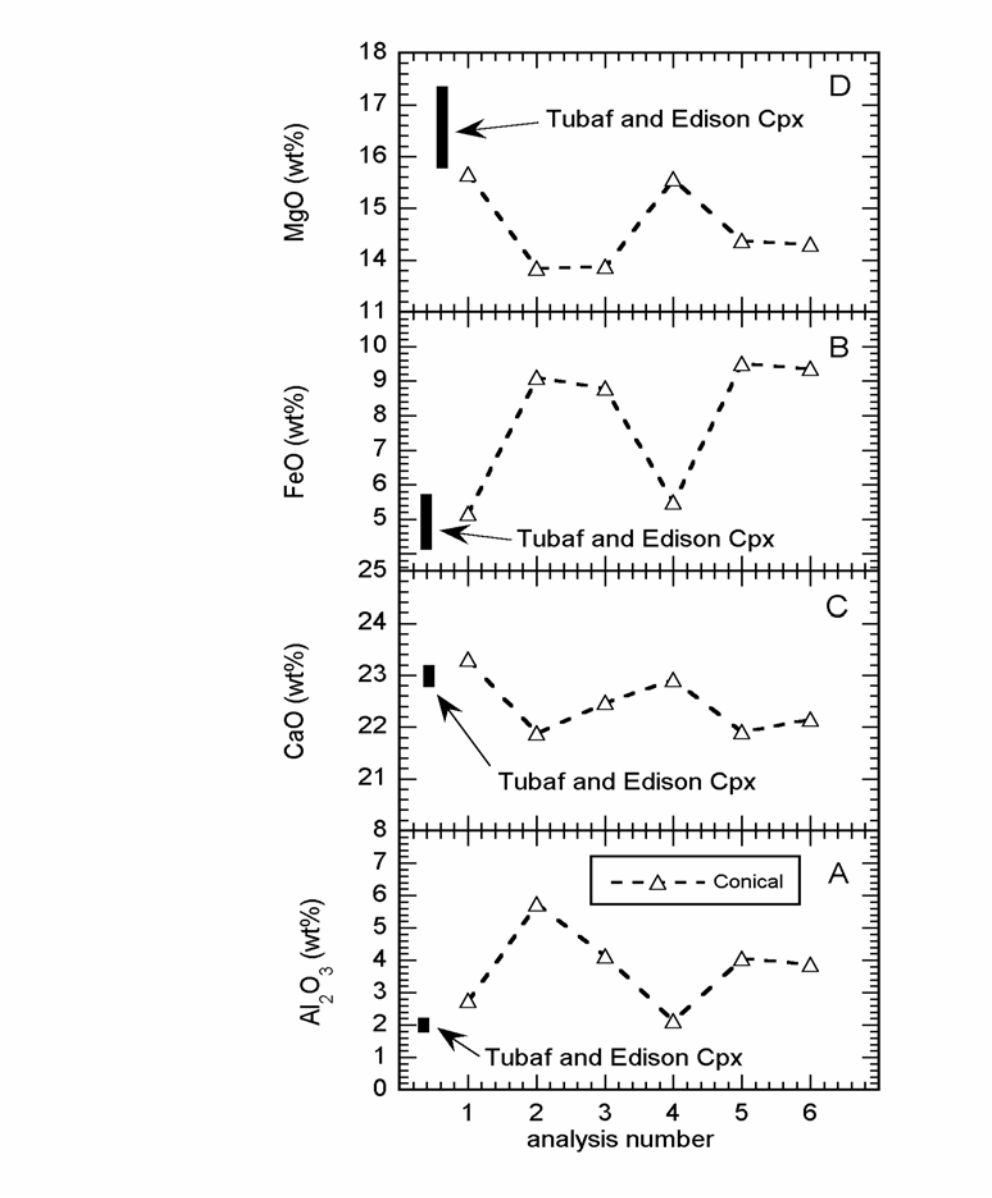

Figure 3-5. Representative compositional changes from core to rim in Conical clinopyroxene shown in Figure 3-6. Bars represent the observed variations in Tubaf and Conical clinopyroxenes.

(2001) conducted an extensive study of Lihir volcanic rocks and minerals exposed in the vicinity of the Ladolam gold deposit and the P-T conditions inferred from mineral analyses suggested that their main evolution stage occurred at a shallow crustal level. Müller et al. (2003) also investigated P-T conditions of crystallization of Conical seamount lavas and calculated crystallization pressures of 10-14 kbar based on Al content in hornblende cores and 0-4.5 kbar (+/-2 kbar) crystallization pressure for clinopyroxenes. This data suggests magma evolution in 2 stages: one deeper, controlled by early hornblende crystallization, and a second stage, shallower (crustal levels) associated with clinopyroxene and plagioclase crystallization (Müller et al., 2003). The presence of plagioclase in Conical lavas also suggests relatively shallower crystallization compared to the Tubaf and Edison magmas. Plagioclase crystallization is suppressed in magmas with high concentration of water (Carmichael et al., 1996), therefore, its presence is consistent with the model that Conical seamount lavas evolved at a shallower level under relatively low water fugacity, probably in a degassing magma chamber close to the surface. Microprobe elemental analyses of Conical clinopyroxenes reveal chemical zoning (Fig. 3-5), whereas Tubaf and Edison clinopyroxenes do not show zoning and their compositions are similar to the central parts of the Conical clinopyroxenes (Table 3-2 and Fig. 3-5). Stracke and Hagner (1998) argue that clinopyroxene was the major fractionating phase during the magmatic evolution of the seamounts and TLTF islands. As a result, Mg and Ca will behave compatibly and decrease in the more evolved lavas. Furthermore, other elements, such as Al and Fe, will not be incorporated preferentially in the clinopyroxenes and their concentrations will increase in the evolving liquid. The observed chemical variations in the interiors of the analyzed clinopyroxenes are

consistent with such an evolutionary trend. The cores of the Conical clinopyroxenes are higher in Mg and Ca and lower in Al, Fe, and Ti, similar to the compositions of Tubaf and Edison clinopyroxenes (Fig. 3-5). The darker colored zones surrounding the lighter zones (Fig. 3-6) show lower Ca and Mg and elevated Al, Fe, and Ti reflecting changes likely occurring in the evolving liquid. Light colored areas toward rims of the crystals, however, have elevated Mg and Ca and lower Fe, Al, and Ti contents and this reverse zoning is consistent with a mafic magma recharge episode in the evolving magma chamber beneath Conical seamount. In addition, careful observation reveals that the darker zones (also along the borders between the lighter and darker zones) contain a number of small inclusions (Fig. 3-6). The inclusions are composed of a glass and fluid phase, and often contain clusters of needle-shaped apatite crystals. The later observation suggests that during the growth of the dark zones the clinopyroxenes were in contact with highly evolved magma. Apatite usually forms toward the end of the crystallizing

Figure 3-6. Photomicrograph of Conical seamount clinopyroxene. Numbers correspond to the analysis numbers presented in Table 3-2 and shown in Figure 3-5.

sequences and is observed in the Conical lavas groundmass (Müller et al. 2003). The presence of a fluid phase in the inclusions along the zones provides evidence for episodes of volatile saturation and magmatic fluid exsolution, processes considered to play important roles in the ore formation.

Pb and Sr Isotopic Variations in the Conical and Lihir Mineralizations

Petersen et al. (2002) observed that the early, high-temperature mineralization stages at Conical seamount are overprinted by a low temperature stage that mainly produced amorphous silica and arsenic sulfides. Sr isotopic compositions of high and low temperature mineralized samples compared with Conical seamount lavas and sediments from the area are shown in Figures 3-2 and 3-7. The high-temperature ore-rich samples with high Cu, Ag, Au, and Pb contents show overall similar $^{87}Sr/^{86}Sr$ to Conical, Lihir, and the other seamount lavas, suggesting that the Sr is mainly derived from the alkaline lavas in the area. One of the high-temperature mineralization samples exhibits elevated $^{87}Sr/^{86}Sr$, which indicates incorporation of more-radiogenic Sr. Two of the analyzed 3 Lihir mineralization samples have Sr isotopic compositions that are slightly elevated compared to the analyzed monzonite sample from Luise volcano (Table 3-1), which is also suggestive of minor incorporation of more-radiogenic Sr. Conical low-temperature mineralized samples with relatively lower Pb, Zn, Cu, and Au contents show either similar or elevated $^{87}Sr/^{86}Sr$ compared to the fresh lavas (Table 3-1, Fig. 3-7). Seawater and/or sediments are the two possible sources for more radiogenic Sr in the area, however, simple mixing can not explain the observed variations (Fig. 3-7, see caption for more discussion). Observations at MOR black smoker systems show only minor increase in Sr concentrations in the emanating fluids compared to the ambient seawater (Teagle et al. 1998). Experiments by Seewald and Seyfried (1990) indicate K_D Sr values

between 0.017 and 0.027 during high-temperature (300 to 500°C) fluid/basalt interactions, which also suggests that Sr will not be strongly enriched in the hydrothermal fluids. Therefore, ore-forming fluids probably will not contain very high Sr content, then, even small amounts of seawater incorporated in the Conical or Ladolam ore-forming hydrothermal fluids will result in elevated $^{87}Sr/^{86}Sr$ in the mineralized zones compared to the host lavas. In addition to seawater, the thick Miocene-Recent sedimentary sequences beneath the seamounts also can be a possible source of more radiogenic Sr. Due to their

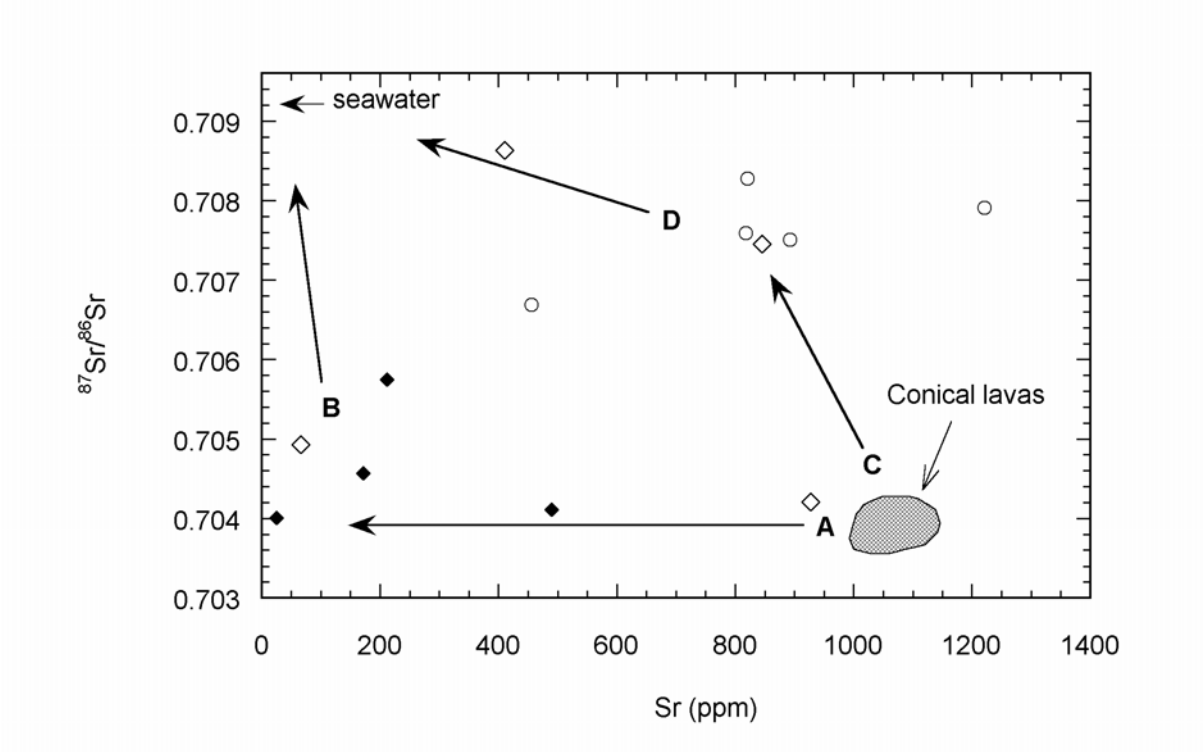

Figure 3-7. 87Sr/86Sr vs Sr concentrations for mineralized samples in comparison with Conical fresh lavas and sediments. Symbols are the same as in figure 2. Arrows show possible mixing trends between the possible end-members in the region: A – exsolution and/or dissolution of Sr from magma/lava without significant seawater or sediment Sr incorporation; B – mixing between magmatic Sr and seawater Sr (note that Sr has low fluid-rock Kd (less than 0.1) and that is why the fluid Sr concentration is expected to be lower that the lavas (for more discussion see the text); C – simple Sr mixing between lava and sediment; D – mixing between lava, sediment, and seawater Sr. Sr data from Table 3-1 and from Stracke and Hagner (1998).

calcareous character, the sediments in the area have $^{87}Sr/^{86}Sr$ values either close to or lower than the present day seawater (Fig. 3-7) and this fact prevents unequivocal distinction based solely on Sr isotopic data whether the more radiogenic end-member in the mineralized zones is seawater or sediment derived Sr.

Seawater contains negligible amounts of Pb compared to the lavas and sediments in the area and, although it may affect the Sr budget, it will not affect the Pb isotopic compositions of the altered and mineralized zones. Overall, the mineralized samples exhibit Pb isotopic compositions similar to the volcanic rocks in the area (Fig. 3-3), suggesting that Pb and possibly other ore metals with similar geochemical behavior were derived from the latter. An complicating issue, however, for the isotopic composition of the lead in the mineralized samples is that their suggested source (i.e., the volcanic rocks in the area) originated from a mantle that has been metasomatically altered by components released from subducted sediments and oceanic crust (Stracke and Hagner 1998, McInnes et al. 2001, Gregoire et al. 2001). These components most probably had Pb isotopic compositions varying between the Pacific sediments (including the sedimentary xenoliths), and the mafic xenoliths (Fig. 3-4), and so make it very difficult to resolve if the isotopic signatures observed in the lavas and mineralizations were acquired in the mantle or in the crust. Althoug the above arguments suggest that the Pb isotopic signature of the lavas is inherited directly from their mantle source, the same arguments can not be applied to the origin of the ore metals in the Conical and Lihir mineralizations. Therefore, two possible scenarios for the origin of the Pb in the mineralized zones must be considered: (1) lead in the mineralized samples can be derived from the host lavas (either hydrothermally leached or exsolved from solidifying magmas at depth), and (2) it

can be hydrothermally scavenged from the thick layer of sediments and underlying oceanic crust.

An Os isotopic study conducted on Au ores from the Ladolam deposit indicates that the primary source of the ore metals is the mantle underlying the TLTF island chain (McInnes et al. 1999), providing evidence that material derived from the Miocene-Recent sediments in the area has not contributed significantly to the metal budget of the ore deposits. Overall, the sediments exhibit much higher $^{207}Pb/^{204}Pb$ and $^{208}Pb/^{204}Pb$ compared to the TLTF lavas (Fig. 3-4), therefore, incorporation of sedimentary Pb in the hydrothermal system will shift the isotopic compositions of the mineralized samples to higher $^{207}Pb/^{204}Pb$ and $^{208}Pb/^{204}Pb$ at relatively constant $^{206}Pb/^{204}Pb$, which is not the case (Fig. 3-3). Pb isotopic compositions of the lavas and mineralized samples do show a minor increase in $^{207}Pb/^{204}Pb$ and $^{208}Pb/^{204}Pb$, however, accompanied with an increase in $^{206}Pb/^{204}Pb$ and form a trend parallel to the NHRL (Fig. 3-3, note that only high-precision MC-ICP-MS data are shown). This trend, and the fact that the mineralized samples fall within the field of the Pacific MORB (Fig. 3-4, note that at the scale of the figure the mineralized samples can not be distinguished from the lavas), suggest mainly oceanic crust (or mantle) control on their Pb isotopic compositions. In addition, the relatively non-radigenic Pb isotopic composition of the Ladolam deposit further argues against scavenging of sedimentary Pb within the hydrothermal system (Fig. 3-3).

Hydrothermal scavenging of Pb from the oceanic crust underlying the thick layer of sediments also must be considered as a possible process for incorporation of ore metals in the mineralizations. The mafic xenoliths recovered from Tubaf lavas are less-radiogenic than the lava and mineralized samples (Table 3-1, Fig. 3-4), but mixing of Pb

from the sediments and the underlying mafic crust within the hydrothermal system may generate Pb isotopic values similar to the observed in the mineralized samples and fresh lavas. However, a Pb isotopic study on Escanaba Trough sulfide deposits indicates that the source for the ore metals is the thick, up to 1 km layer of sediments, without any significant contribution from the underlying Gorda Ridge MORB (German et al. 1995). It is hard to believe, therefore, that the mafic crust that underlies the sediments in the TLTF area, with its low Pb content will have significant impact on the Pb isotopic composition of hydrothermal fluids that must pass through 5 km of sediments and/or volcanic rocks with much higher Pb content (Table 3-1). The most probable sources for the ore metals in the giant Ladolam deposit and the Conical seamount mineralization, therefore, are the magmas in the area.

Intriguingly, mineralized zones bracket the host lavas (Fig. 3-3), with Lihir mineralization plotting at the low-radiogenic end, and Conical mineralization plotting at the high-radiogenic end of the array, suggesting distinct sources for each mineralization. In addition, both mineralizations exhibit less variation in their Pb isotopic compositions than the Conical and Lihir host lavas, suggesting a relatively homogeneous source and/or homogenizing process (Fig. 3-3). The Tubaf and Edison magmas, which rapidly ascended from their source region, also show relatively homogeneous Pb compared to Conical and Lihir lavas, indicating that in some instances single magmatic pulses in the area were composed of relatively homogeneous Pb. The Conical high-temperature mineralized samples have Pb isotopic compositions similar to the nearby Tubaf and Edison seamount lavas (Fig. 3-3), suggesting that a single pulse of magma with similar isotopic composition could be the metal source for the high-temperature mineralization.

Conical low-temperature mineralized samples containing relatively low Pb concentrations and elevated $^{87}Sr/^{86}Sr$, have Pb isotopic compositions scattered between those of the host lavas and the high-temperature, ore-rich samples (Fig. 3-2). This suggests that Pb was remobilized from both the host lavas and from the high-temperature ore zones during the waning stages of the hydrothermal system in order to form the late-stage low-temperature zones.

Mechanism for ore Formation

Sillitoe (1997) suggested that the gold deposits associated with alkaline rocks may be related to formation of highly oxidized magma generated by quenching of a volatile-rich mafic melt during injection into a shallow magma chamber. The resultant volatile phase will be charged with ore-forming metals such as Au, Ag, Cu, Pb, Zn, and Fe. In addition, alkaline rocks usually contain elevated amounts of sulfur and chlorine, important ligands for hydrothermal gold and base metal transport (Candela and Piccoli 1995). Sulfur isotopic ratios in sulfide minerals from mineralized Conical seamount samples are consistent with mineralization from a magmatic fluid (Herzig et al. 1999, Petersen et al. 2002). Chemical compositions of clinopyroxene and petrological observations described above, provide evidence for the presence of a relatively shallow magma chamber beneath Conical seamount and an episode of magma recharge involving a mafic magma similar in composition to Tubaf and Edison lavas. Conical and Lihir lavas are more evolved compared to Tubaf lavas, however, the latter are more volatile-rich (Fig. 3-8). In addition to being highly enriched in chlorine, Tubaf lavas also show about two times higher Pb content than Conical lavas (Table 3-1). The

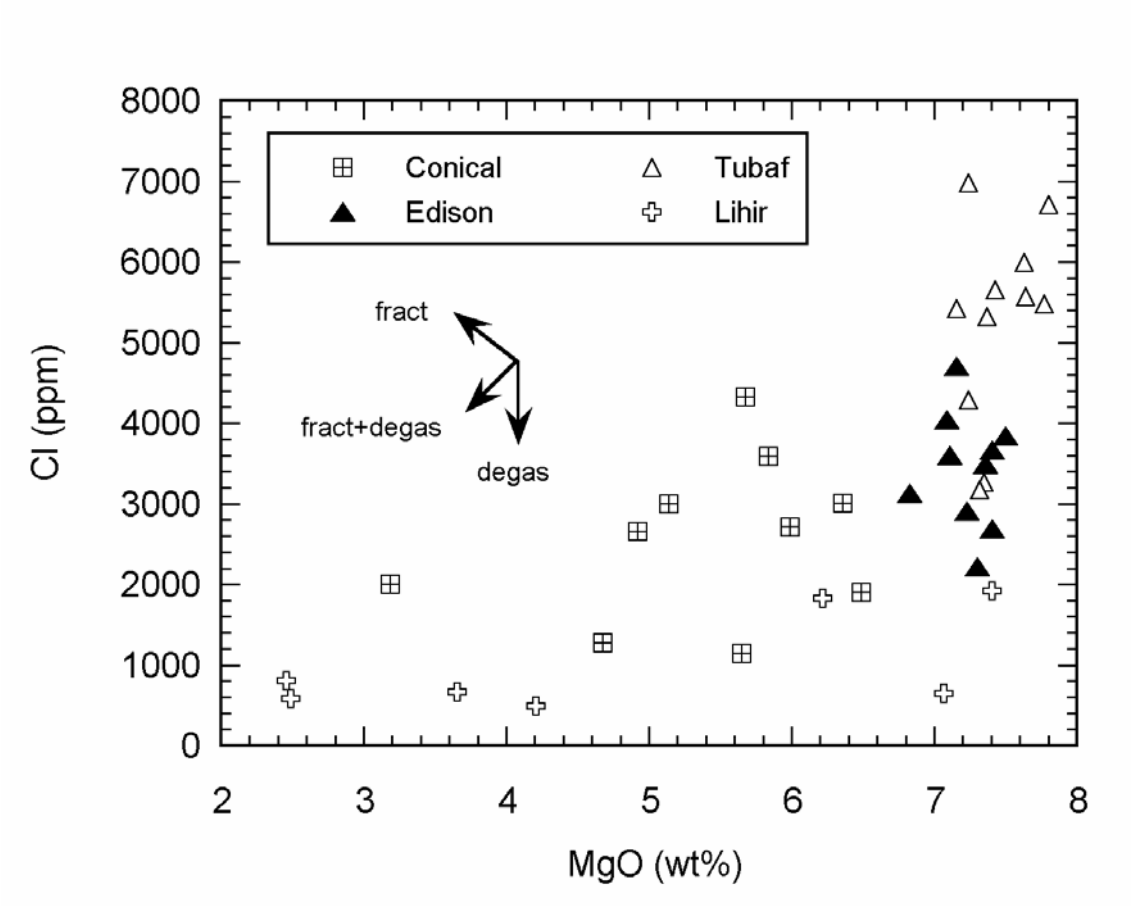

Figure 3-8. MgO vs Cl content of seamounts and Lihir island. Arrows show general direction of changes during magma degassing, fractionation, and fractionation accompanied with degassing. Note the highest Cl content in Tubaf lavas.

presence of chlorine greatly increases the fluid/magma partitioning coefficients of base metals, and fluids with 10^3-10^4 ppm base-metal concentrations can be rapidly generated from magmas with tens of ppm base-metal concentrations (Candela 1989).

Mafic, volatile-rich magmas travel upward through subvertical cracks in brittley fractured rocks as dikes, and in extensional tectonic settings over-pressured magmas may ascend through such self-generated cracks for tens of kilometers, even through less dense rocks (Best and Christensen 2001). Once such rapidly ascending magma encounters magma stored in a shallow magma chamber, then its upward motion will be retarded due

to lack of significant density contrast and because the mechanism of brittle fracturing will not operate in the fluid medium. Quenching of this volatile-rich magma that is recharging the system will cause rapid fluid saturation and metal-bearing solutions will exsolve (note the higher Cl and Pb content in Tubaf compared to the other lavas (Table 3-1, Fig. 3-8) from the magma body at depth (Fig. 3-9). The ore-bearing fluids, therefore, will be primarily derived from the mafic magmas (similar to Tubaf) recharging the system, not from the lavas that host the mineralization close to the surface (Fig. 3-9).

A similar ore-forming mechanism can be proposed for the Ladoloam gold deposit. Sulfur isotopic data, similar to the sulfur data for the Conical seamount hydrothermal system, indicate mineralization from a magmatic fluid (Carman 2003). Similar to the observed relationships between Conical ores and lavas, a small offset between the Pb isotopic compositions of the Ladolam ores and surficial Lihir lavas is apparent (Fig. 3-3), suggesting that the ore metals were also probably not hydrothermally leached from the host lavas, but possibly exsolved from a recharging volatile-rich magma at depth (Fig. 3-9).

Conclusions

High precision lead isotopic measurements conducted with MC-ICP-MS on ores, lavas, and sedimentary and mafic xenoliths in the area of Lihir Island provide a clear picture of the sources of metals in the Ladolam gold deposit and in mineralized zones on Conical seamount. Although Sr isotopic data suggest some involvement of seawater, particularly during the waning stages of the hydrothermal system, Pb isotopes suggest that neither seawater nor the sediments in the area have significantly contributed to the metal budget of the ore mineralizations discovered on the island and the seamount. The ore Pb in the hydrothermal systems and presumably other ore metals with similar

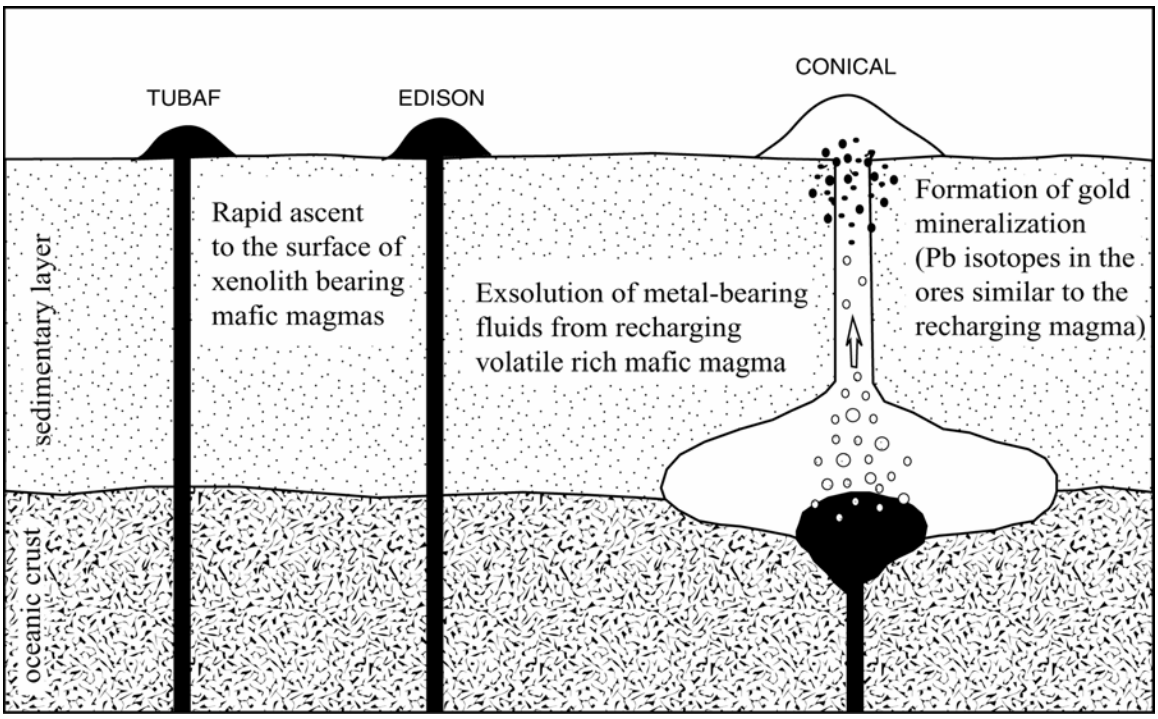

Figure 3-9. Cartoon depicting the inferred ore formation mechanism. Evidences suggest that a magma chamber under Conical seamount was recharged by a mafic magma and the exsolved fluids formed the ore deposit. Pb isotopes in the ore mineralization will inherit their signature from the recharging magma. Note that the Tubaf magmas have the highest Pb content (Table 3-1). Barren seamounts' magmas (Tubaf and Edison) ascended rapidly to the surface from their mantle source region and no ore mineralization was formed. However, during their ascent a number of xenoliths were trapped, thus providing representative samples from the possible lithosphere sources beneath the TLTF volcanoes.

geochemical behavior were derived from alkaline magmas in the area. The extent of mineralization during a magmatic event can be related to the volcano-magmatic evolution of the volcanic complex. I propose that the magmas forming the two barren Tubaf and Edison seamounts ascended rapidly to the surface and preserved their volatile content close to the moment of eruption and thus precluded significant exsolution of metal-bearing fluids and consequent potential for ore formation. On the other hand, Conical seamount, composed of similar lavas to Tubaf and Edison, shows evidences for magmatic

evolution at shallower levels, and thus enhanced ore-forming potential. The triggering ore-mineralization event, however, appears to be related to a mafic, volatile-rich magma recharging event in the evolving magma chamber beneath the seamount. The latter hypothesis is supported by petrologic observations indicative of a complex magmatic history including magma recharge and fluid saturation and exsolution at Conical seamount. In addition, small but distinguishable differences between the Pb isotopic compositions of ores and host lavas were observed, suggesting that the ore metals were not hydrothermally leached out from the host lavas but most probably exsolved from quenched mafic magmas injected into magma chambers existing beneath the Conical seamount and Luise volcano.

CHAPTER 4
DECIPHERING MANTLE AND CRUSTAL CONTROLS IN AN ISLAND ARC ENVIRONMENT: A SR, ND, AND PB ISOTOPIC STUDY OF SW PACIFIC ISLAND ARCS AND SUB-ARC XENOLITHS.

Introduction

In the classical model for magma generation in continental and island arc settings it is believed that magmatism results from lowering the melting point of the mantle wedge peridotite as a result of fluid and/or melt introduction from the subducted slab (Poli and Schmidt 2002, Stern 2002). It can be considered, then, that complex interaction between components derived from the subducted slab, the crust underlying the island arc, and the subarc mantle wedge play major role in arc petrogenesis. Samples from these sources in the form of mantle and crustal xenoliths brought to the surface by arc lavas, therefore, can provide important constrains on the composition and evolution of the mantle wedge and the contribution of the crust to the chemistry of arc lavas. Such samples, however, are rare and limited to only a few localities: Japan, Cascades, Philippines, Mariana, and Kamchatka arcs (McInnes et al. 2001).

The Tabar-Lihir-Tanga-Feni (TLTF) arc, Papua New Guinea provides an outstanding opportunity to look in detail at the components directly involved in the petrogenesis of the island arc because numerous sedimentary, mafic, and ultramafic xenoliths were recovered from TUBAF seamount, located on the flank of Lihir island (Chapter 3). Detailed studies on the mineralogy and trace element geochemistry of the xenoliths indicated that the mantle wedge and crust underlying the TLTF island chain resembles oceanic lithosphere possibly formed at mid-ocean ridge (MOR) settings (Franz

and Wirth 2000, McInnes et al. 2001, Gregoire et al. 2001, Franz et al. 2002). Many of the ultramafic xenoliths exhibit evidence for metasomatic alteration by hydrous fluids, possibly released during the subduction of the Pacific plate underneath the Indo-Australian plate (McInnes et al. 2001, Gregoire et al. 2001, Franz et al. 2002).

TLTF lavas are characterized mainly by silica undersaturated, alkaline rocks and two mechanisms can be invoked to explain their origin: 1) the lavas can be a product of high pressure, small degree melting of a MORB-like mantle source, or 2) the lavas can be derived from partial melting of a metasomatized mantle wedge. Elemental and isotopic data from the xenoliths and the lavas from the region will allow us to determine whether the ultramafic xenoliths are the source or a component for the alkaline magmas. In addition, the mantle xenoliths will provide information for the isotopic composition of the mantle in the region, which will be used to constrain the origin of the isotopic signatures in New Britain and Solomon island arcs and the Manus and Woodlark back-arc basins.

Geological Settings

The oceanic region to the north and east of northeastern Australia includes the island arcs of New Britain, New Ireland, and the Solomon Islands and numerous small basins and seas (Fig. 4-1). The Tabar, Lihir, Tanga, and Feni (TLTF) island chain is located in the former fore-arc region of New Ireland, extending for about 250 km parallel to the presently inactive Manus-Kilinailau trench. Some studies suggest that the Solomons, New Britain, and New Ireland arcs rifted away from the eastern Australian margin around 40 Ma ago, in contrast to other interpretations that indicate that the arcs originated as intra-oceanic arcs within the Pacific plate (Hall 2001 and references therein). The formation of the arcs led to the formation of the Solomon Sea, and recovered

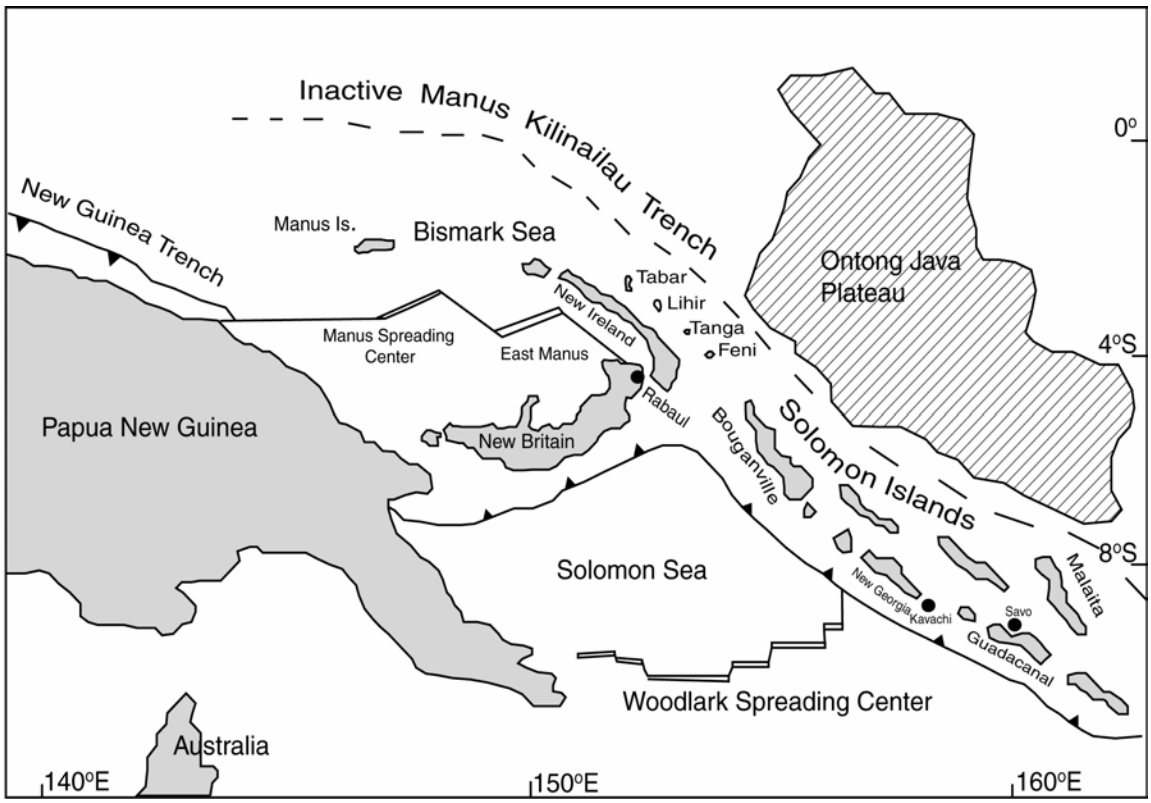

Figure 4-1. Regional map of the study area, modified after Hall (2001). See chapter 3 for more detailed map of the TLTF area.

seafloor basalts show geochemical similarity to evolved MORB from the East Pacific Rise (Davies and Price 1987). Solomon Islands, New Britain, and New Ireland volcanism began during the Eocene as a result of south-westerly subduction of the Pacific plate under the Indo-Australian plate along the Manus-Kilinailau trench (Johnson 1979). During the Oligocene New Ireland and New Britain islands formed continuous arc with the Solomon Islands (Hall 2001). Subduction ceased about 20-10 Ma ago, when the thick and relatively buoyant Ontong Java oceanic plateau collided with the subduction zone (Coleman and Kroenke 1981, Petterson et al. 1997). After the collision, regional relocation of stress caused reversal of the subduction direction and caused Solomon plate subduction beneath New Britain to the north, and beneath Solomon Islands to the east, along the newly formed New Britain-San Cristobal trench (Petterson

et al. 1997). New Britain began to migrate southwestward and as a result, Manus back-arc basin opened at about 3.5 Ma (Taylor 1979). The floor of Manus basin is composed of diverse magmatic rocks, ranging from normal MORB to BAB and lavas with arc-type compositions (Sinton et al. 2002). Woodlark Basin spreading began about 5 to 6 Ma ago and at present, typical MORB erupt at the spreading center, although some of the lavas exhibit back-arc characteristics (Perfit et al. 1987, Trull et al. 1990).

The main part of the New Britain arc is composed of Eocene-Oligocene calc-alkaline rocks, generated during the previous subduction of the Pacific plate along the currently inactive Manus-Kilinailau trench (Woodhead and Johnson 1993). The arc migrated southward after the opening of the Manus back-arc basin as the subduction began along the New Britain trench. A number of Quaternary volcanic centers exposed along the north rim of the New Britain are related to the present Solomon Sea plate subduction and Woodhead et al. (1998) divided the volcanic centers into zones with specific chemical characteristics related to the depth of the subducted slabs. The zones closer to the trench show a Solomon plate slab contribution dominated by altered oceanic crust, and the zones further away from the trench exhibit decreasing slab influence and an increase in the Manus basin mantle component (Woodhead and Johnson 1993, Woodhead et al. 1998).

The TLTF island groups, located about 30 to 70 km off-shore New Ireland, are equally spaced at about 75 km apart. Volcanism in the TLTF area began on Simberi island (part of Tabar island group) about 3.7 Ma ago (Johnson et al., 1976), coeval with the initiation of back-arc spreading in the Manus Basin, and migrated southward to Feni island (2300 y), as the island of New Britain was transported to the southeast. Taylor (1979) suggests

that the local extension and volcanism are related to the opening of the Manus back-arc spreading center. Pliocene-Pleistocene TLTF islands are characterized mainly by silica undersaturated, alkaline rocks, ranging from basanites to trachyandesites with rare occurrences of more evolved tephriphonolites and phonolites (Johnson et al. 1976; Wallace et al. 1983; Kennedy et al. 1990a,b; McInnes and Cameron 1994; Stracke and Hegner 1998). More detailed description of the TLTF geological settings is available in Chapter 3.

Samples and Analytical Methods

Fresh volcanic rocks used in this study were recovered from the seamounts during the "SONNE-133" cruise in 1998. Conical seamount trachybasalts are composed of about 20 to 25% clinopyroxene, 5% plagioclase, and rare olivine and phlogopite phenocrysts embedded in a slightly vesicular, fine-grained groundmass which consists of glass, plagioclase, clinopyroxene, spinel, and apatite microcrysts (Müller et al. 2003). The clinopyroxene phenocrysts are large (up to about 6 mm), euhedral to subhedral, and exhibit distinct zoning. Plagioclase phenocrysts are much smaller, up to about 1mm long. Tubaf and Edison seamounts' lavas are also trachybasalts and contain phenocrysts of clinopyroxene, as well as phlogopite and amphibole embedded in a groundmass containing about 20% vesicles and glass (McInnes et al. 2001). Clinopyroxene crystals in these samples are smaller (up to 1 mm) and more homogeneous than those in Conical lavas.

Sedimentary (limestones and carbonaceous mudstones), mafic (gabbroic and basaltic), and ultramafic (lherzolite, harzburgite) xenoliths were recovered from Tubaf seamount lavas and have been described in detail in several recent publications (Franz and Wirth 2000, McInnes et al. 2001, Gregoire et al. 2001, Franz et al. 2002).

Sedimentary xenoliths are mainly composed of coralline and coralgal limestones, interbeded with layered carbonaceous and volcanoclastic sediments, similar to uplifted sedimentary sequences exposed on New Ireland, and some pelagic deep-sea sediments (McInnes et al. 2001).

The mafic xenoliths are composed mainly of gabbros and few fine-grained basalts. Representative gabbro samples 543E and 563I contained uralitized pyroxene and altered plagioclase common low-temperature alteration products that probably formed as the oceanic lithosphere was transported away from the ridge axis (McInnes et al. 2001). Sample 553E shows little to no alteration of the plagioclase and pristine pyroxene, suggesting that the oceanic crust beneath the arc is not entirely altered.

The ultramafic xenoliths are course-grained spinel lherzolites composed mainly of olivine and lesser amount of orthopyroxene (Opx) crystals, with minor clinopyroxene (Cpx) and spinel. In some cases deformed exsolution lamellae in pyroxenes and kink-banded olivines are present, suggesting a period of ductile deformation (McInnes et al. 2001). Peridotite samples 542D, 562B, 562P, 542S, and 542K contain numerous vein and veinlets composed mainly of fibrous Opx, some amphibole, phlogopite, spinel, and Fe-Ni sulfides. These vein components are secondary in origin and were formed as a result of a release of metasomatic agents from the subducted Pacific oceanic crust underneath the TLTF chain (McInnes et al. 2001, Gregoire et al. 2001, Franz et al. 2002). Samples 562F, 542G, and 552H are spinel harzburgites that do not contain vein assemblages, although 542G and 552H show some areas of irregular metasomatic alteration. Clinopyroxene separates 611B Cpx, 611C Cpx, and 671 Cpx are from ultramafic xenoliths collected from Tubaf seamount during the 1994 SONNE cruise (B. McInnes,

pers. comm.). The clinopyroxens were separated from lherzolites, discussed in detail by McInnes et al. (2001) and Gregoire et al. (2001).

For this study, xenolith samples were separated from the host lavas using a microdrill being particularly careful to avoid any contamination by the host lavas (R. Chopra, pers. comm.). Before isotope analyses fresh lava, mafic and ultramafic xenolith samples were leached for several hours in warm 2N HCl. Then, the residues were rinsed several times with 4xH_2O and were dissolved in sealed Teflon vials for several days at 100˚C in a HF-HNO_3 mixture (see also Chapter 3). Major and trace element concentrations Table 1) were determined by ICP-AES and ICP-MS at the Geological Survey of Canada (http://www.nrcan.gc.ca/gsc/mrd/labs/chem-e.html).

Radiogenic isotopic analyses were performed at the Department of Geological Sciences at the University of Florida. Sr, Pb, and Nd were separated using standard chromatographic methods used in our lab (Heatherington and Mueller 1999). Procedural blanks determined several times during sample preparation were maximum 70 ppt for Sr, 80 ppt for Pb, and 30 ppt for Nd. Sr isotope measurements were collected using a Micromass Sector 54 Thermal Ionization Mass Spectrometer equipped with seven Faraday collectors and one Daly collector. Sr samples were loaded on oxidized W single filaments and run in dynamic collection mode. Data were acquired at a beam intensity of 1.5V for ^{88}Sr, with corrections for instrumental discrimination made assuming $^{86}Sr/^{88}Sr=0.1194$. Errors in measured $^{87}Sr/^{86}Sr$ are better than +/- 0.00002 (2σ) based on long-term reproducibility of NBS 987 ($^{87}Sr/^{86}Sr=0.71024$). Nd isotopic analyses were performed on a Nu Plasma multiple-collector magnetic-sector inductively coupled mass spectrometer (MC-ICP-MS). Samples and standard solutions were aspirated into the

plasma source either via a Micromist nebulizer with GE spray chamber (wet plasma) or through DSN-100 desolvating nebuliser (dry plasma). The instrument settings were carefully tuned to maximize the signal intensities on a daily basis. Preamplifier gain calibration was performed before each analytical session. Nd isotope measurements were conducted for 60 ratios in static mode simultaneously acquiring ^{142}Nd on low-2, ^{143}Nd on low-1, ^{144}Nd on Axial, ^{145}Nd on high-1, ^{146}Nd on high-2, ^{147}Sm on high-3, ^{148}Nd on high-4, and ^{150}Nd on high-5 Faraday detectors. The measured ^{144}Nd, ^{148}Nd, and ^{150}Nd beams were corrected for isobaric interference from Sm using ^{147}Sm/^{144}Sm = 4.88, ^{147}Sm/^{148}Sm = 1.33, and ^{147}Sm/^{150}Sm = 2.03. All measured ratios were normalized to ^{146}Nd/^{144}Nd = 0.7219 using an exponential law for mass-bias correction. The mean value of ^{143}Nd/^{144}Nd for our Ames Nd in-house standard based on 23 repeat analyses during the samples analyses was 0.512140 (2σ = 0.000012). Three repeated analyses of the JNdi-1 and LaJolla Nd standards during the same time interval produced mean values of 0.512106 (2σ = 0.000013) and 0.511856 (2σ = 0.000013), respectively. Three separate dissolutions of USGS SRM BCR-1 were prepared and analyzed for Nd isotopes together with the samples in order to further evaluate the analytical protocol. The mean value of ^{143}Nd/^{144}Nd for the analyses of BCR-1 was 0.512645 (2σ = 0.000011), which is indistinguishable from the published TIMS value of 0.51264 (Gladney et al. 1990).

Pb isotopic analyses were conducted on a Nu Plasma multi collector ICP-MS using the Tl normalization technique on fresh mixtures to prevent oxidation of thallium to Tl^{3+} (for more details see chapter 2 and 3). Analyses of NBS 981 conducted in wet plasma mode during the period of time the samples were analyzed gave the following results (n=42): ^{206}Pb/^{204}Pb=16.937 (+/-0.004 2σ), ^{207}Pb/^{204}Pb=15.490 (+/-0.003 2σ), and

$^{208}Pb/^{204}Pb$=36.695 (+/-0.009 2σ). Due to their low Pb content the ultramafic xenoliths were analyzed in dry plasma mode and the reported data are relative to the following NBS 981 values (n=29): $^{206}Pb/^{204}Pb$=16.937 (+/-0.001, 2σ), $^{207}Pb/^{204}Pb$=15.491 (+/-0.001, 2σ), and $^{208}Pb/^{204}Pb$=36.694 (+/-0.004, 2σ)

Results

Major and trace element concentrations of lava, xenolith, and sediment samples from the study area are shown in Table 4-1. Lihir and the nearby seamount lavas vary from subalkaline basalts to trachyandesites, with the majority of the samples plotting in the field of trachybasalts on an alkali-silica diagram (Fig. 4-2), similar to the lavas found on the other TLTF islands (Wallace et al. 1983; Kennedy et al. 1990a,b; McInnes and Cameron 1994; Stracke and Hegner 1998). Tubaf and Edison lavas are characteristically more primitive, whereas Lihir lavas vary from subalkaline basalts to trachyandesites and include a few phono-tephrites. The seamount lavas have more restricted MgO content, ranging between about 8 and 4 wt % in comparison to Lihir lavas, which have quite variable MgO content, ranging from as high as about 8 wt% to as low as about 1 wt% (Table 4-1, Fig. 4-3). Both, the seamounts and the island exhibit decreasing CaO and Fe_2O_3 and increasing SiO_2, Al_2O_3, Na_2O and K_2O with the decrease in the MgO (Fig. 4-3). TiO_2 data, on the other hand, exhibit large scatter and do not show clear correlation with MgO variation. Compatible trace elements, such as V, Ni, and Cr have relatively moderate concentrations and show an overall decrease with decreasing MgO concentration (Fig. 4-4). Incompatible trace elements, such as Ba, Rb, Cs, Nb, and La show increase with decreasing MgO (Fig. 4-4), although most of the elements exhibit large scatter when plotted on correlation diagrams.

Table 4-1. Major and trace element data for lavas and xenoliths

Location:	Conical	Conical	Conical	Conical	Conical	Conical	Conical
Sample:	7DR	12DR 2A	13DR 4	36GTVA 1	42GTVA-1	42GTVA-3	50DR 1C
Type:	lava	Lava	lava	lava	lava	lava	lava
SiO_2	47.2	48.5	47.6	50.2	51.6	48.7	49
TiO_2	0.69	0.75	0.72	0.77	0.84	0.77	0.74
Al_2O_3	19.3	15.4	18.4	16.5	16.6	16.1	15.4
Fe_2O_3T	9.6	10.1	9.8	10.2	8.45	10.3	10.5
MnO	0.18	0.19	0.2	0.19	0.14	1.08	0.19
MgO	5.99	6.36	5.84	5.68	4.2	3.83	6.49
CaO	10.6	11.4	10.3	11	10.3	9.5	11.7
Na_2O	2.35	2.66	2.94	3.03	3.67	3.41	2.64
K_2O	2.89	2.71	3.02	2.94	2.45	2.81	2.84
P_2O_5	0.31	0.32	0.42	0.36	0.52	0.52	0.36
Total	99.3	98.6	99.5	101.1	99.2	97.4	100.1
LOI	1.3	1.2	1.1	1.3	3.3	3.6	0.9
Ba	202	221	234	245	294	279	210
Be	1	0.9	1.2	1.1	0.9	1.3	1.1
Co	28	30	27	30	27	73	31
Cr	141	124	97	90	98	89	157
Cs	0.77	0.77	0.84	0.85	1.2	0.89	0.82
Cu	84	117	116	107	148	246	102
Hf	1.6	1.7	2.4	1.7	1.5	1.5	1.6
Nb	1.3	1.4	1.6	1.6	1.8	1.8	1.3
Ni	29	30	30	25	22	35	31
Pb	4	4	6	5	10	10	4
Rb	57	56	57	63	32	56	63
Sc	38	40	33	36	30	27	40
Sr	869	936	1195	1011	1180	1100	915
Ta	0.08	0.09	0.1	0.11	0.09	0.09	0.08
Th	0.82	0.75	1.2	0.91	1	0.97	0.84
U	0.52	0.51	0.85	0.64	1.7	1.5	0.58
V	279	302	297	307	247	239	290
Zn	77	82	85	86	75	111	82
Zr	54	57	92	63	55	55	60
Ce	19	20	34	23	23	21	20
Dy	2.8	2.9	3.8	3.2	3	2.9	3.1
Er	1.5	1.5	1.7	1.6	1.6	1.5	1.6
Eu	1.2	1.2	1.6	1.2	1.3	1.2	1.2
Gd	3.6	3.7	4.7	3.8	3.8	3.5	3.9
Ho	0.57	0.58	0.67	0.63	0.6	0.56	0.62
La	8.7	8.6	14	9.8	11	10	8.9
Lu	0.25	0.24	0.29	0.26	0.26	0.25	0.25
Nd	13	14	20	15	14	14	14
Pr	2.8	2.9	4.3	3.2	3.2	3.1	2.9
Sm	3.5	3.6	4.9	3.9	3.7	3.4	3.7
Tb	0.5	0.54	0.66	0.56	0.52	0.49	0.54
Tm	0.22	0.23	0.26	0.25	0.24	0.22	0.23
Y	17	17	20	18	17	17	17
Yb	1.5	1.6	1.8	1.7	1.6	1.6	1.6

Table 4-1. Continued

Location:	Conical	Edison 10GTVA	Edison 10GTVA	Edison 10GTVA	Edison 11GTVA	Edison 11GTVA	Edison 33GTVA
Sample:	52GTVA 1	5A2	6B1	6B2	2A1	2A2	2J2
Type:	lava	lava	lava	lava	lava	lava	lava
SiO_2	48.4	45.7	46.7	47	47.1	47.1	46.5
TiO_2	0.77	0.79	0.78	0.78	0.8	0.82	0.79
Al_2O_3	16.4	14.2	16.9	14	14	14	15
Fe_2O_3T	8.98	11.2	11	11.3	11.3	11.3	11.3
MnO	0.16	0.19	0.19	0.19	0.18	0.19	0.19
MgO	5.14	7.5	7.41	7.09	6.83	7.36	7.3
CaO	11.3	11.9	11.5	11.7	12	12.1	12
Na_2O	2.37	2.22	2.28	2.3	2.13	2.25	2.46
K_2O	2.88	2.31	3.38	2.01	2.17	1.98	2.39
P_2O_5	0.31	0.44	0.44	0.44	0.43	0.43	0.47
Total	96.9	96.7	100.8	97	97.2	97.8	98.6
LOI	3.1	2.2	1.5	2.2	2.6	2.5	1.1
Ba	230	242	250	280	246	252	245
Be	1	0.9	1.1	1	0.9	0.9	1.1
Co	24	35	34	34	32	33	34
Cr	89	98	99	115	110	127	107
Cs	0.64	0.61	0.68	0.65	0.62	0.64	0.74
Cu	108	118	139	127	107	111	141
Hf	1.7	1.9	1.7	1.9	1.9	1.8	1.9
Nb	1.5	1.4	1.5	1.4	1.5	1.4	1.5
Ni	21	57	52	56	46	51	53
Pb	5	5	5	6	4	5	5
Rb	41	26	42	30	28	28	43
Sc	38	43	41	43	45	44	41
Sr	1073	1160	1116	1161	1179	1172	1173
Ta	0.09	0.09	0.09	0.12	0.1	0.1	0.09
Th	0.82	1	1	1.1	1.1	1.1	1
U	0.58	0.82	0.72	0.71	0.78	0.66	0.79
V	317	317	311	317	321	319	316
Zn	80	86	85	85	85	85	87
Zr	56	63	59	65	64	62	65
Ce	20	26	26	26	26	25	27
Dy	3.2	3.4	3.4	3.4	3.6	3.5	3.6
Er	1.6	1.7	1.7	1.8	1.7	1.8	1.8
Eu	1.2	1.5	1.4	1.5	1.4	1.5	1.5
Gd	3.7	4.6	4.7	4.7	4.7	4.7	4.7
Ho	0.63	0.67	0.68	0.67	0.69	0.67	0.69
La	9.3	11	11	11	11	11	12
Lu	0.26	0.26	0.27	0.27	0.28	0.27	0.29
Nd	14	18	18	18	18	17	18
Pr	3	3.7	3.8	3.8	3.8	3.7	3.9
Sm	3.8	4.7	4.5	4.7	4.6	4.6	4.9
Tb	0.58	0.66	0.64	0.65	0.66	0.66	0.67
Tm	0.24	0.25	0.26	0.26	0.26	0.27	0.27
Y	17	19	20	19	20	19	20
Yb	1.7	1.7	1.7	1.7	1.8	1.7	1.8

Table 4-1. Continued

Location:	Edison	Edison	Tubaf	Tubaf	Tubaf	Tubaf	Tubaf
Sample:	34GTVA 3.1	34GTVA 3.2	54GTVA 2R1	54GTVA 2R2	54GTVA 4.1	54GTVA 4.2	55GTVA 5F1
Type:	lava	lava	lava	lava	lava	lava	lava
SiO_2	45.9	45.6	47.1	47.8	47.1	46.4	47.1
TiO_2	0.78	0.78	0.75	0.8	0.76	0.75	0.76
Al_2O_3	14.1	14.6	16.2	16.2	16.9	17.7	16.3
Fe_2O_3T	11	10.8	10.1	10.6	10.1	10.2	10.4
MnO	0.19	0.18	0.21	0.2	0.21	0.2	0.2
MgO	7.16	7.11	7.24	7.64	7.24	7.16	7.8
CaO	11.7	12.2	9.22	9.19	9.07	9.04	9.01
Na_2O	2.29	2.38	3.31	3.34	3.3	3.19	3.3
K_2O	2.35	2.06	2	2.16	2.18	2.1	2.05
P_2O_5	0.44	0.48	0.54	0.34	0.46	0.43	0.47
Total	96.1	96.4	97	98.6	97.6	97.5	97.7
LOI	2.9	3.1	2.2	2	1.6	1.8	2
Ba	245	239	233	238	245	230	240
Be	1	0.9	1.9	1.9	1.9	2	1.9
Co	32	31	31	32	30	32	31
Cr	125	107	140	154	159	180	145
Cs	0.67	0.66	0.53	0.51	0.56	0.55	0.37
Cu	126	124	69	66	82	86	89
Hf	1.8	1.9	2.9	3	2.8	3	2.9
Nb	1.5	1.5	2.8	2.9	2.8	2.8	2.8
Ni	48	45	87	99	89	105	84
Pb	5	5	11	10	10	10	10
Rb	30	28	20	21	23	22	23
Sc	42	43	29	30	29	30	29
Sr	1161	1169	1920	1942	1901	1927	1961
Ta	0.09	0.08	0.16	0.15	0.16	0.16	0.16
Th	1.1	1.1	2.1	1.9	2.1	2.1	2
U	0.75	0.69	1.4	1.4	1.4	1.5	1.3
V	307	299	297	307	297	302	294
Zn	83	80	89	90	89	91	87
Zr	63	65	103	101	100	100	100
Ce	26	27	42	39	39	42	39
Dy	3.5	3.5	4.4	4.2	4.2	4.3	4.1
Er	1.7	1.7	2.3	2.1	2.1	2.1	2.1
Eu	1.5	1.5	1.9	1.9	1.9	1.9	1.9
Gd	4.8	4.6	6.1	5.5	5.8	5.7	5.8
Ho	0.69	0.68	0.86	0.83	0.82	0.81	0.83
La	11	11	20	18	19	19	18
Lu	0.28	0.28	0.35	0.34	0.36	0.37	0.34
Nd	18	18	26	24	25	25	25
Pr	3.8	3.9	5.7	5.2	5.5	5.8	5.6
Sm	4.7	4.7	6.3	5.8	6.1	6.3	6.3
Tb	0.67	0.63	0.83	0.79	0.79	0.81	0.82
Tm	0.26	0.25	0.32	0.33	0.33	0.32	0.3
Y	19	19	24	24	23	24	23
Yb	1.8	1.7	2.3	2.2	2.1	2.2	2.2

Table 4-1. Continued

Location:	Tubaf	Tubaf	Tubaf	Tubaf	Tubaf	Tubaf	Tubaf
Sample:	55GTVA 5F2	56GTVA 2C	56GTVA 3F1	56GTVA 3F2	54GTVA2D	54GTVA2G	54GTVA2J
Type:	lava	lava	lava	lava	lherzolite	harzburgite	lherzolite
SiO_2	47.9	49.5	47.7	47	41.40	37.30	38.60
TiO_2	0.78	0.76	0.79	0.74	0.03	bdl	0.02
Al_2O_3	16.4	16.3	16	16	0.90	2.30	1.70
Fe_2O_3T	10.5	10.4	10.5	10.1	11.80	9.50	11.10
MnO	0.2	0.21	0.2	0.19	0.17	0.13	0.16
MgO	7.37	7.77	7.35	7.63	39.00	48.70	47.20
CaO	9.42	9.2	9.23	9.13	5.20	0.38	2.10
Na_2O	3.37	3.5	3.42	3.33	0.10	bdl	0.04
K_2O	2.13	2.6	2.04	2.08	0.05	bdl	bdl
P_2O_5	0.49	0.45	0.43	0.43	bdl	bdl	bdl
Total	98.9	101	98	97	98.1	98.2	100.8
LOI	1.7	1.5	1.8	2.3	0.0	bdl	bdl
Ba	240	247	229	232	399	bdl	bdl
Be	2	2	2	2	bdl	bdl	bdl
Co	31	31	30	32	131	145	170
Cr	135	166	147	175	3890	4400	7410
Cs	0.49	0.68	0.66	0.63	0.04	bdl	bdl
Cu	92	79	125	142	20	11	16
Hf	3.2	3.2	3.2	3.2	0.17	0.55	0.18
Nb	2.9	2.8	2.8	2.9	0.08	0.10	0.10
Ni	85	109	92	103	2050	2940	2120
Pb	11	10	10	11	19	2	3
Rb	20	29	24	22	0.52	0.13	0.21
Sc	29	29	30	30	18.0	4.4	12.0
Sr	1962	1963	1874	1959	bdl	bdl	10
Ta	0.18	0.15	0.18	0.18	bdl	0.03	0.04
Th	2.2	2.2	2.2	2.3	0.02	0.03	0.03
U	1.5	1.5	1.5	1.6	0.03	0.02	0.04
V	300	297	301	298	69	39	58
Zn	89	93	92	93	68	51	57
Zr	107	103	103	102	6.8	22.0	6.6
Ce	43	43	42	43	0.4	1.7	0.4
Dy	4.5	4.4	4.4	4.5	0.15	0.15	0.07
Er	2.2	2.3	2.3	2.2	0.09	0.03	0.05
Eu	2	2	2	2	0.03	bdl	0.02
Gd	6.2	6	6	6.1	0.10	bdl	0.07
Ho	0.86	0.85	0.87	0.84	0.03	bdl	bdl
La	20	20	20	20	bdl	bdl	0.2
Lu	0.37	0.35	0.38	0.36	bdl	bdl	bdl
Nd	26	25	26	26	0.2	bdl	0.2
Pr	5.9	5.8	5.8	6	0.03	0.02	0.06
Sm	6.4	6.2	6.2	6.3	0.06	0.02	0.06
Tb	0.84	0.83	0.83	0.82	bdl	bdl	bdl
Tm	0.34	0.32	0.33	0.34	bdl	bdl	bdl
Y	24	24	26	25	0.83	0.38	0.49
Yb	2.3	2.2	2.3	2.3	0.09	0.05	0.06

Table 4-1. Continued

Location:	Tubaf	Tubaf	Tubaf	Tubaf	Tubaf	Tubaf	Tubaf
Sample:	54GTVA2L	55GTVA2A	55GTVA2D	55GTVA2F	55GTVA2H	56GTVA2A	56GTVA2B
Type:	lherzolite	lherzolite	lherzolite	lherzolite	harzburgite	lherzolite	lherzolite
SiO_2	42.00	42.60	42.70	41.50	42.60	43.80	39.50
TiO_2	bdl	bdl	bdl	0.02	bdl	bdl	0.02
Al_2O_3	2.10	1.20	1.90	4.90	3.50	1.00	1.50
Fe_2O_3T	9.14	9.10	8.45	8.16	9.12	8.83	12.00
MnO	0.13	0.13	0.13	0.12	0.14	0.13	0.17
MgO	46.40	45.70	44.40	42.80	43.60	46.20	46.00
CaO	0.75	0.72	0.72	0.97	0.79	1.02	1.59
Na_2O	bdl	0.03	bdl	0.09	bdl	0.11	0.06
K_2O	bdl	bdl	bdl	0.09	bdl	bdl	0.05
P_2O_5	0.01	bdl	bdl	bdl	bdl	bdl	bdl
Total	100.2	99.4	98.1	98.4	99.4	100.9	100.4
LOI	bdl	bdl	0.1	bdl	bdl	bdl	bdl
Ba	bdl	60	23	bdl	bdl	bdl	159
Be	bdl	bdl	bdl	bdl	bdl	bdl	bdl
Co	130	124	116	114	120	125	167
Cr	2210	2870	3000	3100	2730	2850	4970
Cs	bdl	bdl	bdl	0.04	bdl	0.06	0.07
Cu	14	23	14	12	10	15	17
Hf	0.46	0.21	0.37	0.71	0.57	0.14	0.94
Nb	0.07	bdl	bdl	0.17	0.07	0.07	0.12
Ni	2710	3930	2510	2380	2480	3210	2040
Pb	1	bdl	bdl	bdl	bdl	bdl	bdl
Rb	0.14	0.07	0.10	1.10	0.25	0.34	1.00
Sc	9.1	9.0	10.0	10.0	10.0	12.0	8.4
Sr	bdl	bdl	bdl	48	bdl	bdl	bdl
Ta	bdl	bdl	bdl	0.03	bdl	0.04	bdl
Th	0.03	bdl	0.02	0.08	0.03	bdl	0.17
U	0.02	bdl	0.02	0.06	0.03	bdl	0.05
V	45	45	50	52	43	54	52
Zn	47	43	43	45	41	40	66
Zr	19.0	9.2	16.0	30.0	25.0	5.4	43.0
Ce	0.1	0.7	1.1	3.9	2.3	bdl	5.0
Dy	0.03	0.08	0.10	0.35	0.19	bdl	0.38
Er	0.03	0.02	0.02	0.08	0.02	bdl	0.05
Eu	bdl	bdl	bdl	0.06	bdl	bdl	bdl
Gd	bdl	bdl	bdl	0.16	0.02	bdl	0.08
Ho	bdl	bdl	bdl	0.04	bdl	bdl	0.02
La	bdl	bdl	bdl	0.6	0.1	bdl	0.5
Lu	bdl	bdl	bdl	0.02	bdl	bdl	bdl
Nd	bdl	bdl	bdl	0.7	0.1	bdl	0.4
Pr	0.02	0.03	bdl	0.18	0.04	bdl	0.12
Sm	bdl	0.03	bdl	0.19	0.04	bdl	0.06
Tb	bdl	bdl	bdl	0.03	bdl	bdl	bdl
Tm	bdl	bdl	bdl	bdl	bdl	bdl	bdl
Y	0.22	0.27	0.24	1.10	0.48	0.12	0.96
Yb	0.05	0.04	0.04	0.10	0.05	0.03	0.06

Table 4-1. Continued

Location:	Tubaf	Tubaf	Tubaf	Tubaf	Tubaf	Tubaf	Tubaf
Sample:	56GTVA2T	56GTVA2P	56GTVA2G	56GTVA2H	56GTVA2X	56GTVA2F	54GTVA3A
Type:	lherzolite	lherzolite	dunite	dunite	dunite	dunite	gabbro
SiO_2	47.10	41.40	40.30	43.40	40.60	38.80	57.70
TiO_2	bdl	bdl	bdl	bdl	0.03	bdl	1.76
Al_2O_3	3.10	2.40	1.70	1.10	2.30	1.60	15.50
Fe_2O_3T	7.94	8.84	11.70	8.72	7.53	10.10	8.89
MnO	0.14	0.13	0.17	0.13	0.11	0.14	0.10
MgO	41.90	47.20	45.90	45.70	44.80	48.00	2.75
CaO	0.87	0.79	1.00	0.84	2.25	0.32	6.70
Na_2O	0.05	0.03	0.07	bdl	0.19	bdl	5.17
K_2O	bdl	0.05	0.06	bdl	0.38	bdl	0.30
P_2O_5	bdl	bdl	bdl	bdl	bdl	bdl	0.13
Total	101.0	100.6	100.0	99.7	99.1	98.6	98.5
LOI	0.1	bdl	bdl	0.2	0.0	bdl	0.2
Ba	bdl	bdl	bdl	bdl	90	bdl	bdl
Be	bdl	bdl	bdl	bdl	bdl	bdl	1.0
Co	101	129	165	128	120	153	17
Cr	4350	3030	682	3200	4250	3460	bdl
Cs	0.03	0.06	0.08	bdl	0.35	0.02	0.10
Cu	14	19	15	bdl	71	bdl	bdl
Hf	0.47	0.58	0.70	0.18	0.23	0.17	6.50
Nb	0.08	0.06	bdl	bdl	0.08	0.06	3.00
Ni	1430	3090	1870	2650	4060	2510	bdl
Pb	bdl	3	bdl	bdl	1	8	bdl
Rb	0.34	0.50	0.88	0.15	11.00	0.14	3.20
Sc	10.0	9.5	7.9	11.0	11.0	5.0	28.0
Sr	bdl	bdl	bdl	bdl	24	bdl	142
Ta	bdl	bdl	bdl	bdl	bdl	bdl	0.21
Th	0.03	0.05	0.04	bdl	0.10	bdl	0.32
U	bdl	0.02	0.02	bdl	0.03	bdl	0.17
V	46	45	29	53	50	32	161
Zn	44	42	55	45	38	46	73
Zr	21.0	27.0	32.0	7.3	9.0	7.3	242.0
Ce	2.1	0.1	3.7	bdl	0.9	bdl	23.0
Dy	0.19	0.03	0.33	bdl	0.24	bdl	12.00
Er	0.04	0.03	0.05	0.02	0.12	bdl	6.60
Eu	bdl	bdl	bdl	bdl	0.07	bdl	2.10
Gd	0.04	0.02	0.05	bdl	0.21	bdl	9.60
Ho	bdl	bdl	0.02	bdl	0.05	bdl	2.40
La	bdl	bdl	0.1	bdl	0.3	bdl	6.5
Lu	bdl	bdl	bdl	bdl	0.02	bdl	1.10
Nd	bdl	bdl	0.1	bdl	0.4	bdl	21.0
Pr	0.03	bdl	0.03	bdl	0.11	bdl	3.90
Sm	0.03	bdl	0.04	bdl	0.18	bdl	7.20
Tb	bdl	bdl	bdl	bdl	0.04	bdl	1.70
Tm	bdl	bdl	bdl	bdl	bdl	bdl	1.10
Y	0.55	0.23	0.82	0.14	1.30	0.12	72.00
Yb	0.06	0.05	0.06	0.04	0.14	0.03	7.20

Table 4-1. Continued

Location:	Tubaf	Tubaf	Tubaf	Tubaf	Tubaf	Tubaf	Tubaf
Sample:	54GTVA3D	54GTVA3E	54GTVA3I	55GTVA3E	55GTVA3F	56GTVA3I	56GTVA3H
Type:	gabbro	gabbro	gabbro	gabbro	gabbro	gabbro	gabbro
SiO_2	57.30	50.50	52.60	42.60	42.50	50.10	47.00
TiO_2	1.98	1.44	2.20	2.38	2.14	0.86	0.43
Al_2O_3	16.00	15.70	13.50	15.80	15.30	16.60	16.40
Fe_2O_3T	9.90	10.80	15.70	17.40	17.30	11.20	8.12
MnO	0.14	0.17	0.16	0.19	0.20	0.21	0.14
MgO	2.69	6.39	5.26	7.57	8.83	8.00	9.29
CaO	5.55	10.80	4.85	12.60	11.80	11.80	14.40
Na_2O	4.73	2.93	4.06	1.58	1.65	2.18	1.91
K_2O	0.69	0.30	0.36	0.11	0.30	0.09	1.56
P_2O_5	0.07	bdl	0.09	bdl	bdl	bdl	0.01
Total	98.4	98.2	98.0	99.4	99.1	100.2	98.8
LOI	0.9	0.3	1.2	bdl	0.4	0.1	0.3
Ba	29	36	93	bdl	bdl	21	38
Be	1.1	0.5	0.9	bdl	bdl	bdl	bdl
Co	24	38	40	56	66	40	42
Cr	bdl	112	11	12	200	253	135
Cs	0.16	0.07	1.40	0.04	0.35	0.02	0.75
Cu	11	29	bdl	80	82	36	66
Hf	5.50	2.50	4.70	0.93	0.62	0.98	0.32
Nb	3.00	1.90	2.30	0.40	0.21	0.31	0.13
Ni	40	51	24	68	129	61	85
Pb	bdl	bdl	bdl	5	4	bdl	bdl
Rb	6.60	2.80	13.00	1.00	8.50	0.57	30.00
Sc	29.0	41.0	35.0	50.0	52.0	49.0	52.0
Sr	148	120	102	161	106	130	316
Ta	0.25	0.15	0.19	0.04	0.04	0.04	0.02
Th	0.30	0.12	0.20	0.07	0.10	0.03	0.05
U	0.18	0.10	0.14	0.06	0.07	0.03	0.06
V	169	330	382	1030	1120	301	299
Zn	60	105	60	128	121	123	122
Zr	207.0	81.0	169.0	31.0	22.0	35.0	9.2
Ce	17.0	14.0	21.0	4.6	3.9	5.7	1.7
Dy	11.00	7.70	9.50	2.80	1.80	3.70	1.50
Er	6.50	4.30	5.30	1.50	0.99	2.20	0.90
Eu	2.20	1.40	1.90	0.67	0.42	0.97	0.43
Gd	9.20	6.10	8.00	2.30	1.30	3.00	1.20
Ho	2.40	1.60	2.00	0.56	0.36	0.79	0.33
La	4.3	3.7	6.3	1.2	1.2	1.1	0.7
Lu	1.10	0.70	0.87	0.23	0.16	0.36	0.13
Nd	19.0	14.0	18.0	3.8	1.9	4.8	1.7
Pr	3.30	2.50	3.50	0.67	0.41	0.76	0.28
Sm	6.60	4.50	5.90	1.40	0.78	1.90	0.77
Tb	1.60	1.10	1.40	0.40	0.25	0.56	0.24
Tm	1.00	0.71	0.85	0.23	0.16	0.34	0.12
Y	67.00	49.00	57.00	16.00	11.00	22.00	8.40
Yb	7.00	4.70	5.70	1.50	1.00	2.20	0.80

Table 4-1. Continued

Location:	Tubaf	Tubaf	Tubaf	Tubaf	Tubaf	Tubaf	Tubaf
Sample:	56GTVA3O	56GTVA4D	56GTVA.4E	56GTVA.4F	54GTVA.6F	54GTVA.6B	54GTVA.6E
Type:	basaltic	sedimentary	sedimentary	sedimentary	sedimentary	sedimentary	sedimentary
SiO_2	51.00	42.20	46.50	15.30	48.40	41.30	32.70
TiO_2	2.56	0.19	0.51	0.12	0.68	0.43	0.34
Al_2O_3	14.10	10.90	13.90	4.20	16.00	9.80	6.70
Fe_2O_3T	15.00	2.34	6.29	1.21	5.80	4.31	3.31
MnO	0.28	0.07	0.32	0.04	0.12	0.12	0.11
MgO	4.89	2.14	2.89	0.76	2.25	1.60	1.15
CaO	9.14	22.30	17.40	43.10	13.10	23.50	29.70
Na_2O	3.52	2.34	2.21	0.67	2.82	1.77	1.26
K_2O	0.12	1.02	0.64	0.33	2.27	0.78	0.74
P_2O_5	0.20	0.12	0.15	0.12	0.08	0.16	0.11
Total	100.9	83.8	90.9	66.0	91.6	83.9	76.3
LOI	bdl	16.1	9.9	32.3	7.5	15.9	22.7
Ba	bdl	163	92	64	212	70	201
Be	0.5	0.5	0.5	bdl	0.5	bdl	bdl
Co	34	bdl	11	bdl	12	6	7
Cr	37	16	19	12	24	30	22
Cs	0.04	0.69	10.00	0.52	4.00	0.57	0.44
Cu	47	96	223	25	123	38	49
Hf	2.20	1.70	1.40	0.70	1.30	1.50	1.10
Nb	3.40	2.50	1.40	0.99	1.30	1.50	1.20
Ni	15	13	23	bdl	18	12	11
Pb	bdl	5	3	2	4	2	2
Rb	1.00	15.00	42.00	7.70	45.00	15.00	13.00
Sc	36.0	3.9	18.0	2.1	24.0	12.0	9.0
Sr	144	1221	518	911	537	892	818
Ta	0.25	0.16	0.07	0.06	0.09	0.10	0.07
Th	0.05	1.20	0.59	0.48	0.37	0.52	0.40
U	0.04	0.66	0.68	0.65	0.79	1.00	1.40
V	454	28	114	23	165	83	74
Zn	134	65	81	68	80	67	68
Zr	81.0	64.0	51.0	28.0	46.0	61.0	42.0
Ce	14.0	24.0	13.0	7.5	7.5	17.0	8.3
Dy	9.30	1.50	3.00	1.10	2.60	2.50	2.00
Er	5.40	0.86	1.90	0.69	1.60	1.40	1.20
Eu	2.40	0.54	0.80	0.28	0.63	0.72	0.41
Gd	8.20	1.80	2.90	1.10	2.30	2.60	1.80
Ho	2.00	0.31	0.65	0.24	0.56	0.52	0.44
La	3.3	13.0	7.2	5.9	4.0	9.2	5.2
Lu	0.88	0.18	0.32	0.12	0.25	0.25	0.22
Nd	15.0	12.0	9.6	5.4	5.9	11.0	5.9
Pr	2.40	3.30	2.00	1.30	1.20	2.50	1.30
Sm	5.90	2.00	2.40	1.00	1.80	2.50	1.40
Tb	1.50	0.26	0.47	0.16	0.41	0.43	0.30
Tm	0.81	0.14	0.30	0.11	0.26	0.22	0.20
Y	53.00	12.00	22.00	11.00	16.00	17.00	14.00
Yb	5.40	0.96	1.90	0.72	1.60	1.50	1.30

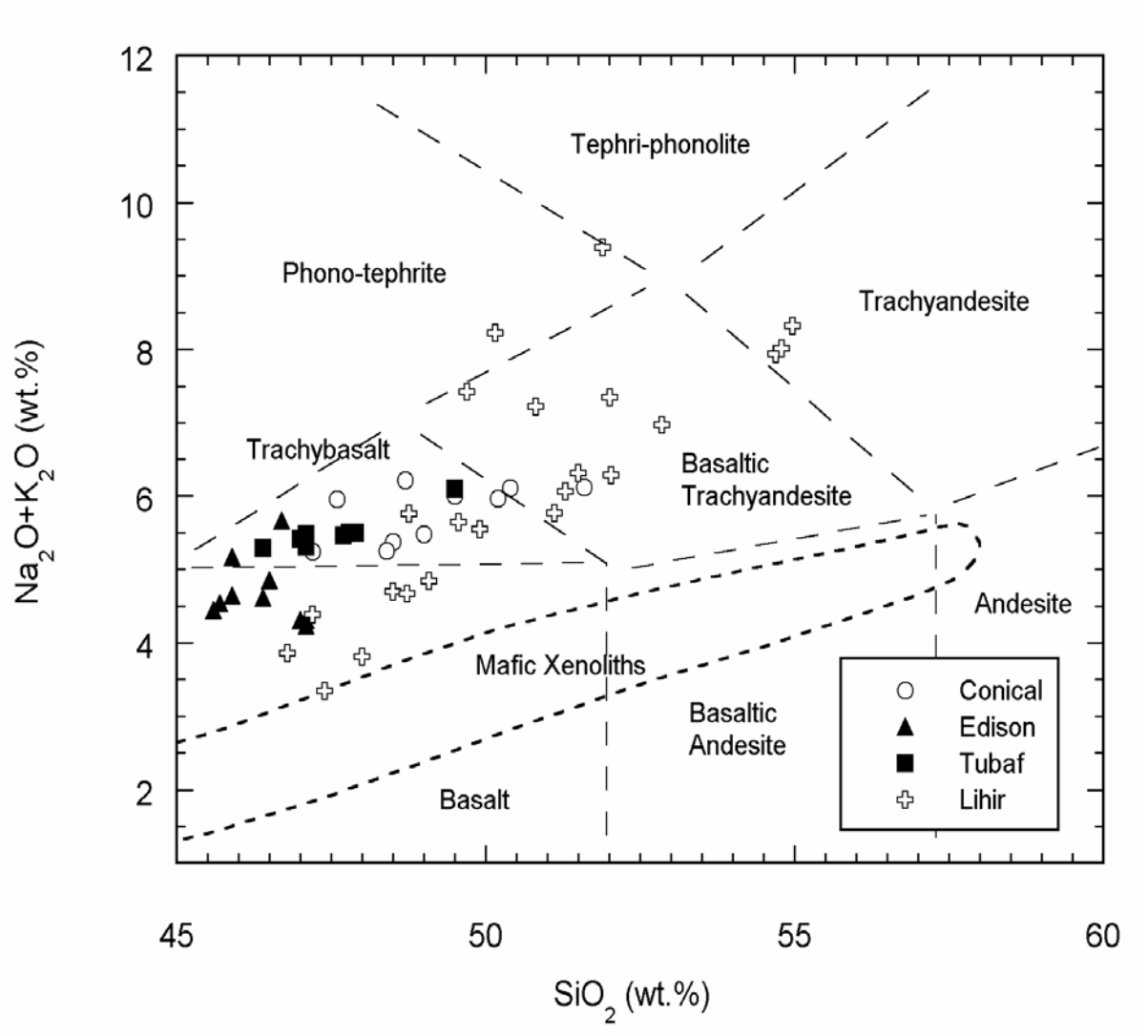

Figure 4-2. Classification of the Conical, Edison, Tubaf, and Lihir lavas based on their SiO_2 vs Na_2O+K_2O concentrations (after LeMaitre, 1989). Data from this study and from Kennedy et al. (1990a), Stracke and Hegner (1998), and Müller et al. (2001). The field for the mafic xenoliths is based on the several analyses presented in Table 4-1. Note that although the mafic xenoliths show relatively wide range in their SiO_2 content, they plot at lower alkali contents relative to the TLTF lavas.

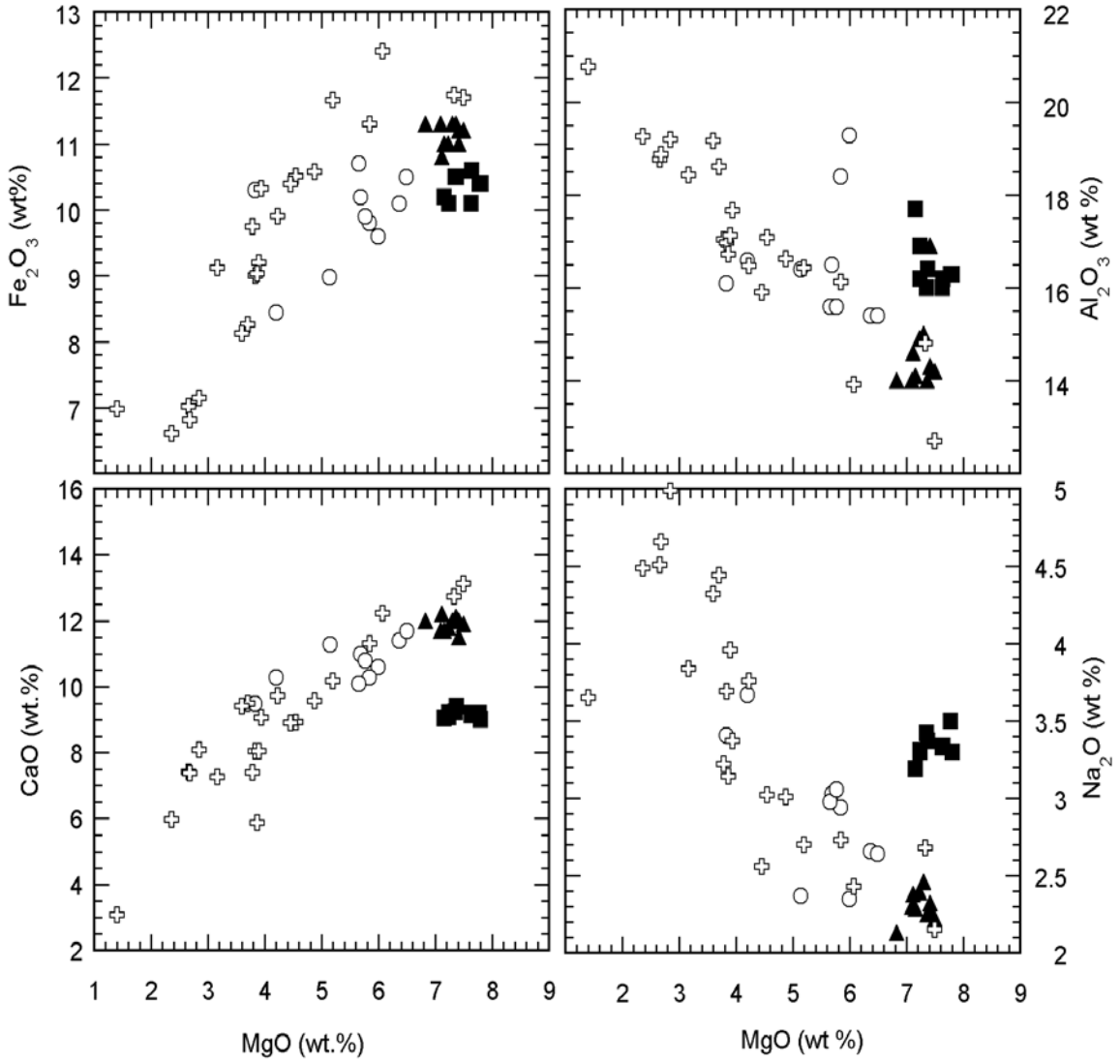

Figure 4-3. Comparison of MgO vs CaO, Fe2O3, Na2O, and Al2O3 between Lihir and seamount lavas. Note that CaO and Fe2O3 decrease, and Na2O, and Al2O3 increase with the decrease in the MgO, suggesting that lavas were affected by fractionation processes (for more discussion see the text). Data sources and symbols are the same as in Figure 4-2.

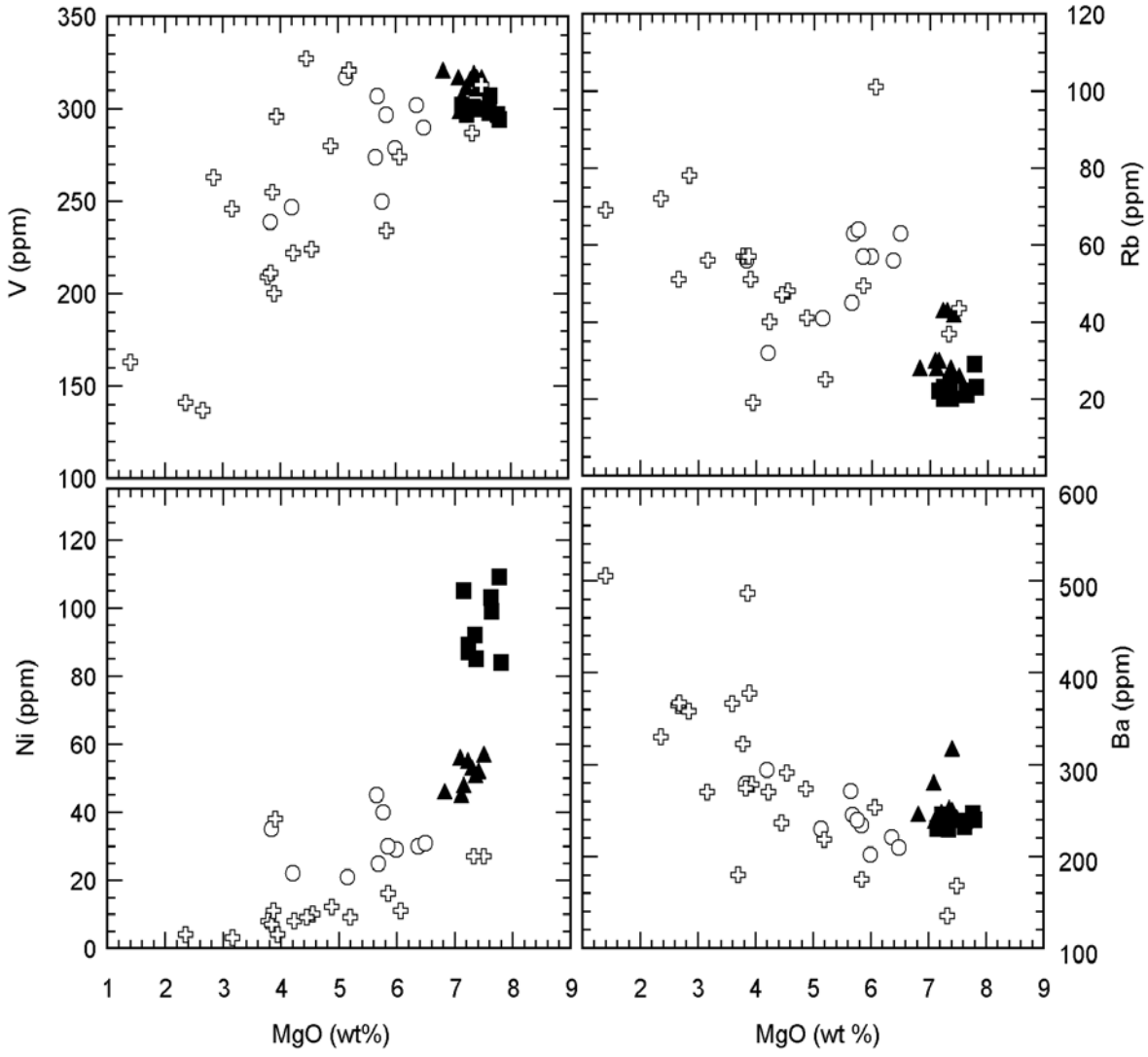

Figure 4-4. Comparison of MgO vs Ni, V, Ba, and Rb between Lihir and seamount lavas. Ni and V behave compatible and decrease with the decrease in MgO, and Ba and Rb behave incompatible and increase with the decrease in MgO, both trends indicating fractination (see the text for more discussion). Data sources and symbols are the same as in Figure 4-2.

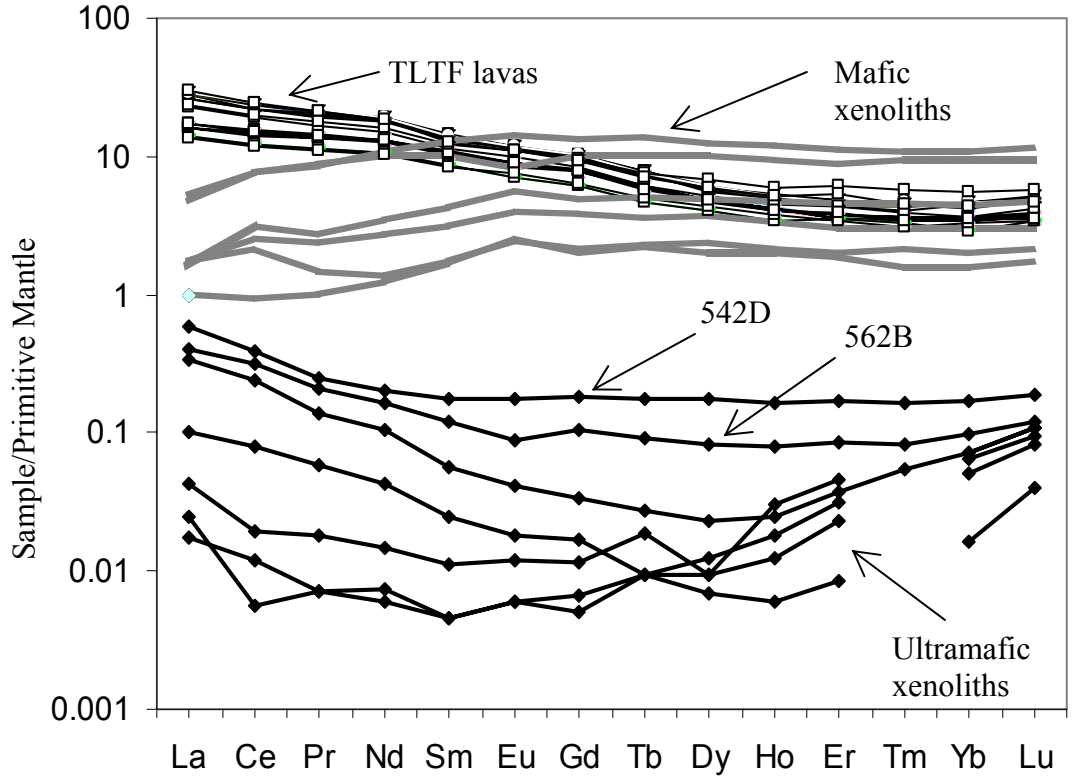

Figure 4-5. Normalized REE patterns of TLTF lavas and mafic and ultramafic xenoliths. TLTF data from this study and from Stracke and Hegner (1998). Ultramafic xenoliths data from Gregoire et al. (2001) and Franz et al. (2002).

Primitive mantle-normalized rare-earth elements (REE) patterns for the seamounts and TLTF islands are subparallel and show enrichments in light rare-earth elements (LREE) relative to heavy rare-earth elements (HREE) (Fig. 4-5). Similarly, the primitive mantle-normalized trace element variations (spider diagram) for the seamount lavas follow the same pattern as the Lihir and the other TLTF island lavas (Fig. 4-6). They are characterized by negative Nb and Ti anomalies, and positive U, K, Pb, and Sr anomalies, typical for island arc volcanics (Perfit et al. 1980).

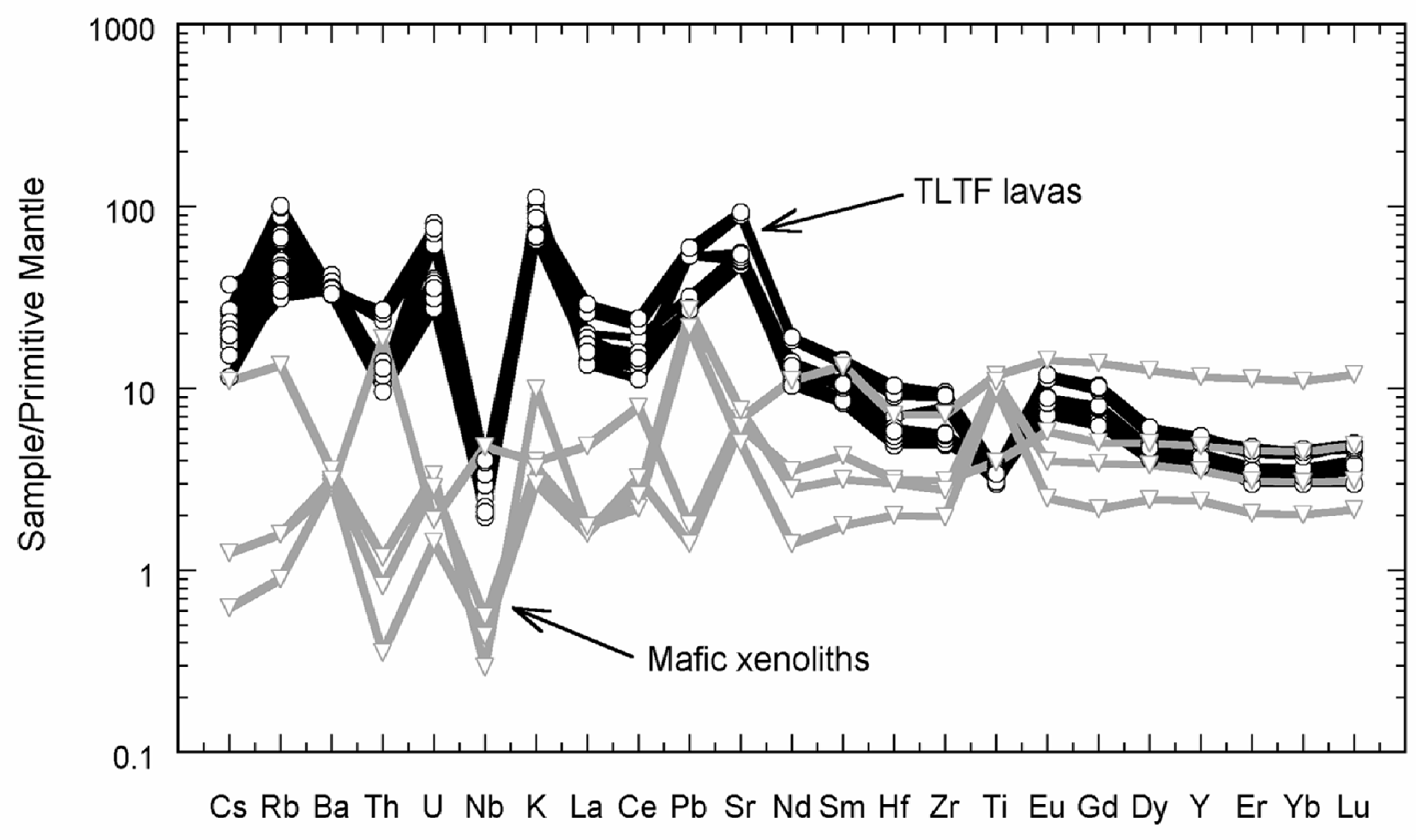

Figure 4-6. Primitive Mantle normalized trace element patterns of TLTF lavas and mafic xenoliths. Primitive Mantle values from Sun and McDonough (1989).

The mafic xenoliths contain 42.5 to 57.7 wt % SiO_2 (i.e., from gabbro to diorite, Table 4-1, Fig. 4-2). A few plagiogranite xenoliths also have previously been recovered (McInnes et al., 2001). Overall, the mafic xenoliths are subalkaline with low total alkalis relative to the Lihir and seamount lavas (Fig. 4-2). They exhibit depleted LREE patterns (Fig. 4-5) and enrichments in some fluid-mobile elements, such as Ba, K, U, and Pb (Fig. 4-6).

Ultramafic xenoliths have high MgO content, ranging from 26% to 48.7% and low contents of CaO, Na_2O, Al_2O_3 (Table 4-1). They are also enriched in compatible elements, such as Ni and Cr, and depleted in incompatible elements, most below detection limits (Table 4-1).

Isotopic analyses of lavas, xenolith, and sediment samples from the study area are presented in Table 4-2 and also in Kamenov et al. (2004b) (Chapter 3). Sr isotopic compositions of fresh lavas from the region, including TLTF, New Britain, and Solomon Islands and Manus and Woodlark Basins, show relatively small $^{87}Sr/^{86}Sr$ variations with values close to 0.704 (Table 4-2), similar to previously published data (Wallace et al. 1983; Johnson et al. 1988; Trull et al. 1990; Kennedy et al. 1990b; Stracke and Hegner 1998; Woodhead et al. 1993, 1998). Measured $^{87}Sr/^{86}Sr$ in sedimentary xenoliths recovered from Tubaf seamount lavas have more radiogenic $^{87}Sr/^{86}Sr$ values, ranging from 0.7067 to 0.7083, compared to the lavas in the area (Table 4-2). Sr isotopic compositions of the analyzed ultramafic xenoliths exhibit a wider range than the TLTF lavas, ranging from 0.7037 to 0.7059 (Table 4-2).

Table 4-2. Pb, Sr, and Nd isotopic analyses of lava and xenolith samples

Location	Type	sample	$^{206}Pb/^{204}Pb$	$^{207}Pb/^{204}Pb$	$^{208}Pb/^{204}Pb$	$^{87}Sr/^{86}Sr$	$^{143}Nd/^{144}Nd$
Tabar	lava	TAB 3	18.773	15.553	38.377	0.70355	0.513037
Tabar	lava	TAB 4	18.714	15.547	38.345	-	-
Tanga	lava	DR11.1/2A	18.735	15.542	38.342	0.704195[A]	0.51301
Feni	lava	DR12.1/8A	18.679	15.555	38.370	0.704005[A]	-
Rabaul	lava	RAB 2	18.813	15.543	38.423	0.70367	0.513006
Rabaul	lava	RAB 981	18.815	15.545	38.423	-	-
Bouganville	lava	69B	18.573	15.533	38.283	0.70370	0.512988
Solomon	lava	24-12	18.622	15.580	38.448	0.703916[B]	-
Solomon	lava	31-1	18.443	15.509	38.252	0.703503[B]	-
Savo	lava	SAVO 2	18.424	15.515	38.225	0.70408	0.512971
Kavachi	lava	35-2	18.394	15.518	38.203	0.703724[B]	-
Woodlark	lava	4 29-H	18.273	15.484	37.927	0.702826[B]	-
Woodlark	lava	4 26-5	18.288[C]	15.522	38.005	0.70258[B]	0.513095
Woodlark	lava	4 26-14	17.947[C]	15.492	37.629	0.70270	-
Woodlark	lava	4 29-8	17.890[C]	15.511	37.591	0.70282	0.513078
Woodlark	lava	4 32-10	18.117[C]	15.494	37.758	0.70267	0.513151
Woodlark	lava	4 32-16	18.116[C]	15.530	37.910	0.703311[B]	0.513063
Woodlark	lava	4 32-17	-	-	-	0.70351	0.513028
Tubaf	lava	54 4-2	18.759	15.554	38.391	0.70397	0.5130017
Tubaf	lava	56 2C	18.756	15.550	38.377	0.70397	0.513003
Tubaf	lava	56 2M	18.767	15.550	38.366	-	-
Xenoliths:							
Tubaf	sedimentary	54 6G	18.640	15.568	38.255	0.70828	0.5129289
Tubaf	sedimentary	54 6B	18.627	15.557	38.302	0.70751	0.5129586
Tubaf	sedimentary	56 4F	18.770	15.583	38.495	0.70669	0.5129378
Tubaf	sedimentary	54 6E	18.901	15.560	38.494	0.70759	0.5128994
Tubaf	sedimentary	54 6F	18.771	15.567	38.441	-	0.5129111
Tubaf	sedimentary	56 4D	18.712	15.528	38.307	0.70791	-
Tubaf	veined lherzolite	54 2D	19.120	15.652	38.633	0.70374	0.513010
Tubaf	harzburgite	562F	18.694	15.557	38.321	0.70398	0.512910
Tubaf	veined lherzolite	56 2B	18.340	15.567	38.263	0.70437	-
Tubaf	harzburgite	54 2G	18.499	15.641	38.523	0.70592	0.512920
Tubaf	veined lherzolite	56 2P	18.800	15.577	38.414	0.70453	-
Tubaf	harzburgite	55 2H	18.514	15.524	38.192	0.70404	-
Tubaf	veined lherzolite	54 2S	18.853	15.672	38.652	-	-
Tubaf	veined lherzolite	54 2K	19.099	15.759	38.781	-	-
Tubaf	lherzolite	55 2F	-	-	-	0.70398	-
Tubaf	CPx separate	61 1C CPx	17.859	15.567	37.672	0.70446	0.51298
Tubaf	CPx separate	67 1 CPx	17.591	15.561	37.429	0.70411	0.51292
Tubaf	CPx separate	61 1B CPx	17.892	15.567	37.716	0.70457	0.512963
Tubaf	basaltic	56 3O	18.692	15.509	38.163	0.70297	0.513077
Tubaf	gabbro	55 3E	18.722	15.533	38.280	0.70333	0.513030
Tubaf	gabbro	56 3I	18.647	15.529	38.191	0.70293	-
Tubaf	gabbro	54 3E	18.747	15.509	38.196	0.70302	0.513056
Tubaf	gabbro	56 3H	-	-	-	0.70366	-
Tubaf	gabbro	55 3F	-	-	-	0.70343	-

A-data from Johnson et al. 1988; B-data from Trull et al.1990; C-TIMS Pb analyses;

Sr isotopic compositions in the analyzed 3 clinopyroxene separates from the ultramafic xenoliths range from 0.7041 to 0.7046. The mafic xenoliths have slightly less radiogenic $^{87}Sr/^{86}Sr$ values, ranging from 0.7029 to 0.7036 (Table 4-2).

Fresh volcanic rocks from Lihir and the seamounts exhibit small, but distinguishable variations in their Pb isotopic compositions, with Conical seamount lavas having slightly less, and Tubaf and Edison seamount lavas having slightly more radiogenic ratios (Kamenov et al. 2004b). Lavas from Tabar and Tanga show overall similar Pb isotopic compositions to Lihir and the seamounts (Table 4-2). Feni lavas have slightly less radiogenic, whereas Rabaul lavas have slightly more radiogenic Pb isotope values compared to the other TLTF lavas (Table 4-2). Solomon Islands and Woodlark Basin samples show less radiogenic Pb isotopic ratios than the TLTF islands (Table 4-2). Sedimentary xenoliths recovered from the Tubaf seamount lavas exhibit a larger range in their lead isotope compositions compared to the fresh volcanic rocks in the area (Table 4-2, Chapter 3) with values ranging from $^{206}Pb/^{204}Pb$=18.627 to 18.901, $^{207}Pb/^{204}Pb$=15.509 to 15.585, and $^{208}Pb/^{204}Pb$=38.163 to 38.512. Surprisingly, the ultramafic xenoliths exhibit a very wide range in their Pb isotopic compositions, ranging from $^{206}Pb/^{204}Pb$=18.340 to 19.120, $^{207}Pb/^{204}Pb$=15.524 to 15.759, and $^{208}Pb/^{204}Pb$=38.192 to 38.781. The 3 clinopyroxene separates, however, show distinct Pb isotopic compositions from the ultramafic xenoliths, with $^{206}Pb/^{204}Pb$=17.591 to 17.892, $^{207}Pb/^{204}Pb$=15.561 to 15.567, and $^{208}Pb/^{204}Pb$=37.429 to 37.716. The mafic xenoliths, on the other hand, show Pb isotopic compositions from similar to the lavas to slightly less-radiogenic, ranging from $^{206}Pb/^{204}Pb$=18.647 to 18.747, $^{207}Pb/^{204}Pb$=15.509 to 15.533, and $^{208}Pb/^{204}Pb$=38.163 to 38.280 (Table 4-2).

Nd isotopic compositions of the lavas from the region show small variations, ranging from 0.51297 to 0.51315, similar to previously published data (Stracke and Hegner 1998). The mafic and ultramafic xenoliths overall exhibit similar Nd isotopic compositions to the lavas (Table 2). Sedimentary xenoliths have slightly lower $^{143}Nd/^{144}Nd$ compared to the lavas and igneous xenoliths (Table 4-2).

Discussion

Major and Trace Element Variations in Seamount and Lihir Lavas

Although the lavas in the TLTF area are relatively alkaline, their overall major and trace element abundances are typical for potasic magmatic rocks recovered in island arc settings (Müller et al. 2001**)**. Elemental variations in the seamount and Lihir samples suggest that most of the lavas were modified to some degree by fractional crystallization. The observed decrease in CaO and increase in Al_2O_3 with decreasing MgO (Fig. 4-3) suggests that plagioclase fractionation did not play a major role in magmatic evolution. Although a common phenocryst in the Conical seamount and Lihir lavas, plagioclase is not common in Edison and is rare in Tubaf lavas. The Cpx is the most abundant phenocryst observed in the lavas from the area, and Lihir island samples form a positive correlation between the MgO and CaO/Al_2O_3 ratio (Fig. 4-7), indicating Cpx as a dominant phase in the crystallization sequence, in agreement with previous observations (Stracke and Hegner 1998). An experimental study on Lihir lavas also provided evidences that the magmatic evolution was mainly controlled by clinopyroxene, accompanied by amphibole, magnetite, and minor olivine fractionation (Kennedy et al. 1990a).

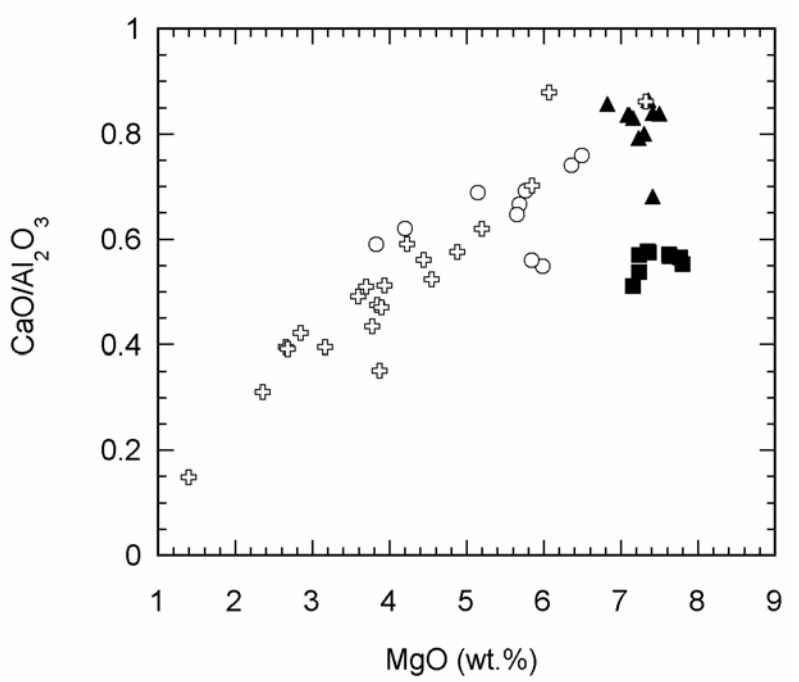

Figure 4-7. Plot CaO/Al_2O_3 vs MgO indicating clinopyroxene as a major fractionation phase. Symbols and data sources are the same as in Figure 4-2.

Müller et al. (2001 and 2003) conducted extensive P-T studies on mineral phases in Lihir and Conical seamount lavas and suggested that magma evolution occurred in two stages: one deeper, controlled by early hornblende crystallization, and a second shallower stage, associated with clinopyroxene and plagioclase crystallization. Plagioclase is not a stable phase at higher pressures and in addition, the plagioclase stability field is suppressed in magmas with high H_2O concentrations (Carmichael et al. 1996). The absence of plagioclase in the more primitive Tubaf lavas is consistent with the Tubaf lavas containing the highest volatile contents of the TLTF suite (Chapter 3). Furthermore, the abundance of ultramafic xenoliths in Tubaf suggest that this magma rose rapidly to the surface, without much time for low-pressure evolution close to the surface (Chapter 3), another potential explanation for absence of plagioclase from the phenocryst assemblage. Decreasing Fe_2O_3 with decreasing MgO indicates removal of a Fe-rich

phase, most probably magnetite, during fractional crystallization. Magnetite is abundant in the lavas and also was suggested to play a role in the magma evolution by the experimental study of Kennedy et al. (1990a). It is a common feature for arc magmas to show a decrease in Fe_2O_3 with evolution indicating high fO_2, which stabilizes magnetite early in the crystallization sequence. Indeed, several previous studies confirmed the high fO_2 state of the magmas in the area (Kennedy et al. 1990a, McInnes and Cameron 1994, McInnes et al. 2001). In addition, the positive correlation between MgO and Ni (Fig. 4-4) also indicates that olivine was present in the early fractionation sequence, even though it is not observed as a phenocryst in the lavas.

The major element data for Lihir Island and the seamounts show considerable scatter on Harker diagrams, which suggests that the magmas did not evolve along a single liquid line of descent from a common parental magma. Incompatible trace elements, such as Rb, Ba, La, Ce, U, Th, and Pb plotted versus MgO also show considerable scatter indicating multiple parental magmas (Fig. 4-4), similar to the observations derived from the major element variations. This is further supported by the observed small, but significant differences in the lavas' isotopic compositions (Stracke and Hegner 1998, Kamenov et al. 2004b). Variations in parental melt compositions, on the other hand, are probably a result of small differences in the source materials, as indicated by the isotope data, and as well as a result of different degrees of partial melting. For example, Sr is higher in the relatively more primitive lavas from Tubaf seamount, and the higher Sr content correlates with higher La/Yb, suggesting smaller degrees of partial melting created parental Tubaf magmas (Fig. 4-8). Alternatively, these differences can be

explained by magma derivation from sources with different Sr, La, and Yb concentrations.

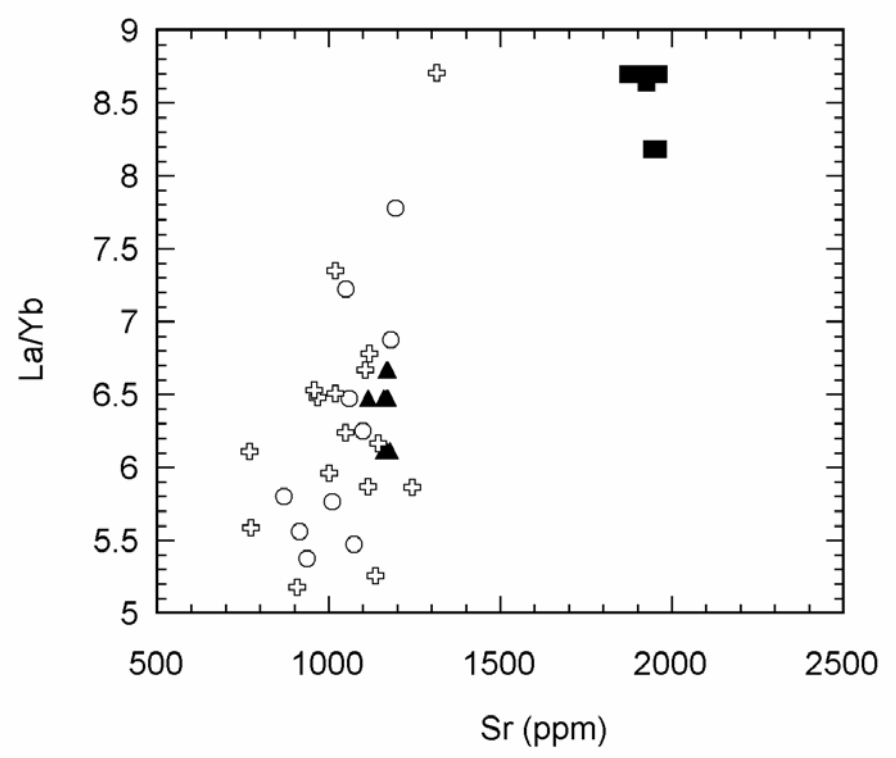

Figure 4-8. La/Yb vs Sr for Lihir island and seamount lavas. For more discussion see the text, data symbols same as Fig. 4-2.

Overall, the TLTF lavas exhibit trace element signatures typical for subduction-related volcanism, in particular exhibiting high LILE/HFSE and elevated LREE relative to HREE ratios (Fig. 4-5 and 4-6). Although currently not associated with active subduction, this observation indicates that the TLTF volcanism is related to a previous episode of subduction, as suggested previously by a number of studies (Kennedy et al. 1990b, McInnes et al. 1994; Stracke and Hegner 1998; Franz et al. 2002).

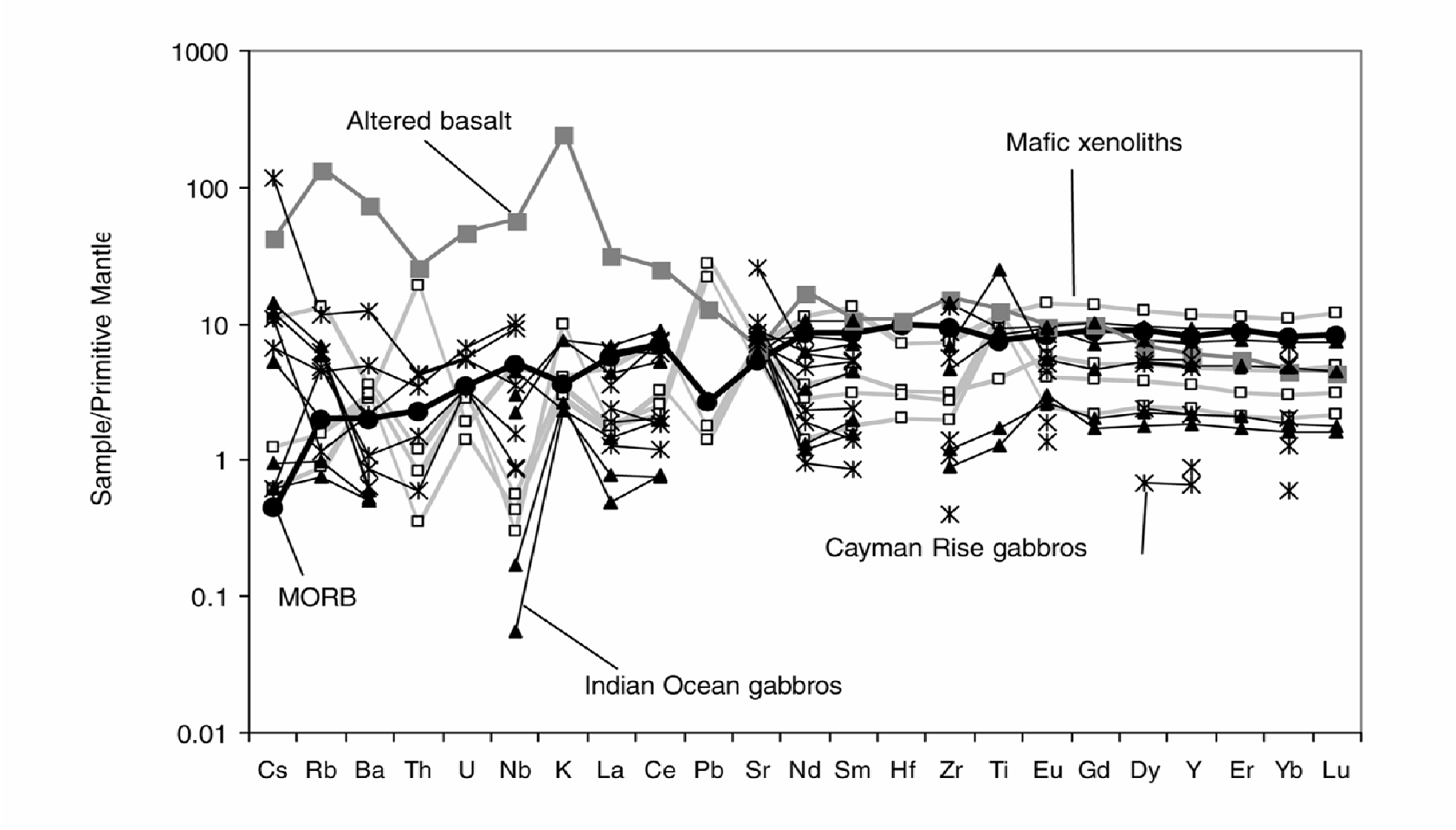

Figure 4-9. Primitive Mantle normalized trace element patterns of mafic xenoliths compared with MORB, altered MORB, and oceanic gabbros. Primitive Mantle values from Sun and McDonough (1989), MORB data from Kelley et al. (2003), Indian Ocean gabbros from Coogan et al. (2001), and Cayman Rise gabbros from Perez-Suarez (2001).

Major and Trace Element Variations in Mafic and Ultramafic Xenoliths

The wealth of xenoliths recovered from Tubaf seamount allow us to look more closely at the processes and sources in the crust and mantle and/or subducted slab and their role in the formation of the TLTF magmas. The gabbroic xenoliths have major and trace element abundances similar to gabbros recovered from oceanic settings. This observation is in agreement with the McInnes et al. (1999) study that suggested that the mafic crust underlying the TLTF islands originated at an oceanic spreading system. The mafic xenoliths exhibit depletion in the LREE (Fig. 4-5) indicating origin from a depleted mantle source. Their extended trace element patterns exhibit overall lower abundances than typical MORB (Fig. 4-9) indicating that the gabbros are cumulates, similar to other mid-ocean ridge gabbros (Coogan et al. 2001). The elevated concentration of Ti in some samples (Fig. 4-9) is due to Ti-magnetite accumulation, a common accessory mineral observed in the mafic xenoliths (McInnes et al. 2001). The mafic xenoliths trace-element patterns exhibit enrichments in fluid-mobile elements, such as Ba, U, K, and Pb (Fig. 4-9) suggesting that part of the mafic crust was affected by alteration probably after its formation at an oceanic spreading system. Indeed, a majority of the studies on ODP cores penetrating into the basaltic and gabbro layer of the oceanic crust provide evidences for chemical exchange between the oceanic lithosphere and seawater (Bach et al. 2001, Kelley et al. 2003).

The overall high MgO and low CaO, Na_2O, Al_2O_3 content observed in the ultramafic xenoliths (Table 4-1) indicates that they are residues after partial melting event (Gregoire et al. 2001, McInnes et al. 2001, Franz et al. 2002, for detailed discussion). Almost all of the xenoliths exhibit metasomatic alteration features, such as veins and irregular alteration areas (Gregoire et al. 2001, Franz et al. 2002). Overall, the

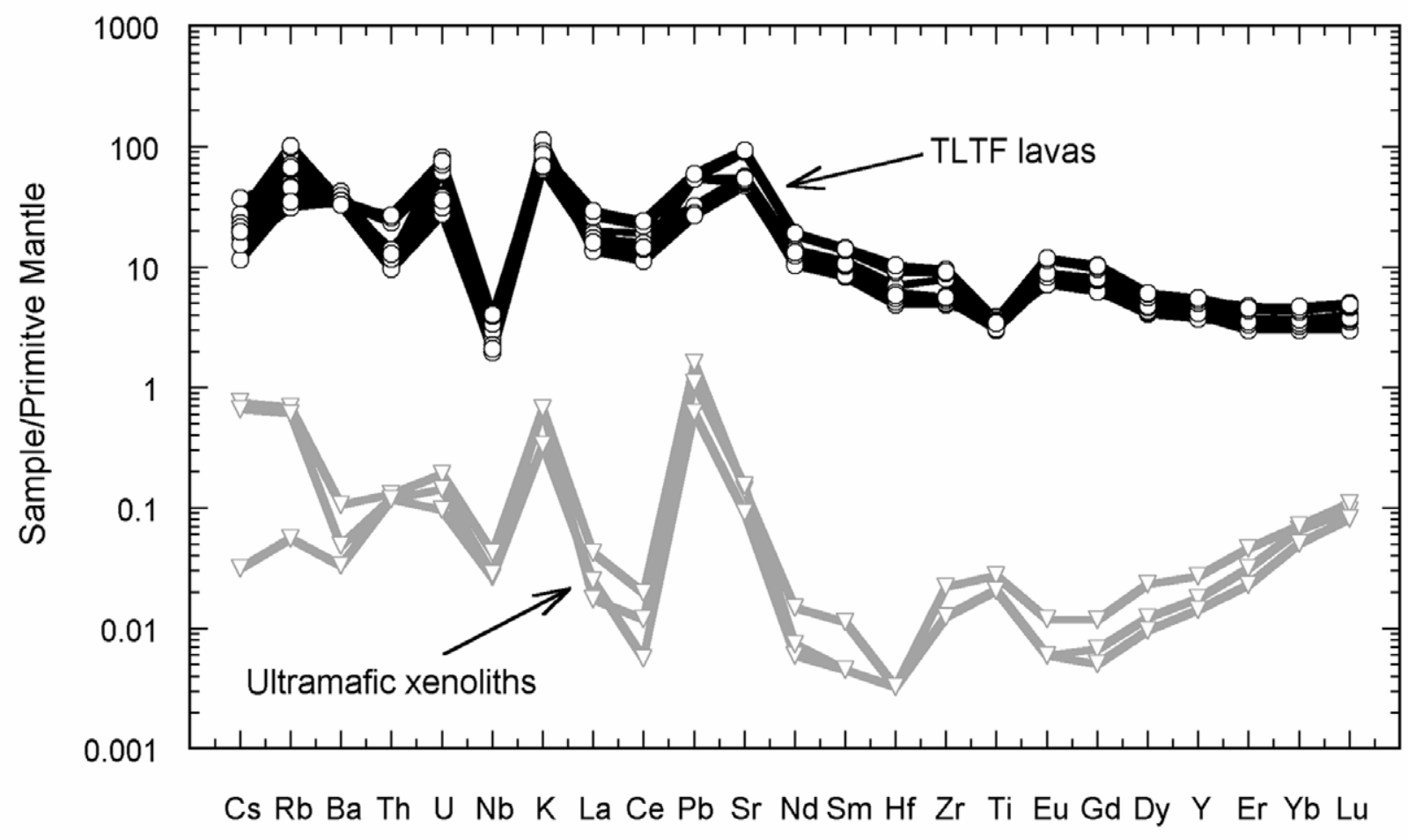

Figure 4-10. Primitive Mantle normalized trace element patterns of ultramafic xenoliths compared to TLTF lavas. Primitive Mantle values from Sun and McDonough (1989), ultramafic xenoliths data from Gregoire et al. (2001).

ultramafic xenoliths have strongly depleted trace element abundances compared to the TLTF lavas and mafic xenoliths. The REE patterns observed in the ultramafic xenoliths range from LREE and HREE enriched, so called "spoon-shape" pattern, to almost flat, slightly LREE enriched pattern (Fig. 4-5). The LREE enrichment can be explained by a metasomatic enrichment from a hydrous fluid phase (Gregoire et al. 2001, Franz et al. 2002). In addition, the metasomatized xenoliths exhibit high LILE/HFSE and LREE/HFSE ratios (Fig. 4-10), also indicative of enrichment by hydrous fluids (Gregoire et al. 2001).

Sr and Nd Isotopic Variations in Xenolith and Lava Samples.

The measured Sr and Nd isotopic compositions in the mafic xenoliths are similar to the Pacific-Indian MORB (Fig. 4-11), indicating derivation from a depleted mantle source which is consistent with their trace element and REE patterns. Some of the ultramafic xenoliths, on the other hand, exhibit elevated $^{87}Sr/^{86}Sr$ at relatively high $^{143}Nd/^{144}Nd$ (Table 4-2, Fig. 4-11) and their trace element patterns provide evidence for metasomatic alteration by hydrous fluid released most probably from the subducted slab.

Experiments show that Sr is partitioned in hydrous fluid phase while the REE are relatively immobile and do not partition into the fluid (Brenan et al. 1995). Therefore, fluids released during dehydration of subducted sediments and/or altered oceanic crust are expected to have relatively high Sr and low Nd contents. Metasomatism of the TLTF mantle wedge by such fluids will shift the Sr isotopic compositions of the ultramaifc xenoliths to more radiogenic ratios, but at the same time will not have strong effect on the Nd isotopic ratios, which appears to be the case (Fig. 4-11).

$^{143}Nd/^{144}Nd$ measured in the lavas from the region are generally similar to Indian and Pacific MORB, indicating that Nd reflects derivation from a depleted mantle source.

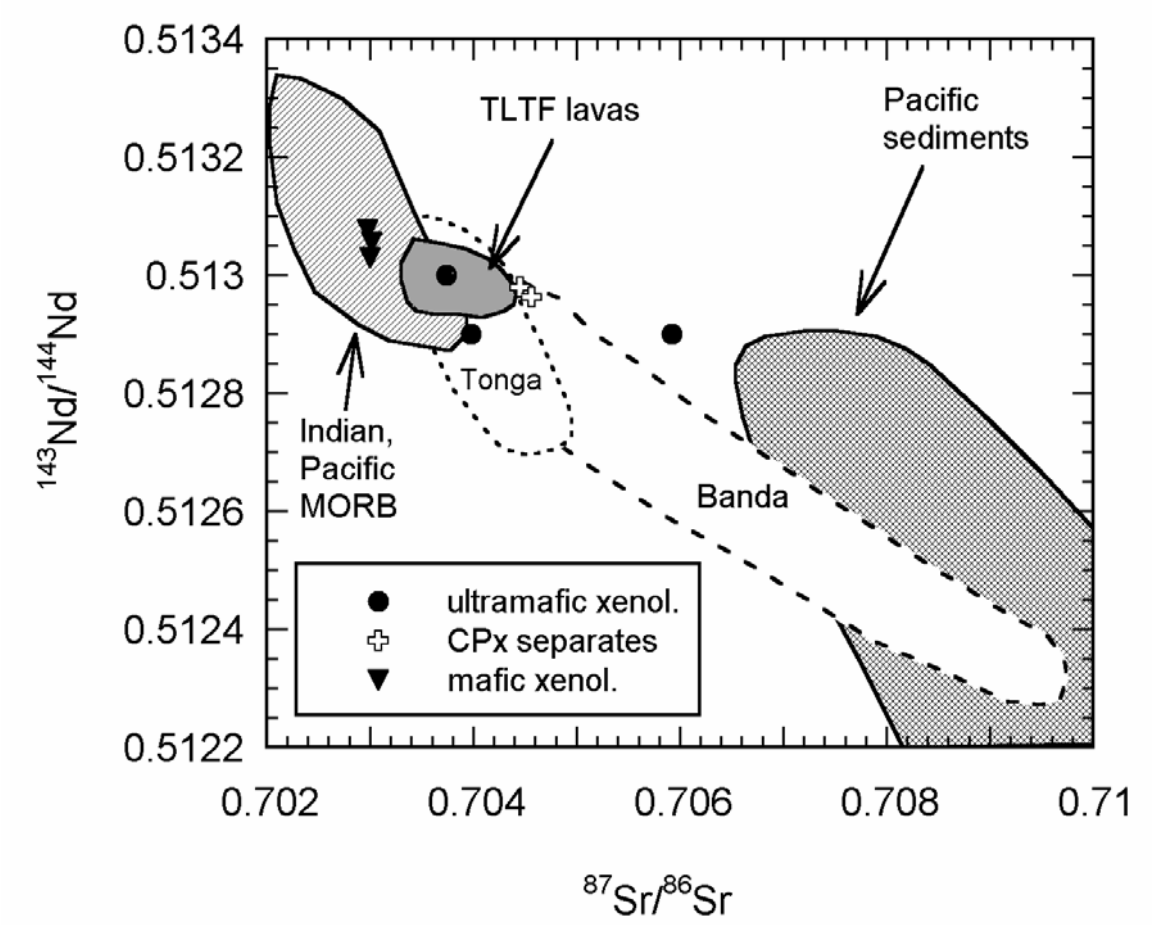

Figure 4-11. Nd vs Sr isotopic compositions of the mafic and ultramafic xenoliths relative to possible source in the area. Data from this study; and White (1987), Othman et al. (1989), Ewart and Hawkesworth (1987) Vroon et al. (1993), and Stracke and Hegner (1998).

Although the TLTF lavas have a MORB-type Nd isotopic signature, some of them are displaced to slightly elevated $^{87}Sr/^{86}Sr$ values compared to the Indian and Pacific MORB. The elevated Sr isotopic ratios suggest involvement of sedimentary and/or altered oceanic crust material. Altered oceanic crust is expected to acquire higher $^{87}Sr/^{86}Sr$ as a result of interaction with seawater, but at the same time it will preserve its $^{143}Nd/^{144}Nd$ due to the relative immobility of the REE during hydrothermal alteration. Incorporation of material in the TLTF magmas from altered oceanic crust, therefore, may produce the trend exhibit by the TLTF volcanoes (Fig. 4-11). In addition, incorporation of small amount of

sediment or material from the metasomatized mantle wedge in the TLTF magma also can produce the observed elevated $^{87}Sr/^{86}Sr$ ratios coupled with elevated $^{143}Nd/^{144}Nd$ and this mechanism will be discussed in greater details later below.

Pb Isotopic Variations in the Mafic and Ultramafic Xenoliths

The mafic xenoliths show an overall small range in their Pb isotopic compositions with two of the analyzed samples having compositions similar to the TLTF lavas, and two exhibiting slightly lower $^{207}Pb/^{204}Pb$ compared to the TLTF lavas (Fig. 4-12). The mafic xenoliths plot entirely within the field of the Pacific MORB, in agreement with their trace element and Nd isotopic characteristics indicating derivation from a depleted mantle source. The similarity between the Pb isotopic compositions of the mafic xenoliths with the Pacific MORB indicates that the oceanic crust beneath the TLTF islands most probably originated at a spreading center in the Pacific Ocean.

The ultramafic xenoliths trace element patterns and petrographic observations indicate that the New Ireland forearc mantle wedge (i.e., at present, the area beneath the TLTF island chain) has been metasomatically modified by fluids released during earlier subduction of the Pacific plate beneath the Indo-Australian plate (McInnes et al. 2001, Grégoire et al. 2001, Franz et al. 2002). It is difficult to put a time frame on the metasomatic events, but it is plausible to suggest that the forearc region was continuously flushed by hydrous fluids more or less as long as the Pacific plate subduction was active. TLTF volcanism, however, postdates the active subduction by several million years (McInnes et al. 2001), indicating that it is not directly caused by the metasomatic event.

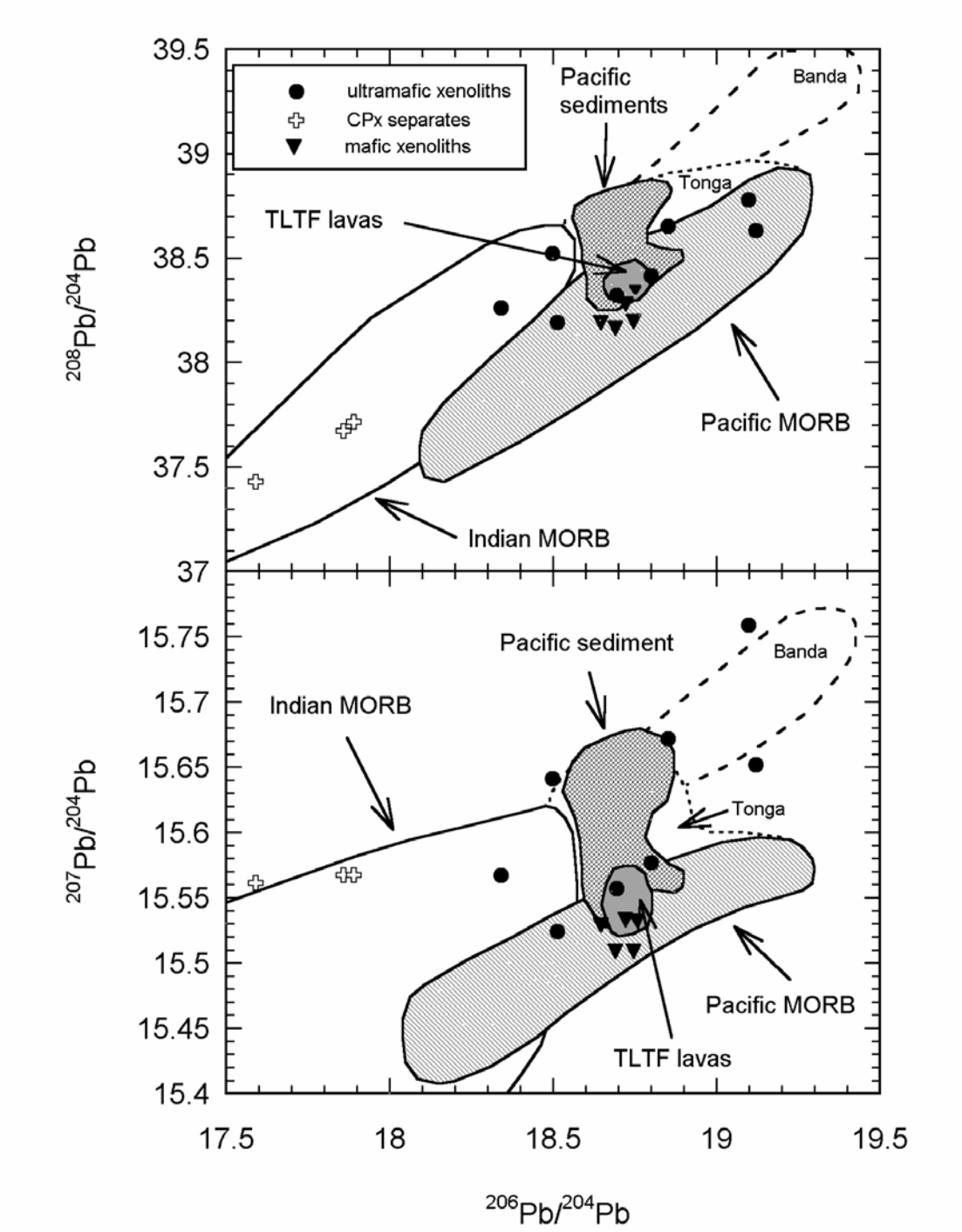

Figure 4-12. Pb isotopic compositions of mafic and ultramafic xenoliths relative to possible sources in the area. Data sources form this study and same sources as in Figures 4-11.

During active subduction, the cold oceanic lithosphere will maintain a relatively cold thermal regime in the forearc region, unless very young oceanic lithosphere is subducted (Harry and Green 1999). It is difficult to determine the age of the subducted slab beneath New Ireland, but we can speculate that it was relatively old, Jurassic or Cretaceous in age, formed probably sometime before the Ontong Java Plateau emplacement (Cretaceous). The thermal regime, therefore, was probably not suitable to induce partial melting in the fore-arc mantle wedge, and during that time fluids released mainly from compaction and dehydration of the sedimentary layer of the subducted oceanic slab flushed the fore-arc mantle wedge and caused the widespread metasomatism observed in the ultramafic xenoliths. The Pb isotopic compositions of most of the ultramafic samples show elevated $^{207}Pb/^{204}Pb$ relative to the Pacific MORB and plot close to the Pacific sediment field and Banda arc volcanics (Fig. 4-12). Previous studies showed that the isotopic compositions of Tonga and Banda arc volcanics are result of subduction of continental material (Vroon et al. 1993) and, therefore, the Pb isotopic compositions of the ultramafic xenoliths with elevated $^{206}Pb/^{204}Pb$ and $^{207}Pb/^{204}Pb$ can be best explained by addition of Pb by dehydration and compaction of the subducted sediments during the earlier period of subduction. Two of the analyzed ultramafic xenoliths (562F and 552H), however, plot within the field of the Pacific MORB indicating that they may represent samples from the Pacific oceanic mantle more or less uncontaminated by sedimentary material (Fig. 4-12, Table 4-2). Sample 562F have Pb isotopic composition similar to the TLTF lavas and its Pb isotopic composition can be generated also by contamination of the xenolith with Tubaf magma during the eruption. On the other hand, sample 562B, and particularly the 3 clinopyroxene separates from

ultramafic xenolith samples show higher $^{207}Pb/^{204}Pb$ at relatively lower $^{206}Pb/^{204}Pb$ and plot away from the fields defined by the Pacific MORB and sediments (Fig. 4-12). Several authors have suggested involvement of Indian-type mantle in the SW Pacific arcs (Hickey et al. 1995, Woodhead et al. 1998) and in the Eastern Australia Cenozoic basalts (Zhang et al. 2001). The clinopyroxenes and sample 562B show Pb isotopic compositions similar to the Indian type mantle indicating that there may be remnants of old lithosphere in the TLTF mantle wedge. Alternatively, their isotopic compositions can be a result of involvement of Australian subcontinental mantle in the mantle wedge beneath the TLTF, as will be discussed below. Regardless of the origin of the Pb isotopic signature in the clinopyroxene separates, the ultramafic samples show a very wide range and point toward 3 different Pb sources involved in the mantle wedge beneath TLTF, which can be identified as Pacific-type mantle, Pacific sediments, and either Indian-type mantle or Australian subcontinental mantle.

Indian Ocean-Type Mantle Versus Australian Subcontinental Mantle Incorporation in the Mantle Wedge Beneath TLTF

Two possibilities must be considered for the origin of the Indian Ocean-type Pb end-member identified in the mantle wedge beneath the TLTF islands. It can be either a result of involvement of Indian-type mantle or Australian subcontinental mantle in the TLTF mantle wedge, or alternatively, it could be created by local processes. The origin of the Indian-type mantle signature has been attributed to a contamination of a depleted mantle source, isotopically similar to Pacific-Atlantic MORB, with either deep plume material or with Gondwana subcontinental lithosphere (Hickey-Vargas et al. 1995 for extensive discussion). In the case of the plume hypothesis, it is considered that one or a number of plumes that presumably caused the Gondwana break-up, contaminated the

depleted mantle in the region. In the case of the sub-Gondwana lithosphere contamination hypothesis, the isotopic signature was acquired as a result of a long-term subduction along the Gondwana margins that supplied sedimentary material to the deep mantle beneath the region. The Pb isotopic signature in both scenarios requires involvement of old (continental) material that has evolved initially at high μ ($^{238}U/^{204}Pb$) and then has experienced U loss (or Pb gain) and has evolved after that at low μ for a long period of time. Subcontinental lithosphere, Earth's core, and subducted slabs have been considered as candidates for the low μ reservoir (Murphy et al. 2002).

Locally, contamination of the TLTF mantle wedge with ancient low μ material can explain the origin of the isotopic signature of the clinopyroxenes and sample 562B. Contamination as a result of the most recent subduction or by deep mantle plumes, however, can be ruled out because the Pacific subducted sediments do not have the required Pb isotopic composition, and the isotopic signature of the TLTF magmas does not support deep plume material involvement. Therefore, it is highly unlikely that the observed isotopic compositions can be created as a result of local processes, suggesting that Indian-type mantle material or Australian subcontinental mantle was incorporated in the TLTF mantle wedge. On Figure 4-13, the xenoliths are shown in comparison with Cenozoic alkali basalts from Eastern and North Eastern Australia. The basalts tap different parts of the Australian subcontinental mantle (Zhang et al. 2001) and it can be seen that overall they plot within the field of the Indian Ocean-type MORB. Basically, it appears that whether we will call the elevated $^{207}Pb/^{204}Pb$ end-member "Indian Ocean-type mantle" or "Australian sublithospheric mantle" is more or a less circular argument, because Australia was part of the Gondwana before the super-continent breakup.

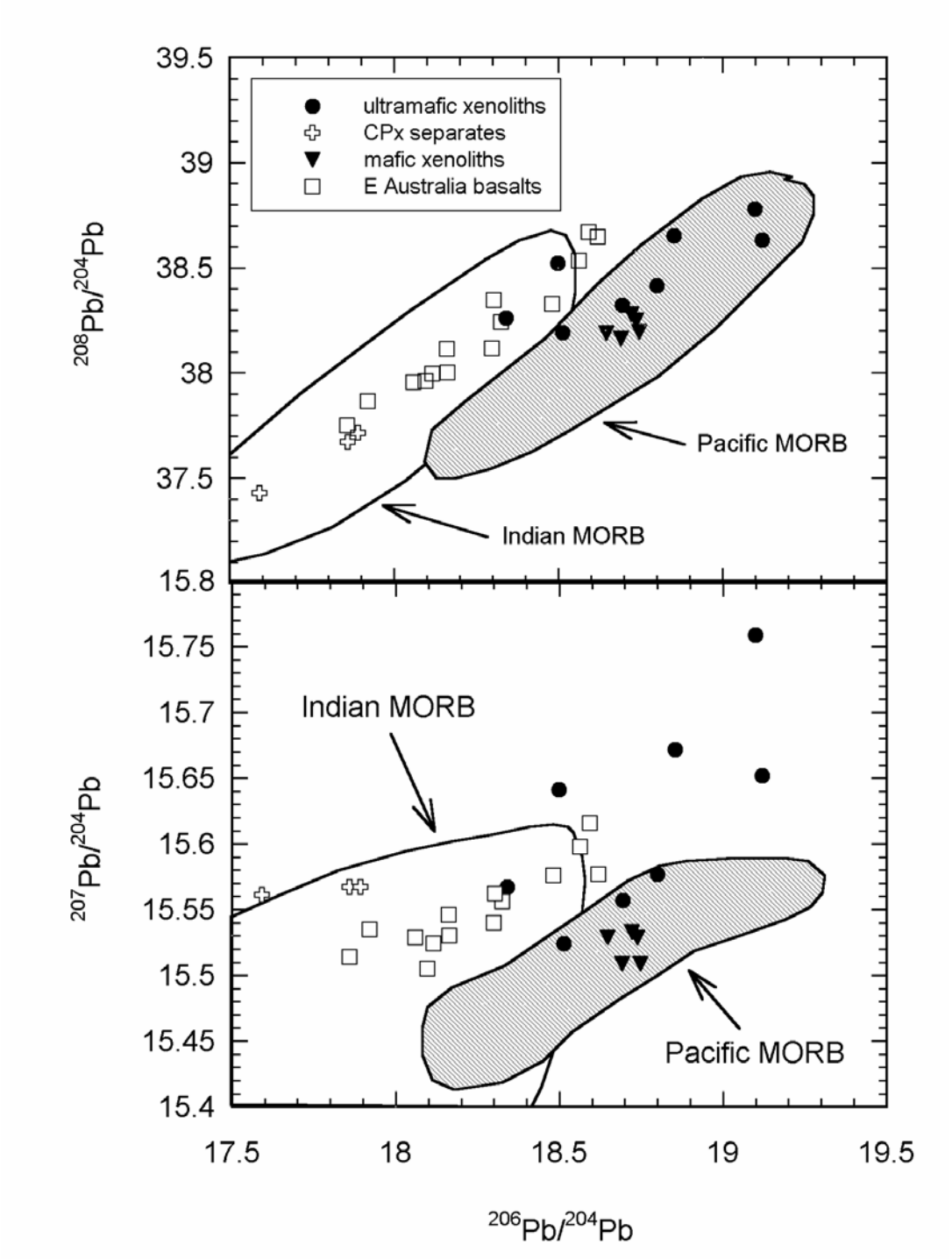

Figure 4-13. Pb isotopic compositions of xenoliths relative to Indian, Pacific MORB, and Eastern and North Eastern Australia basalts. Data sources same as in Figure 4-11. Australian basalts data from Zhang et al. (2001).

The Australian sub-lithospheric mantle, therefore, is expected to have more or less similar Pb isotopic signature to the Indian-type mantle. It is not clear, however, how this component was incorporated beneath the TLTF island arc. Some studies demonstrate that clinopyroxene can be very refractory and preserve its chemical signatures even if the rest of the rock is altered (Machado et al. 1986). Therefore, it is possible that the clinopyroxenes are surviving fragments from the old sub-Gondwana lithosphere, trapped in the area after the super-continent breakup. Alternatively, it is possible that the Australian sublithospheric mantle is displaced east and northeast with the northward movement of the Australian continent (R. Russo, personal communication) and so becomes incorporated in the source of the magmas in the region. Further support for the latter possibility comes from isotopic compositions of lavas from Woodlark and Manus back-arc basins, as will be discussed below.

Relationships between Compositions of Xenoliths and Regional Volcanism

TLTF lavas show a very restricted range in their Pb isotopic compositions, compared to the possible sources in the area and they plot within the field of the Pacific MORB (Fig. 4-12). In addition, if only the high-precision Pb isotopic compositions of Lihir and seamount lavas (and ores) are considered, they form a trend parallel to the NHRL and plot in the Pacific MORB field (Fig. 3-3 and 3-4, Chapter 3), indicating that the Pb is mainly contributed by Pacific MORB-type source. There are, however, small, but distinct isotopic variations between the volcanic centers, indicating of some variations in the source components. The Sr isotopic compositions in the lavas indicate involvement of material from either altered oceanic crust or sediments or from the metasomatized ultramafic assemblage beneath the volcanoes (Fig. 4-14). The TLTF lavas plot at the higher $^{207}Pb/^{204}Pb$ end of the Pacific MORB array, which may also indicate

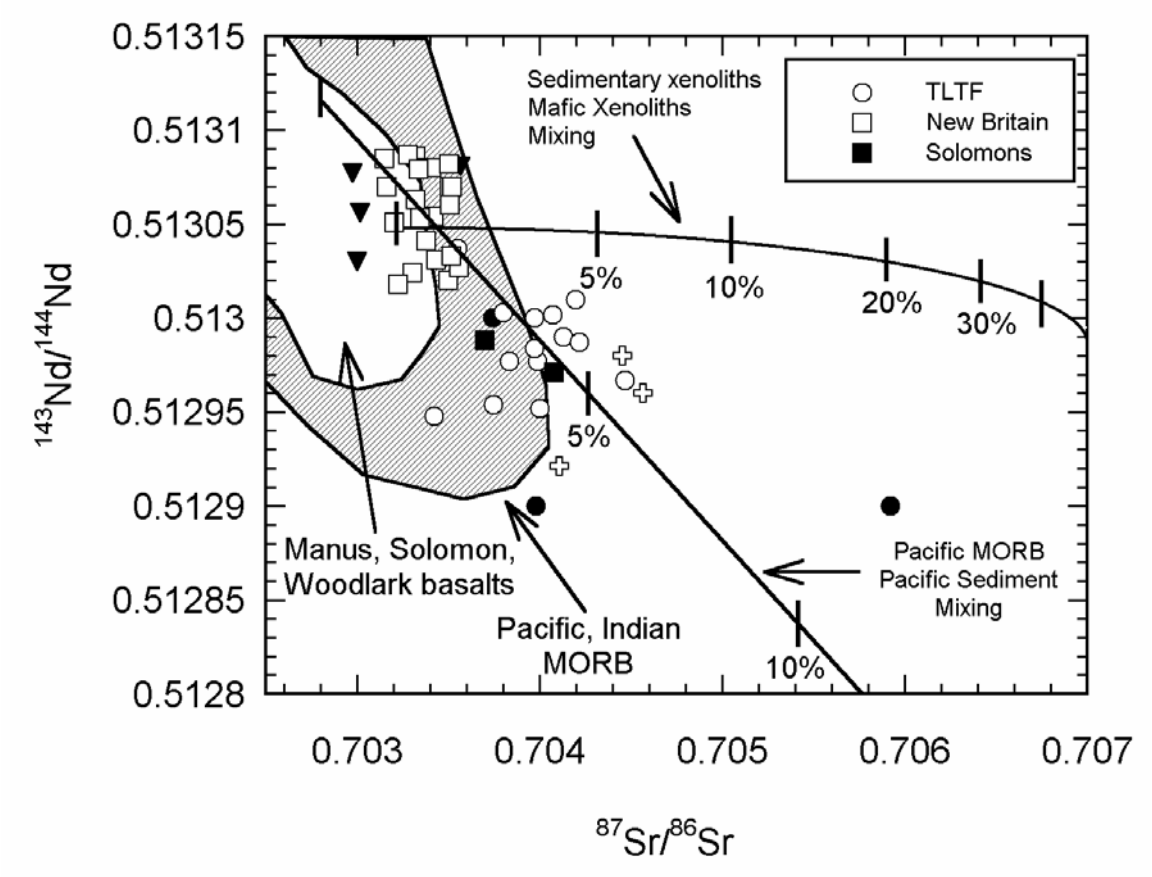

Figure 4-14. Nd vs Sr isotopic compositions for island arc and back-arc basins lavas in the region with possible mixing relationships between Indian-Pacific MORB and Pacific sediments or mafic and sedimentary xenoliths. Note that some of the TLTF lavas overlap with the Pacific-Indain MORB field, and some show elevated $^{87}Sr/^{86}Sr$ that can be explained by small amount of sedimentary component contribution, for more discussion see the text. Data from this study, White (1987), Othman et al. (1989), Hickey-Vargas et al. (1995), Woodhead et al. (1998), and Kamenetsky et al. (2001).

minor incorporation of more radiogenic Pb, either from subducted sediments or from the metasomatized xenoliths. Overall, the Pacific sediments show much higher $^{207}Pb/^{204}Pb$ than the lavas in the area (Fig. 4-12), and mixing calculations indicate that only minor (ca. from 0% to maximum around 5-6%) incorporation of Pacific sediments can explain the isotopic compositions of the TLTF lavas (Appendix C). Using sedimentary and mafic xenoliths as end-members in the mixing calculations indicates very high (more than 50%) sedimentary contribution (Appendix C), which is not supported by the lavas' Sr and Nd

isotopic compositions. Sr and Nd isotopic values indicates maximum of about 5 to 6% sedimentary material incorporation in the lavas, more or less independent on whether the Pacific MORB-Sediment or mafic-sedimentary xenolith components are used as end-members in the mixing calculations (Fig. 4-14). The mixing calculations involving sedimentary xenoliths (and also near-surface sediments) from the region must be interpreted with care because some of the analyzed sediments, notably sediments from the Solomon plate (Woodhead et al. 1998) show isotopic similarity with the TLTF and New Britain volcanics. These Late Cenozoic sediments, however, contain large amount of pyroclastic material delivered to the basin from the surrounding arcs (Lackschewitz et al. 2003). Therefore, it is plausible to suggest that the Pb and Nd (note for example the elevated $^{143}Nd/^{144}Nd$ end of the Pacific sediment field on Figure 4-11) isotopic similarity in this case is simply due the fact that a significant amount of material was provided to the local sediments from the surrounding volcanoes. An argument in favor of this suggestion is the fact that the metasomatic signature in the ultramafic xenoliths suggests that fluids released from the subducted sediments had quite variable Pb isotopic compositions compared to the Cenozoic Solomon plate sediments. The Cretaceous Ontong Java Plateau must had been emplaced in Cretaceous or older oceanic crust, which is now subducted underneath TLTF area. We can thus argue that the sediments subducted beneath the TLTF islands were quite variable, in age and composition, consisting of young and Cretaceous or older deep marine sediments, therefore, spanning the whole range of the Pacific sediment field shown of Figure 4-12.

Lavas from the New Britain arc front and Eastern Manus Basin spreading center (Fig. 4-1) show very similar Pb isotopic compositions to the TLTF volcanoes (Fig. 4-15).

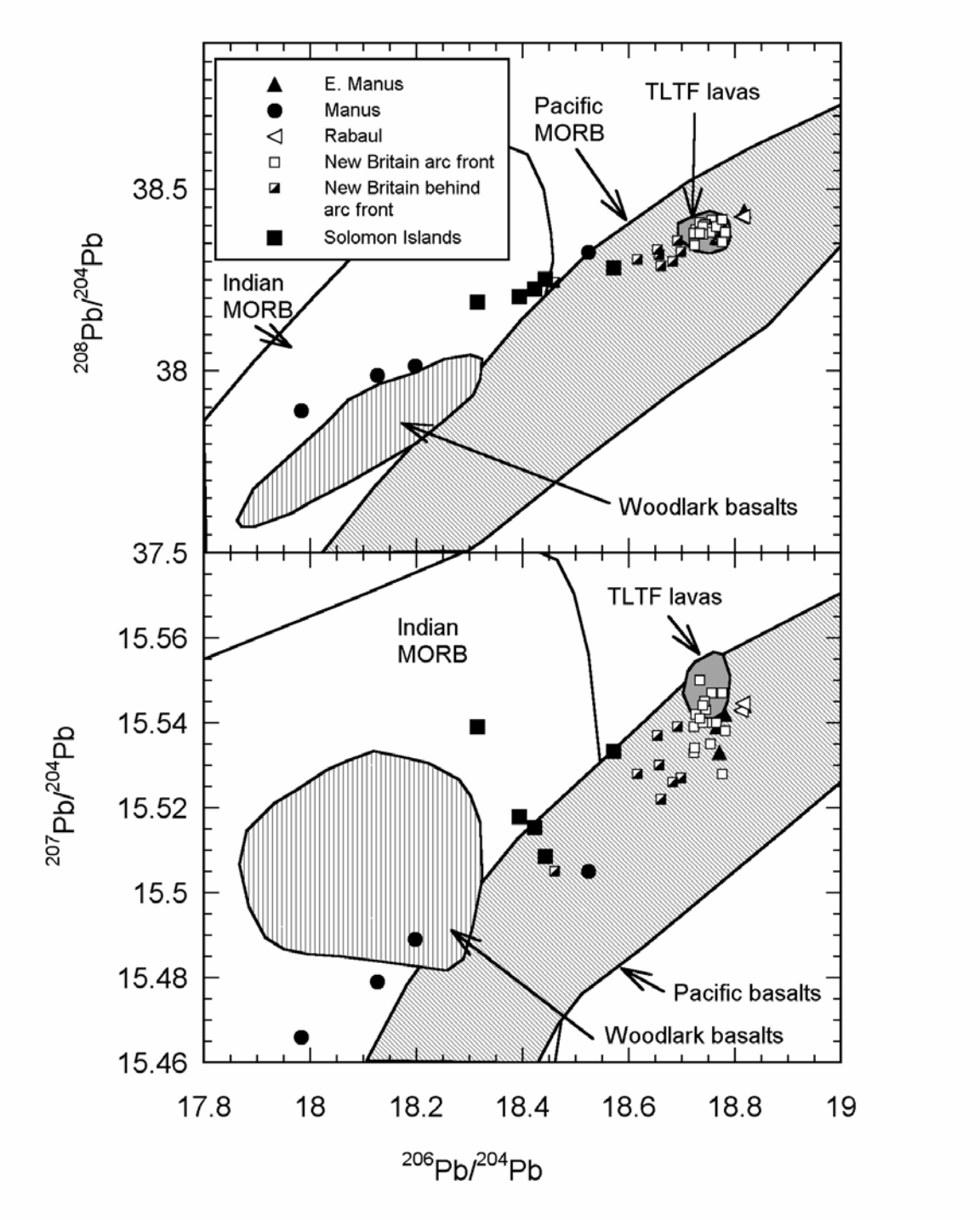

Figure 4-15. Pb isotopic compositions of lavas from TLTF, New Britain, Solomon Islands, Manus and Woodlark back-arc basins. Data sources form this study and same sources as in Figure 4-11.

The current volcanism on New Britain is related to the Solomon plate subduction, which is composed of basalts with geochemical and isotopic similarity to Pacific MORB (Woodhead et al. 1998). The Pb isotopic signature in New Britain frontal arc volcanoes was interpreted to reflect derivation from subducted altered oceanic crust with Pacific affinity (Woodhead et al. 1998). The eastern part of the Manus spreading center (Fig. 4-1) with its Pb isotopic similarities to TLTF and New Britain arc lavas, suggest that the magma composition is either inherited from the previous Pacific plate subduction, or is related to the present-day Solomon plate subduction. New Britain, E. Manus, and the TLTF lavas plot within the field of the Pacific MORB indicating that their Pb is primarily controlled by the subducted oceanic slab (Fig. 4-15). Once, however, the active volcanism in the region is located relatively far away from a subduction zone, it appears that an isotopic signal from the local mantle begins to be identifiable in the lavas. For example, the New Britain lavas erupting behind the volcanic front show lower $^{206}Pb/^{204}Pb$ and not so low $^{207}Pb/^{204}Pb$ and $^{208}Pb/^{204}Pb$, a trend interpreted to be a result of mixing between Indian and Pacific type mantle, as the subducting slab influence decreases with the increase in the distance from the trench (Woodhead et al. 1998). A similar trend is identifiable in the lavas from the Manus basin. The eastern part of the basin is in close proximity to active subduction and the Pb isotopes indicate derivation from subducted slab with Pacific affinity, similar to the TLTF and New Britain lavas. The Pb isotopic composition of the lavas in the NW part of the basin, however, is different (Fig. 4-15). There is probably no subducting slab underneath the NW part of the basin and appears that the Indian-type mantle signal begins to show in the local upwelling mantle as evidenced by the lavas plotting at slightly higher $^{207}Pb/^{204}P$ and $^{208}Pb/^{204}Pb$ relative to

Pacific MORB (Fig. 4-15). Solomon Islands, located south-south east of TLTF and New Britain, show less radiogenic $^{206}Pb/^{204}Pb$ compared to TLTF and New Britain, and also form a trend that can be explained by mixing of components between Pacific and Indian type mantle components (Fig. 4-15). The older volcanism in the Solomons was related to the Pacific plate subduction, however, after the collision of the Ontong Java plateau, the Pacific plate subduction ceased and subduction of the Woodlark Basin slab underneath the Solomon Islands began in an eastward direction (Mann and Taira 2004). The origin of the islands isotopic signature can be explained by mixing between Pacific and Woodlark material because the available data from young eruptive centers in the Solomon Islands form a trend toward the Woodlark basin samples (Fig. 4-15). The basin basalts exhibit higher $^{207}Pb/^{204}Pb$ than the Pacific MORB, and plot entirely within the Indian mantle field (i.e. apparently the local mantle Pb isotopic composition), identifiable also in the New Britain behind-arc volcanoes, NW Manus spreading center, and in the Tubaf ultramafic xenoliths. The Woodlark Basin samples have Pb isotopic compositions similar to young Eastern Australia basaltic centers (compare Fig. 4-13 and Fig. 4-15), indicating that the Woodlark lavas may be related to material derived from the Australian subcontinental mantle. Recent studies indicate the importance of lateral flow in the mantle, and in this case, the northward movement of Australia may cause lateral displacement of the mantle in the region (R. Russo 2004 personal comm.). Therefore, it may be that the Woodlark basin lavas are tapping Australian sublithospheric mantle laterally “squeezed out” by the northward motion of the continent. Alternatively, fragments from the subaustralian mantle can be entrapped in the upwelling mantle

underneath Woodlark basin and so can influence the isotopic compositions of the ridge lavas.

Model for the Alkaline Magmatism in the TLTF Area

It is generally accepted that island arc calc-alkaline magmatism results from lowering the melting point of the mantle wedge peridotite as a result of fluid introduction from the dehydration of subducted slab (Tatsumi 1989). Some models also indicate that the subducted slab may undergo partial melting and produce adakites (Martin 1999), or the resultant melts may metasomatize the depleted mantle wedge peridotites, which subsequently melt to produce the island-arc magmas (McInnes and Cameron 1994, Schiano et al. 1995). Some recent experiments, however, indicate that there is a complete miscibility between silicate melts and hydrous fluids at high temperatures and pressures, suggesting that it may be difficult or even irrelevant to attempt to distinguish fluids and melts in subduction zones, unless we are concerned with relatively low temperature and pressure zones, such as the forearc region, where hydrous fluids are expected to dominate (Bureau and Kepler 1999). So, in the TLTF island-arc system, therefore, we can suggest that part of the fluids, mainly from the subducted sedimentary assemblages, is released in the forearc area and the fluid reacts with the mantle wedge to create the observed metasomatic features in the ultramafic xenoliths (Fig. 4-16A). No significant mantle melting occurs at this stage because the temperature is relatively low due to the subducting cold oceanic slab. It is quite possible that most of the metasomatized ultramafic xenoliths recovered from Tubaf lavas are samples representative of this hydrated forearc mantle wedge. They contain hydrous minerals such as amphibole and phlogopite (Franz et al. 2002) and my results indicate that their

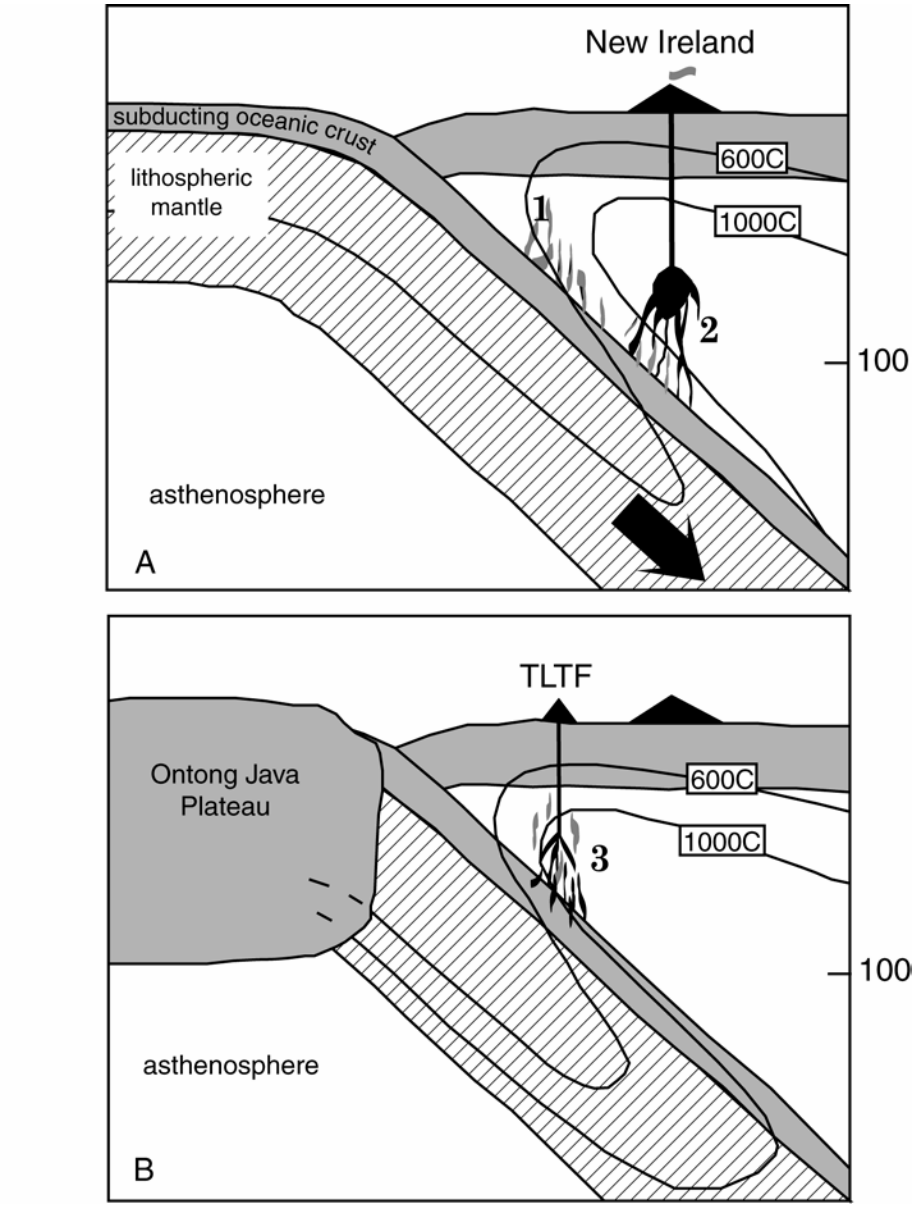

Figure 4-16. Cartoon summarizing the suggested origin of the TLTF volcanism. Mantle isotherms after Tatsumi (1989). A. Normal Pacific plate subduction under the Indo-Australian plate and formation of New Ireland, New Britain, and Solomon Islands island arcs as a result of dehydration of the subducting slab and melting in the mantle wedge (zone 2). Dehydration of the sedimentary layer of the subducting slab without melting due to cold thermal regime causing widespread hydrous metasomatism in zone 1. B. Ontong Java plateau collision and termination of the New Ireland volcanism due to the cease in the active subduction. Mantle isotherms gradually recover and eventually cause release of melt-fluid phase from the stalled slab in zone 3, which leads to the TLTF volcanism (see text for more discussion).

Pb and Sr isotopic compositions are quite variable, a result of incorporation of material from at least 3 sources, including contribution from the Pacific sediments.

The TLTF lavas are alkaline, and although not uncommon in island arc settings, they are not the dominant rock series associated with subduction zones, nor are they common in the island arcs around Paupua New Guinea. In general, such alkaline magmas is believed to be generated either by low degrees of partial melting at high pressures (e.g. alkaline basalts) or by low degrees of melting of metasomatized mantle source (e.g. lamproites, kimberlites) (Winter 2001). Experiments show that low degrees of partial melting of metasomatized mantle xenoliths generate highly alkaline magmas, such as lamproites and kimberlites (Lloyd et al. 1985), not observed in the TLTF area. Although the ultramafic xenoliths are metasomatized, their major and trace element data indicate that they are overall very depleted (Table 4-1, Fig. 4-5 and 4-10). Unrealistically small degrees of partial melting (ca. 0.1% or less) of these mantle wedge samples are required to produce the enrichment of trace elements observed in the TLTF lavas. Isotopically, the TLTF lavas are very different from the ultramafic xenoliths (Fig. 4-12), also indicating that the magmas can not be a direct result of partial melting of this hydrated part of the mantle wedge.

The isotopic compositions of the TLTF lavas suggest that a major portion of their incompatible elements was probably derived from the subducted oceanic slab. However, there are no samples directly available from the subducted oceanic slab in the region, therefore, we can either estimate it from available data for fresh Pacific MORB or alternatively, we can use the data for the mafic xenoliths, obtained in this study as a proxy for the composition of the subducted oceanic crust. Tectonic considerations

suggest that the oceanic crustal portion of the slab subducted beneath the TLTF arc could be similar to the mafic xenoliths. If the New Ireland-New Britain arc originated as an intra-oceanic arc, then we can assume that the Pacific oceanic crust began to subduct underneath its own detached fragment, probably sometime during Oligocene-Eocene time, based on the oldest subduction-related volcanic rocks on New Britain (Woodhead et al. 1998). Therefore, at some point at the past, the subducted slab and the oceanic crust underlying the TLTF chain, probably were parts of the same oceanic slab. The trace-element compostitions of the mafic xenoliths (Fig. 4-9) indicate that the oceanic crust beneath the arc is altered; in agreement with many studies that show oceanic crust slab alteration shortly after its formation (Bach et al. 2001, Kelley et al. 2003). Therefore, the use of altered oceanic crust is likely a better proxy for the composition of the subducted slab compared to fresh MORB. The question remains as to how material from the subducted slab was incorporated in TLTF magmas.

Components can be released from the subducted lithosphere either as hydrous fluids or melts, or as a homogeneous mixture of both (Bureau and Kepler 1999). Extended trace element patterns (Fig. 4-6) and elemental ratios, such as K_2O/Ba vs Ba/La (Fig. 4-17) for the TLTF lavas indicate enrichment by hydrous fluids. K and Ba are fluid mobile and highly incompatible elements, La is also highly incompatible but is fluid immobile element. Elevated Ba/La ratios indicate fluid-generated enrichment or sediment contribution, if the ratios are greater than 70 (Patino et al. 2000). The TLTF lavas show relatively low Ba/La, notably the Tubaf lavas, indicating very minor sediment contribution, in agreement with the isotope data. The K2O/Ba ratios of the TLTF lavas are close to MORB, especially altered MORB, and overlap with the data for the mafic

xenoliths (Fig. 4-17), further indicating that the TLTF magmas are probably related to components from the subducted oceanic slab. The increase in the alkalinity (mainly K_2O) in island arc lavas is generally attributed to either a decrease in the amount of melting as a result of a decrease in the slab H_2O content with depth or to K-rich fluid/melt release as a result of phlogopite or phengite breakdown with increasing depth of subduction.

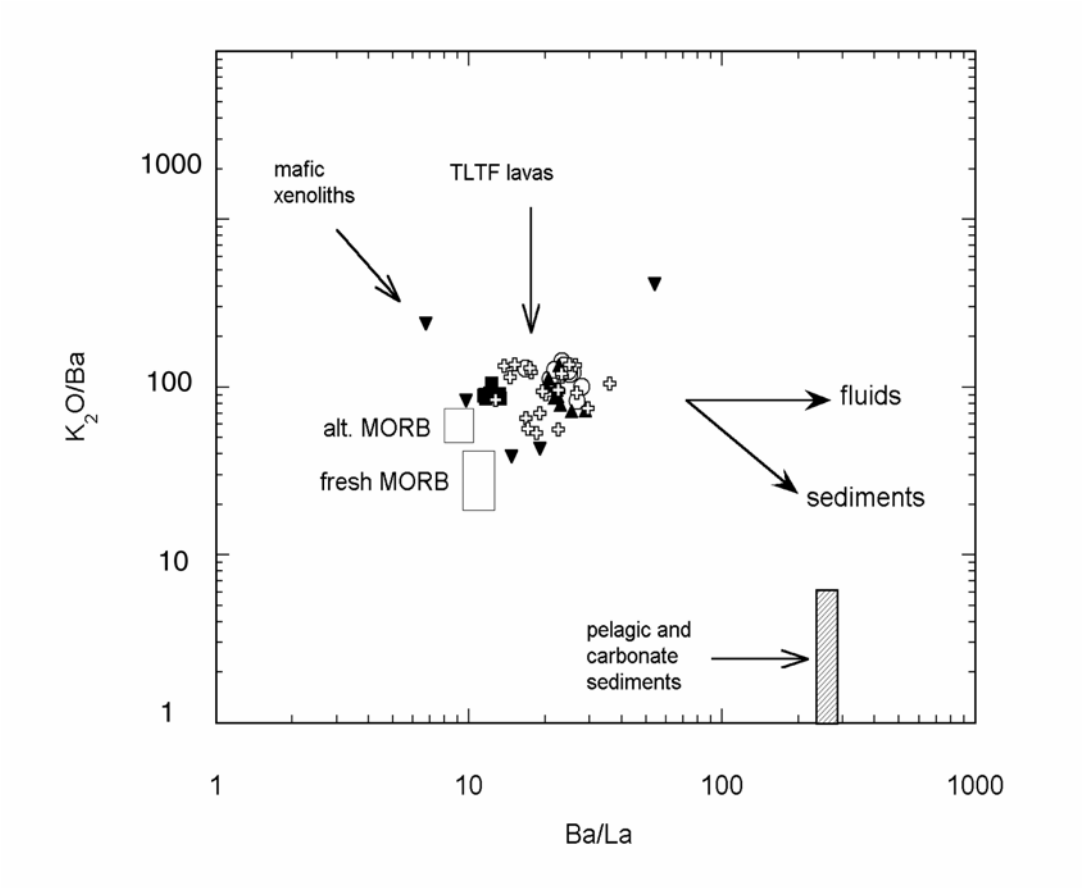

Figure 4-17. Comparison of K_2O/Ba vs Ba/La between lavas and mafic xenoliths and pelagic and carbonate sediments. Increase in Ba/La at relatively constant K/Ba is expected if the elements were derived from the subducted slab via aqueous fluids, which is not the case. Data for sediments from Patino et al. (2000).

Schmidt (1996) demonstrated that during low-T dehydration of a subducting slab most of the K is contained in phengite, which is stable to about 300 km depth. Fluids and/or melts released during the phengite breakdown would be strongly enriched in K and as a

consequence, arc magmas erupting behind the volcanic front, over deeper Benioff zone, will be enriched in K (Schmidt 1996). The high volatile contents in TLTF magmas, notably the Tubaf mafic lavas (Chapter 3, Fig. 3-8), suggests abundant fluid presence in the magma source, and thus a decrease in H_2O content with depth along the slab was probably not responsible for the alkaline character of the TLTF magmas.

It is generally considered that melting of the slab does not occurs in subduction zones because the geothermal gradient along the Benioff zone is low and subducted oceanic lithosphere dehydrates before it reaches the wet solidus temperature. Only in some extreme situations, such as subduction of very young lithosphere or cessation of the subduction, is the geotherm high enough to potentially melt the oceanic crust. In the case of subduction termination, as is the TLTF situation, rising temperature in the mantle wedge will transfer its heat to the once cold slab and the solidus front will move to the forearc region (Fig. 4-16B). The resultant melts are expected to have adakitic, sodic-alkaline, or potassic-ultrapotassic affinity (Martin, 1999, Defant and Kepezhinskas 2001, Hermann and Green 2001, Mungall 2002). Adakitic compositions, (andesitic to dacitic lavas with relatively high alkali, MgO, and Sr contents, and very low Y and HREE), are indicative of melting of a mafic source where garnet and/or amphibole are residual phases (Martin 1999). Although the TLTF magmas exhibit some features similar to adakites, such as high Sr and alkali contents, their SiO_2 is much lower than typical adakites and they do not show the characteristic Y and HREE depletions of slab melts. Some experimental studies, however, indicate that alkalic melts are generated during reaction between slab-derived partial melt with mantle wedge peridotite (Yaxley 2000). Intriguingly, McInnes and Cameron (1994) observed hydrous, alkali-rich

alumosilicate melt inclusions in xenoliths and xenocrysts from Simberi Island, part of TLTF chain. The melt in these inclusions, named SCHARM (sulfate-carbonate-H_2O-alkali-rich-alumosilicate melt), is similar to phonolite and is enriched in Sr, Ba, Cl, F, S, and CO_2. Partial melting of the stalled hydrated altered oceanic crust beneath TLTF with a feldspathic or phengite phase contributing to the initial melt probably produced the alkali-rich alumosilicate melts observed in the inclusions (McInnes and Cameron 1994). Sr content in the SCHARM is very high, ranging from 2000 to 4800 ppm, and Sr isotopic compositions in the host xenoliths range from 0.7036 to 0.7042, similar to the range observed in the TLTF lavas (McInnes and Cameron 1994). These melt inclusions provide direct evidence for partial melting of the oceanic crust beneath TLTF islands. Dilution and mixing of this hydrous slab melt with peridotite melts from the hot mantle wedge could possibly produce magmas with major and trace element compositions similar to the TLTF alkaline lavas. For example, on Figure 4-18 (A and B) the SCHARM composition is shown relative to the ultramafic xenoliths from the area. TLTF lava major element characteristics can be modeled by diluting the slab melt with ultramafic material from the mantle wedge. Simple mixing between SCHRAM and ultramafic xenoliths, and subsequent crystal fractionation may produce magmas with chemical characteristics similar to the lavas in the region. In such scenario, the incompatible elements will be mainly derived from the slab component because even the metasomatized ultramafic xenoliths are very depleted in incompatible elements (Table 4-1, Fig. 4-5 and 4-10). It is difficult to produce a definitive quantitative model due to the lack of trace element data for the slab component, however, the Pb isotopic compositions of the lavas support this

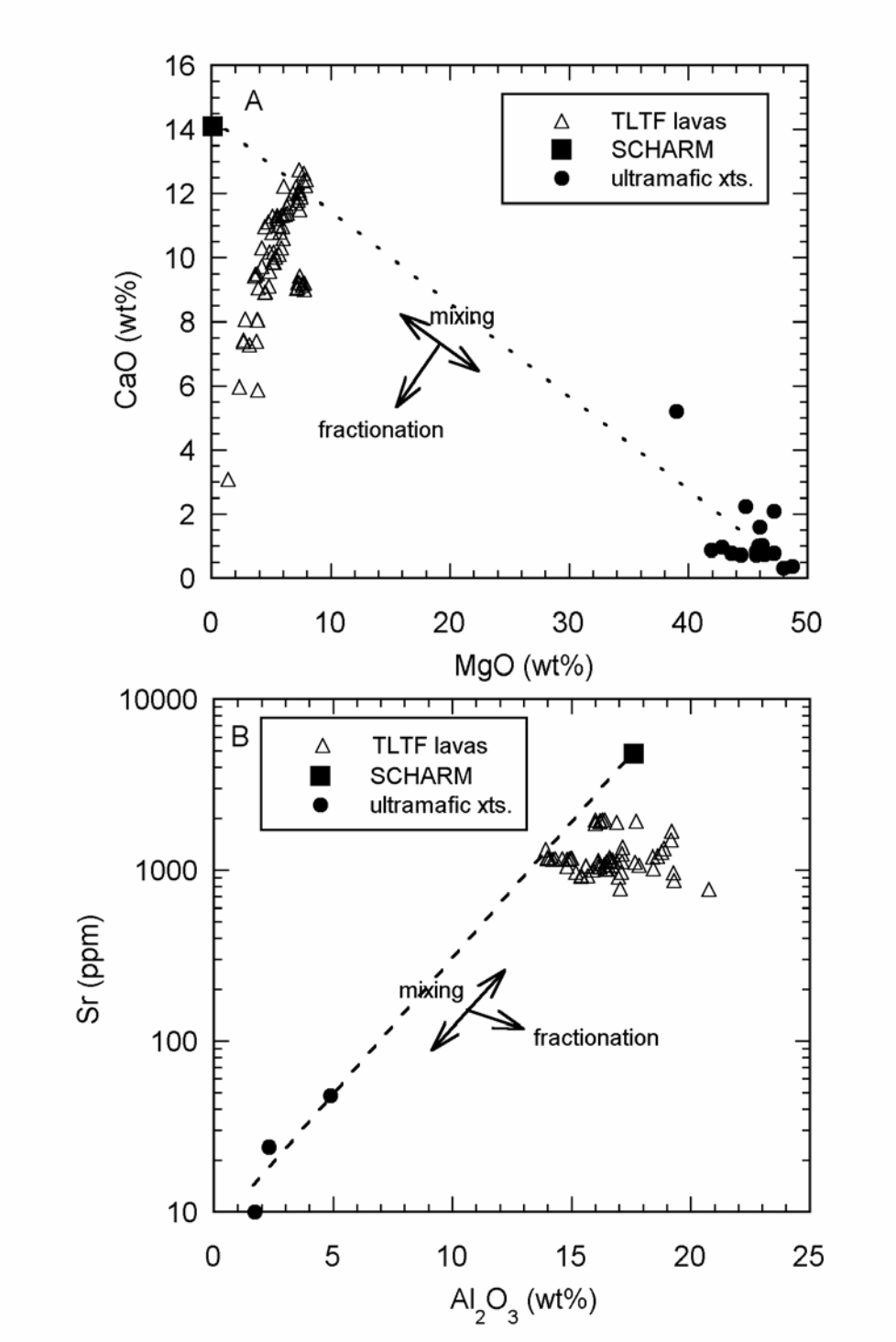

Figure 4-18. Interaction of slab melt (SCHARM) with ultramafic mantle and formation of the TLTF magmas. Note that simple mixing accompanied with crystal fractionation may account for the chemistry of the TLTF lavas. SCHARM data from McInnes et al. (1994).

model, because they suggest involvement of subducted oceanic crust. Sr and Nd isotopic data are also consistent with derivation from altered oceanic crust.

The mantle-isotherm rebound mechanism summarized on Figure 4-16 may provide explanation for the origin of the TLTF magmatism, however, the inactive Manus-Kilinailau trench appears to extend further to the north and northwest (Fig. 4-1), without any evidences for active volcanism. If the mantle isotherm rebound mechanism is correct, then it will be expected that the TLTF-type volcanism will continue further to the north, parallel to the inactive trench, which apparently is not the case. An alternative model for the development of the TLTF arc, based on extensional tectonics was proposed by McInnes (1992). In this model, the back-arc spreading in the Manus basin caused formation of pull-apart basins in the TLTF area which lead to decompressional meting in the mantle wedge underneath the islands. The isotope data for the mantle xenolith samples presented here do not support origin of the magmas only by partial meting of the metasomatized mantle wedge. However, the extensional tectonics in the area probably played important role for the generation of conduits for the magma ascend to the surface. In addition, large-scale extension in the area will lead to mantle upwelling underneath the TLTF islands. Then, if there is no stalled subducted slab, there won't be a barrier to prevent Pacific mantle influx in the region. Such scenario for Pacific mantle incorporation is consistent with the Pacific isotopic signature in the lavas, however, decompressional melting involving Pacific mantle is not consistent with the island-arc signature in the TLTF lavas. The isotope and trace-element data for the TLTF lavas, in combination with tectonic considerations can probably be best explained by a hybrid model involving mantle isotherm rebound, which generated the required thermal regime

to induce partial slab melting, accompanied by extensional tectonics that created suitable conditions for ascent of the magmas that formed the volcanic islands. Then, the absence of extensional tectonic regime north of the TLTF islands may explain the lack of volcanic activity further north along the inactive Manus-Kilinailau trench.

It is difficult to conclude if the slab component was solely melt or fluid derived, based on the existing data. Fluid-mobile elements will be readily released during dehydration of the slab and so will easily swamp the isotopic and fluid-mobile traceelement characteristics of the mantle wedge. Observed enrichments in fluid-mobile elements,uch as Ba, K, U, and Pb in the TLTF lavas (Fig. 4-6) are in good agreement with slab dehydration. Other incompatible, but fluid immobile element concentrations, however, can not be solely derived from the mantle wedge, due to its very depleted nature (Fig. 4-5 and Fig. 4-10). Therefore, a hybrid melt+fluid component release from the slab will probably best explain the chemical features of the TLTF lavas. Experiments by Bureau and Keppler (1999) show that any proportion of melt and fluid can exist as a homogeneous mixture at subduction P-T regime. This homogeneous mixture separates into a hydrous melt and fluid phase with decreasing in temperature and pressure, conditions that will occur during magma ascent to the surface. Therefore, erupted lavas (even the ones with highest volatile content, e.g. Tubaf lavas) will not preserve the starting volatile content of such a fluid:melt mixture. The fate of the fluid component, however, may be important for the ore formation mechanism. If, for example, a homogeneous 50:50 fluid-melt mix is formed at the slab-mantle interface and then this mixture ascends quickly and encounters a stalled magma body close the surface, the ascent will stop and rapid exsolution of great amount of volatile components will occur.

This component will be highly charged with ore-forming metals and may form large ore deposits, as described in Chapter 3.

In addition to this study, it has been noted before that Au and Cu deposits are associated with slab melts (Defant and Kepezhinskas 2001, and references therein). Mungall (2002) also suggested that arc magmas with high potential to generate Au and Cu deposits will be either adakitic, sodic-alkaline, or potassic-ultrapotassic. Favorable tectonic settings for generation of such magmas include regions of subduction of very young lithosphere or very slow or oblique convergence, flat subduction, and the cessation of subduction and subsequent release of slab-derived melt:fluid component, as is the TLTF case. Indeed, our Pb isotope study on the Au deposit on Lihir Island, and Au mineralization on Conical seamount show that the ore formation is intimately related to the magmatism in the area.

CHAPTER 5
SUMMARY AND CONCLUSIONS

The wealth of isotope and chemical composition data, including precise Pb isotope measurements, obtained in this study allowed me to look in details in the relationships between magmatism and ore deposit formation in SW Pacific island arcs. Important step was the development of the method for precise Pb isotope measurements by MC-ICP-MS (Nu Plasma). During the initial experiments, Pb and Tl from single-element, concentrated stock solutions were mixed in 2% HNO_3 prior to isotope ratio measurements. The results revealed relatively poor precision and accuracy of the Pb isotope measurements, large variations in ε^{205}Tl in the same standard (ranging from –3.9 to +30.1), and large variations in the observed Pb/Tl intensity ratios. When analyses were restricted to freshly mixed (<1 hour) Pb-Tl solutions, however, highly precise isotopic ratios were obtained for lead ($^{206}Pb/^{204}Pb$=16.9373 (+/-0.0011, 2σ), $^{207}Pb/^{204}Pb$=15.4907 (+/-0.0012, 2σ), and $^{208}Pb/^{204}Pb$=36.6935 (+/-0.0039, 2σ)) and for thallium (ε^{205}Tl=1.5 (+/-0.8, 2σ)). In addition, Pb/Tl intensity ratios were constant and corresponded to the mixing ratios of the prepared solutions. A series of experiments revealed that the poor precision and accuracy observed for the initial set of isotope ratio measurements resulted from variable photoxidation of Tl^+ to Tl^{3+} that occurs in the presence of Pb and solar UV radiation. This reversible reaction generates Tl^{3+} that behaves distinct from Tl^+ during desolvation and leads to consistently higher measured Pb/Tl and $^{205}Tl/^{203}Tl$ ratios. The extent of the interaction between Pb and Tl and the subsequent effect on isotope ratio measurements is sensitive to a combination of factors, including differences in the acid matrix and

molarity, desolvation conditions, and UV light exposure. It appears that the observed $\varepsilon^{205}Tl$ variations in the Pb-Tl^{3+}-bearing solutions dominantly result from mass-dependant differential diffusion of Tl during desolvation. Utilizing high-precision Pb isotope measurements allowed me to look in unprecedented details in the connection between magmatism and Lihir and Conical seamount gold deposit formation.

Lihir Island, part of the Tabar-Lihir-Tanga-Feni island chain in the SW Pacific, hosts the giant Ladolam gold deposit. Polymetallic gold mineralization also was discovered offshore at Conical Seamount in 1998 during RV SONNE cruise "SO-133". The seamount and the island are composed mainly of trachybasalts and basaltic trachyandesites, although some monzonites are found on Lihir. Sr isotopic analyses of mineralized samples from the island and the seamount suggest that most of the Sr is derived from the local alkaline lavas. Elevated $^{87}Sr/^{86}Sr$ ratios in some of the samples suggest that during the waning stages of the hydrothermal system, part of the Sr was contributed either from seawater or the thick sequence of marine sediments underlying the island.

High-precision Pb isotopic analyses conducted with MC-ICP-MS show that the ores and volcanic rocks share similar Pb isotopic compositions, suggesting that the Pb in the mineralized zones was ultimately derived from the local magmatic sources. The Pb isotopic data, however, reveal small, but significant, differences between the mineralized zones and the associated host lavas. Mineralized samples from Lihir have slightly less radiogenic lead isotopic ratios than their host lavas. These lead isotopic compositions are similar, however, to some of the fresh lavas recovered from Conical seamount and to a monzonite intrusion underlying the Ladolam deposit. Lead isotopic ratios in mineralized

samples from Conical seamount, however, are slightly more radiogenic than their host lavas and similar to those of fresh lavas recovered from nearby Tubaf and Edison seamounts. Petrographic observations and microprobe elemental analyses reveal a complex magmatic history for the magma chamber inferred beneath Conical seamount. Based on zoning patterns in the Conical clinopyroxenes, it appears that a sub-seamount magma chamber was recharged with a mafic magma similar to the most primitive, volatile-rich, and xenolith-bearing lavas recovered from Tubaf and Edison seamounts. Rapid cooling of this mafic magma accompanied by exsolution of metal-bearing fluids in the relatively shallow magma chamber is proposed as the mechanism that ultimately resulted in the observed gold mineralization. Similarity of the lead isotopic ratios between the ores and the mafic magmas in the area suggest that the ore metals were primarily derived from the recharging magma, not by hydrothermal leaching of the host lavas by seawater-derived hydrothermal fluid.

Numerous xenoliths recovered from TUBAF seamount, located in Tabar-Lihir-Tanga-Feni (TLTF) island chain (Papua New Guinea) provide a unique view of the elemental and isotopic composition of the mantle wedge beneath the arc and its relationship to the magmatism in the region. The ultramafic xenoliths exhibit a wide range in their Pb isotopic compositions, suggesting involvement of at least 3 components. Two of the components appear to be the Pacific oceanic mantle and Pacific sediments. Clinopyroxene separates from some of the ultramafic xenoliths exhibit low $^{206}Pb/^{204}Pb$ and high $^{207}Pb/^{204}Pb$, suggesting that the third component was Indian Ocean-type mantle or Australian subcontinental lithospheric mantle. The Sr and Nd isotopic compositions of

the xenoliths are also consistent with involvement of Pacific and/or Indian mantle and sediment components in the mantle wedge beneath TLTF islands.

Compared to the mantle wedge samples, TLTF lavas have very restricted Pb isotopic compositions within the Pacific MORB range, suggesting that the metasomatized part of the mantle did not play a major role in determining the isotopic characteristics of the magmas. Comparison of the volcanic rocks from the TLTF arc to lavas from New Britain arc and Eastern Manus basin suggests that the isotopic compositions of the lavas in the area are mainly controlled by subducted oceanic crust with Pacific MORB affinity. Intriguingly, once the subducted slab influence decreases, the Indian Ocean-type mantle signal begins to appear in the isotopic signature of the lavas in the region, as is demonstrated in lavas from the Solomon Islands, NW Manus and Woodlark back-arc basins.

The fact that TLTF lavas have isotopic compositions mainly inherited from the subducted oceanic crust suggests that the volcanism in the area is intimately related to the stalled oceanic crust beneath the islands. During active subduction of the Pacific plate the thermal regime in the fore-arc region was not suitable to induce partial melting. Once, however, active subduction ceased, the mantle isotherms gradually recovered and warmed up the subducted oceanic crust beneath the fore-arc region. The triggering event that caused the TLTF volcanism is probably related to hydrous melts released from the subducted oceanic crust accompanied by extensional tectonics caused by the spreading in the Manus back-arc basin. Dilution of the slab melt with depleted peridotitic component during melting of the mantle wedge resulted in magmas with similar chemical characteristics to the TLTF lavas. In such scenario the incompatible elements will be

completely controlled by the slab melts, which is evident in the Pacific isotopic signature observed in the TLTF lavas. In addition, the formation of highly hydrous melt or homogeneous fluid-melt mixture has important implications for the formation of ore deposits. If such fluid-melt mixture ascends quickly through the mantle and encounters a stalled magma body close the surface, the ascent will be terminated and rapid separation into hydrous melt and fluid component will occur. The exsolved fluid component will be highly charged with ore-forming metals and may contribute to the formation of large ore deposit close to the surface.

CHAPTER 6
FUTURE RESEARCH

A number of new questions that can be investigated further arose as a result of this study. The proposed ore deposit formation mechanism can be further addressed by detailed study of the fluid-melt inclusions discovered in the Conical Seamount clinopyroxenes. It is difficult to analyze these samples due to the fact that they contain fluid phase that will be lost if an attempt is made to open the inclusions. However, it may be possible to open the inclusions with small diameter laser beam (5-10 microns) while scanning on-line for certain ore-forming metals such as Cu, Zn, Au, Ag, and Pb on the high-resolution Element 2 mass-spectrometer. By utilizing time-resolved analysis software it may be possible to obtain quantitative information for the concentration of these elements in the inclusions and so provide evidences if they really trapped samples of the ore-forming solutions exsolving from a recharging magma. In addition, the developed high-precision Pb isotope measurement technique must be utilized in other studies of ore deposits associated with volcanic complexes. Such studies will confirm or rule out if the proposed ore-formation mechanism is a valid explanation for the origin of other ore deposits, or is applicable only for the Lihir and Conical seamount mineralizations. This will contribute to our understanding of the ore-formation mechanisms, and so will enhance our capabilities for finding new ore deposits.

More detailed study of young volcanic rocks from the arcs in the region, specifically if new samples from New Ireland and the Solomon Islands can be obtained, will provide further constrains on the magmato-tectonic evolution in the region. Useful

information about the changes through time in the subduction settings also can be obtained from studies of older magmatic rocks that at present built the cores of the arcs in the region. Important tectonic question, that remained unanswered, is why there is no volcanism along the inactive trench north of the TLTF chain. Topographic mapping and geophysical survey in the region of the inactive trench may reveal presence of subducted slab, thermal anomalies in the mantle wedge, and young seamounts.

One lava sample from Manus Island has very unusual Pb isotopic composition ($^{206}Pb/^{204}Pb$=16.240, $^{207}Pb^{204}Pb$=15.404, and $^{208}Pb/^{204}Pb$=35.899) that may represent important end-member in the mantle in the region. These results were not included in the dissertation because more samples are needed from the Manus Island to asses if this is the real isotopic composition or is a result of contamination. In addition, further useful information can be derived from new isotopic analyses of the available lava and xenolith samples. For example, Hf isotope measurements can provide invaluable constrains on the origin of HFSE signature in the arcs. An attempt can be made to separate vein material from the xenolith samples. In addition, separation of the xenolith samples on their main mineral constituents (i.e., Ol, Opx, Cpx) and subsequent elemental and isotopic analyses of the separated phases can provide useful information about the original composition of the mantle and the metasomatic agents (i.e., the vein material). This will contribute to our quest for deciphering of the composition of the mantle wedge in subduction zones.

APPENDIX A
MC-ICP-MS ANALYSES OF NBS 981 LEAD ISOTOPIC STANDARD MIXED WITH QCD ICP-MS THALLIUM STANDARD. TABLE INCLUDES WET PLASMA AND DSN FRESH AND AGED, EXPOSED TO LIGHT MIXED PB-TL SOLUTIONS ANALYSES.

Wet plasma analyses (fresh and aged mixtures)

date	time	Pb(ppb)	Tl(ppb)	Pb(V)	Tl(V)	Pb/Tl	$^{205}Tl/^{203}Tl$	$^{206}Pb/^{204}Pb$	error	$^{207}Pb/^{204}Pb$	error	$^{208}Pb/^{204}Pb$	error
4/9/2003	15:47	100	25	2.33	0.62	3.8	2.428083	16.93839	0.0013	15.49278	0.0012	36.7019	0.0033
4/9/2003	17:35	100	25	2.41	0.64	3.8	2.42749	16.93873	0.0015	15.49294	0.0013	36.70266	0.0036
4/10/2003	16:35	100	25	3.22	0.85	3.8	2.422347	16.93712	0.0012	15.49134	0.0012	36.69602	0.0028
4/10/2003	16:45	100	25	3.16	0.83	3.8	2.422695	16.93406	0.0012	15.48756	0.0014	36.69166	0.0034
4/10/2003	17:14	100	25	3.09	0.81	3.8	2.422703	16.93411	0.0009	15.48776	0.0011	36.68809	0.0031
4/10/2003	17:27	100	33	3.12	1.1	2.8	2.422574	16.93626	0.0011	15.49027	0.0009	36.69268	0.0024
4/10/2003	17:40	100	50	3.05	1.62	1.9	2.422236	16.93344	0.0011	15.48801	0.001	36.6878	0.0024
4/15/2003	15:08	100	25	2.87	0.75	3.8	2.424311	16.93694	0.0012	15.49196	0.0013	36.69877	0.0032
4/15/2003	15:36	100	25	2.76	0.73	3.8	2.424916	16.93693	0.0013	15.49151	0.0014	36.69651	0.0036
4/16/2003	11:42	100	33	3.07	1.06	2.9	2.423438	16.93728	0.0012	15.49082	0.0011	36.69555	0.0028
4/16/2003	13:46	100	25	3.04	0.8	3.8	2.419924	16.93752	0.0015	15.49203	0.0013	36.69769	0.0034
4/16/2003	15:18	100	33	3.09	1.07	2.9	2.420987	16.93562	0.0012	15.48968	0.0012	36.69069	0.0028
4/16/2003	16:08	100	33	2.49	0.85	2.9	2.426636	16.93395	0.0017	15.48901	0.0014	36.69096	0.0035
4/16/2003	16:19	100	25	2.41	0.62	3.9	2.426396	16.93787	0.0011	15.49222	0.0012	36.698	0.0029
4/16/2003	17:34	100	25	2.38	0.61	3.9	2.426063	16.93501	0.0012	15.49009	0.0011	36.69259	0.003
4/18/2003	14:50	50	12.5	1.79	0.47	3.8	2.413887	16.93834	0.0018	15.49158	0.0017	36.69704	0.0041
4/18/2003	16:14	50	12.5	1.7	0.45	3.8	2.416825	16.93423	0.0019	15.48863	0.0018	36.68889	0.0045
4/18/2003	17:24	~30	~9	1.26	0.37	3.4	2.41719	16.93765	0.0026	15.49079	0.0025	36.69517	0.0059
4/18/2003	18:40	~30	~11	1.33	0.45	3.0	2.417309	16.93446	0.0021	15.48931	0.0023	36.69089	0.0053
4/18/2003	20:00	100	25	3.27	0.86	3.8	2.416442	16.93934	0.0009	15.49234	0.0012	36.69809	0.0025
4/24/2003	11:46	100	10	2.55	0.27	9.4	2.426466	16.93575	0.0016	15.48898	0.0019	36.6941	0.005
4/24/2003	12:19	100	10	2.47	0.27	9.1	2.426784	16.93876	0.0016	15.49272	0.0016	36.70267	0.0042
4/24/2003	12:35	100	33	2.59	0.89	2.9	2.427411	16.93843	0.0011	15.49191	0.0011	36.70167	0.0029
4/30/2003	12:46	100	25	3.01	0.79	3.8	2.4236	16.93893	0.001	15.4926	0.0009	36.70008	0.0021
4/30/2003	14:03	100	25	3.11	0.82	3.8	2.421732	16.93965	0.0011	15.49267	0.001	36.70033	0.0027
4/30/2003	16:02	60	15	2.25	0.59	3.8	2.417424	16.93736	0.0012	15.49025	0.0012	36.69381	0.0028
4/30/2003	17:50	60	15	2.12	0.56	3.8	2.417969	16.93196	0.0015	15.48568	0.0015	36.68265	0.0033

4/30/2003	18:01	60	15	2.13	0.56	3.8	2.418011	16.93634	0.0015	15.48963	0.0014	36.69259	0.0034
5/19/2003	16:02	100	25	3.04	0.801	3.8	2.422256	16.93312	0.0013	15.48761	0.0013	36.69085	0.0032
5/19/2003	17:50	100	25	2.97	0.79	3.8	2.422927	16.93621	0.0013	15.48972	0.0012	36.69285	0.0032
5/19/2003	18:50	100	25	2.94	0.78	3.8	2.423181	16.93726	0.0013	15.49064	0.0013	36.69631	0.0029
6/17/2003	13:53	150	37.5	4.43	1.01	4.4	2.425222	16.9382	0.00064	15.49128	0.00064	36.69752	0.0017
6/17/2003	15:00	150	37.5	3.64	0.83	4.4	2.427048	16.93839	0.0009	15.49084	0.00099	36.69604	0.0025
6/17/2003	16:33	150	37.5	3.46	0.81	4.3	2.427193	16.93987	0.0009	15.49159	0.0009	36.69683	0.0021
6/17/2003	16:44	150	37.5	3.42	0.79	4.3	2.427209	16.93718	0.00092	15.49078	0.0011	36.69592	0.0027
6/18/2003	15:19	150	37.5	5.11	1.17	4.4	2.423866	16.93729	0.00072	15.48866	0.0007	36.69168	0.0017
6/26/2003	10:45	150	37.5	4.69	1.06	4.4	2.425101	16.93913	0.0009	15.49174	0.0009	36.69796	0.0024
6/26/2003	12:39	150	37.5	4.16	0.95	4.4	2.426988	16.93753	0.0013	15.49046	0.0014	36.69438	0.0029
6/26/2003	14:24	150	37.5	4.27	0.98	4.4	2.426716	16.93709	0.0008	15.49002	0.0008	36.69328	0.0021
6/29/2003	15:47	150	37.5	3.98	0.97	4.1	2.427079	16.93874	0.0009	15.49019	0.0009	36.69629	0.0024
6/29/2003	18:02	150	37.5	4.21	0.99	4.3	2.427373	16.93749	0.0009	15.48933	0.00085	36.69143	0.0021
8/4/2004	10:05	150	37.5	5.28	1.18	4.5	2.421467	16.93667	0.0007	15.4905	0.0007	36.69382	0.0017
8/4/2004	11:15	150	37.5	4.76	1.06	4.5	2.422327	16.93683	0.0007	15.49096	0.0009	36.69546	0.0022
8/4/2004	12:39	150	37.5	4.92	1.1	4.5	2.422691	16.93729	0.0007	15.49104	0.0008	36.69461	0.0019
5/24/2004	12:20	150	37.5	5.05	1.13	4.5	2.423905	16.93849	0.0006	15.49276	0.0006	36.70134	0.0016
5/24/2004	13:52	150	37.5	5.12	1.1	4.7	2.423473	16.93766	0.0009	15.49254	0.001	36.69913	0.0031
5/24/2004	17:07	150	37.5	5.14	1.15	4.5	2.42434	16.9364	0.0007	15.49059	0.0007	36.69534	0.0019

DSN analyses (only fresh mixtures)

6/27/2003	11:33	30	15	6.33	2.93	2.16	2.43142	16.9372	0.0007	15.49037	0.0006	36.69368	0.0014
6/27/2003	13:21	30	15	5.94	2.81	2.11	2.429287	16.93817	0.0011	15.49172	0.001	36.69416	0.0024
6/27/2003	18:26	30	15	5.8	2.9	2.00	2.428392	16.93736	0.0008	15.49052	0.0007	36.69332	0.0018
6/29/2003	12:10	30	15	6.58	3.24	2.03	2.429962	16.93753	0.0008	15.49166	0.0006	36.69706	0.0018
6/29/2003	13:27	30	15	6.72	3.38	1.99	2.426896	16.93721	0.0004	15.49079	0.0004	36.69423	0.001
6/29/2003	15:13	30	15	6.09	2.98	2.04	2.428361	16.93697	0.0007	15.48969	0.0006	36.6905	0.0016
7/7/2003	13:58	30	7.5	6.74	1.6	4.21	2.428993	16.93792	0.0008	15.49195	0.0006	36.69843	0.0018

7/7/2003	14:30	30	7.5	6.54	1.67	3.92	2.429184	16.93787	0.0005	15.49113	0.00047	36.69477	0.0011
7/17/2003	12:09	30	5	6.16	0.99	6.22	2.430151	16.93796	0.0007	15.49089	0.00075	36.69515	0.0018
7/17/2003	12:28	30	10	6.05	1.94	3.12	2.430076	16.93666	0.00055	15.49024	0.00054	36.69326	0.0012
7/17/2003	12:44	30	5	6.14	0.99	6.20	2.430005	16.93751	0.00075	15.49067	0.0007	36.69286	0.0019
7/17/2003	13:41	30	5	5.87	0.93	6.31	2.430216	16.93639	0.0005	15.48991	0.00046	36.69044	0.0013
7/25/2003	12:31	35	6	6.52	1.11	5.87	2.427294	16.9365	0.00077	15.49013	0.00078	36.69213	0.0019
7/25/2003	13:04	35	7	6.58	1.38	4.77	2.427246	16.93718	0.0006	15.49025	0.00062	36.69288	0.0018
7/28/2003	10:37	35	8.75	7.32	1.72	4.26	2.427816	16.93728	0.0006	15.49128	0.0007	36.69338	0.0017
7/28/2003	12:24	35	7	8.39	1.94	4.32	2.427203	16.93746	0.00047	15.49042	0.00038	36.69278	0.0011
7/28/2003	12:45	25	6.25	5.24	1.29	4.06	2.427322	16.93744	0.00083	15.4905	0.00083	36.69278	0.0022
8/4/2003	11:10	35	8	9.46	2.14	4.42	2.429772	16.93789	0.0004	15.4909	0.0004	36.69409	0.0009
8/4/2003	12:46	30	10	7.95	2.43	3.27	2.427151	16.93671	0.00045	15.4897	0.00044	36.68978	0.0014
8/11/2003	11:09	35	11	7.8	2.33	3.35	2.42999	16.93803	0.00039	15.49155	0.00038	36.69588	0.0009
8/11/2003	14:16	35	7	8.02	1.65	4.86	2.428814	16.93651	0.0005	15.49026	0.0006	36.69296	0.0015
8/11/2003	14:27	35	7	7.92	1.61	4.92	2.42895	16.93695	0.00057	15.48995	0.00058	36.69175	0.0017
8/30/2003	11:27	30	7.5	7.65	1.87	4.09	2.429561	16.93809	0.0006	15.4912	0.0006	36.6946	0.0016
8/30/2003	12:35	30	5	7.14	1.23	5.80	2.429206	16.93745	0.0006	15.49028	0.0008	36.69353	0.0014
9/9/2003	11:30	30	6	9.2	1.65	5.58	2.428018	16.93726	0.0004	15.4902	0.0004	36.69323	0.001
1/16/2004	11:45	30	5	14.3	1.9	7.53	2.43584	16.93775	0.00024	15.49001	0.0003	36.69566	0.0007
1/16/2004	12:15	-	-	7	1.2	5.83	2.435932	16.9373	0.0007	15.4892	0.0007	36.69238	0.0025
1/16/2004	12:30	-	-	5.92	1.7	3.48	2.436826	16.93821	0.0007	15.49174	0.0007	36.69983	0.0015
1/16/2004	12:45	-	-	6.1	1	6.10	2.435133	16.93665	0.0006	15.48869	0.0006	36.6912	0.0016
1/16/2004	13:00	-	-	5.8	0.8	7.25	2.436877	16.93666	0.0025	15.48961	0.0025	36.69389	0.0062
1/28/2004	11:22	30	1.5	10.15	0.46	22.07	2.434523	16.93753	0.0009	15.491	0.0009	36.69798	0.0026
3/20/2004	11:50	30	6	6.08	1.11	5.48	2.426919	16.93671	0.0007	15.49018	0.0007	36.69198	0.0019
3/20/2004	10:28	30	7	6.2	1.45	4.28	2.428351	16.93667	0.0007	15.4888	0.0008	36.69082	0.0019

DSN analyses (only aged mixtures)

1/31/2003	14:38	25	6.25	3.91	0.81	4.83	2.425995	16.92747	0.0007	15.47911	0.0007	36.66228	0.0017
3/7/2003	14:57	25	6.25	3.88	0.79	4.91	2.42585	16.92768	0.0007	15.47957	0.0007	36.66337	0.0034
3/7/2003	12:29	25	6.25	3	0.4	7.50	2.431511	16.92131	0.0013	15.47028	0.0016	36.63652	0.0037
3/7/2003	13:45	25	6.25	2.82	0.35	8.06	2.430128	16.92479	0.0014	15.47405	0.0015	36.64273	0.0043
3/7/2003	14:32	25	6.25	2.75	0.33	8.33	2.430539	16.92527	0.0015	15.47463	0.0015	36.64484	0.0039
4/14/2003	15:55	25	6.25	5.61	0.4	14.03	2.436885	16.90209	0.0009	15.44429	0.001	36.55217	0.0028
4/14/2003	16:29	25	12.5	4.59	0.43	10.67	2.439107	16.88809	0.0011	15.4265	0.0011	36.49594	0.0027
4/14/2003	16:43	25	6.25	4.71	0.34	13.85	2.437605	16.89876	0.0009	15.44126	0.0009	36.54276	0.0027
4/14/2003	16:53	25	6.25	4.52	0.33	13.70	2.437095	16.90074	0.0009	15.44337	0.0014	36.55172	0.0033
4/14/2003	17:06	25	12.5	4.12	0.39	10.56	2.438322	16.89115	0.0009	15.43005	0.0011	36.50629	0.0028
5/1/2003	9:54	25	12.5	4.61	0.6	7.68	2.432966	16.90446	0.001	15.44745	0.001	36.55822	0.0029
5/1/2003	10:05	25	12.5	4.57	0.62	7.37	2.433105	16.90472	0.0008	15.44633	0.0007	36.55523	0.0033
6/17/2003	10:27	30	15	9.07	2.19	4.14	2.42782	16.94429	0.00049	15.50005	0.00056	36.72487	0.0018
6/17/2003	11:58	30	15	7.87	1.78	4.42	2.429406	16.94533	0.00054	15.50076	0.00076	36.72605	0.0012
6/17/2003	11:04	20	10	4.08	1.88	2.17	2.430352	16.93843	0.00097	15.49086	0.00097	36.69435	0.00218
6/17/2003	11:27	20	10	4.99	2.26	2.21	2.430697	16.93709	0.00084	15.4891	0.00085	36.68974	0.0019
6/17/2003	11:39	20	10	4.89	2.23	2.19	2.43063	16.93606	0.00062	15.4885	0.00057	36.68808	0.0015
6/18/2003	16:33	30	15	10.6	2.44	4.34	2.424665	16.94188	0.00045	15.49872	0.00045	36.723	0.0012
6/18/2003	16:43	30	15	9.7	2.23	4.35	2.425039	16.9459	0.0004	15.50152	0.0005	36.72995	0.0014
6/18/2003	17:02	20	10	4.54	2.07	2.19	2.42668	16.93618	0.0009	15.48832	0.0009	36.68654	0.0021
6/27/2003	11:05	30	15	6.94	1.3	5.34	2.430499	16.94407	0.0007	15.50022	0.0006	36.72609	0.0014
6/27/2003	13:00	30	15	6.2	2.87	2.16	2.428866	16.93925	0.0009	15.49179	0.0009	36.69594	0.002
7/7/2003	15:14	30	15	7.4	0.93	7.96	2.429591	16.93539	0.00052	15.48757	0.00065	36.68606	0.0017
7/7/2003	16:12	30	15	7.13	0.91	7.84	2.429926	16.93383	0.00055	15.48591	0.0007	36.67956	0.0019
7/9/2003	11:21	30	7.5	9.13	0.37	24.68	2.432247	16.91608	0.0013	15.46207	0.0017	36.60579	0.0053
7/9/2003	11:34	30	7.5	8.46	0.23	36.78	2.43694	16.88894	0.0009	15.42336	0.0011	36.48609	0.0035
7/9/2003	11:56	20	10	4.31	1.34	3.22	2.431438	16.92969	0.0009	15.478	0.0011	36.65302	0.0028
7/18/2003	11:12	30	5	6.97	1.06	6.58	2.431888	16.93518	0.0006	15.48854	0.0006	36.68767	0.0016

7/18/2003	11:28	30	3.3	6.46	0.65	9.94	2.431786	16.93477	0.0006	15.48829	0.0006	36.68743	0.0016
7/18/2003	11:44	30	5	6.51	0.95	6.85	2.431789	16.93478	0.0009	15.48808	0.0009	36.68764	0.002
7/25/2003	11:45	30	3.3	5.33	0.52	10.25	2.427554	16.93397	0.0007	15.48726	0.0008	36.68437	0.0022
7/25/2003	12:00	30	5	5.48	0.73	7.51	2.427259	16.93548	0.0007	15.48988	0.0008	36.69147	0.0019
7/28/2003	11:34	30	5	6.2	0.916	6.77	2.427692	16.93424	0.0011	15.48771	0.00062	36.68274	0.0027
7/28/2003	11:51	30	3.3	5.82	0.54	10.78	2.427588	16.9348	0.0007	15.48855	0.0009	36.68694	0.0022
7/28/2003	12:06	30	5	6.03	0.61	9.89	2.427538	16.93341	0.0008	15.48644	0.0009	36.6812	0.0023
7/28/2003	13:00	30	5	6.16	0.37	16.65	2.42872	16.92823	0.001	15.4793	0.001	36.65755	0.0033
7/28/2003	13:41	30	5	6.02	0.72	8.36	2.428334	16.93579	0.0007	15.48782	0.0009	36.68416	0.0023
7/28/2003	14:15	30	10	6.06	1.17	5.18	2.42813	16.93683	0.0006	15.4901	0.0006	36.69353	0.0012
7/28/2003	14:35	30	5	6.31	0.89	7.09	2.428283	16.93605	0.0007	15.48947	0.00076	36.6901	0.0019
7/28/2003	14:50	30	3.3	6.04	0.55	10.98	2.428343	16.93248	0.0006	15.48494	0.0007	36.67786	0.002
7/28/2003	15:06	35	1.75	7.44	0.31	24.00	2.428129	16.93212	0.00077	15.48503	0.0009	36.67919	0.0026
8/4/2003	11:31	30	5	7.97	0.84	9.49	2.430205	16.93298	0.0006	15.48504	0.0006	36.67574	0.0018
8/4/2003	11:59	30	10	7.89	1.28	6.16	2.428692	16.94049	0.0005	15.49543	0.0005	36.70888	0.0012
8/4/2003	13:04	30	5	7.8	0.7	11.14	2.427786	16.93514	0.0006	15.48794	0.0008	36.68531	0.0021
8/4/2003	13:31	30	3.3	7.5	0.52	14.42	2.428532	16.92716	0.0005	15.4786	0.0006	36.65861	0.0022
8/4/2003	13:54	30	5	7.54	0.29	26.00	2.428887	16.92593	0.0007	15.47625	0.0009	36.65009	0.0027
8/4/2003	14:16	30	5	7.02	1.1	6.38	2.427826	16.93439	0.00045	15.48732	0.0005	36.68501	0.0011
8/11/2003	11:49	30	5	7.55	0.748	10.09	2.430022	16.93321	0.0006	15.48512	0.0008	36.67716	0.0022
8/11/2003	12:29	30	10	7.37	1.08	6.82	2.428507	16.94217	0.0006	15.49706	0.0006	36.71342	0.0017
8/11/2003	12:52	30	5	7.46	0.49	15.22	2.429095	16.93461	0.0008	15.48749	0.0009	36.68453	0.0025
8/11/2003	13:10	30	3.3	7.15	0.39	18.33	2.430377	16.92745	0.0009	15.47646	0.001	36.65055	0.0027
8/11/2003	13:26	30	5	7.23	0.24	30.13	2.430564	16.92407	0.0013	15.47411	0.0013	36.64125	0.0039
9/9/2003	11:11	30	5	8.81	1.31	6.73	2.427693	16.93839	0.0004	15.49219	0.0004	36.69981	0.0012
9/9/2003	11:41	30	5	8.76	1.37	6.39	2.427364	16.94009	0.0005	15.49383	0.0006	36.7053	0.0012
9/9/2003	13:36	30	3.3	8.36	0.54	15.48	2.429	16.92854	0.0008	15.47801	0.001	36.65691	0.0027
9/9/2003	14:23	30	5	8.13	0.31	26.23	2.429496	16.92261	0.0009	15.47144	0.0012	36.63511	0.0039
9/9/2003	14:37	30	5	7.47	0.72	10.38	2.429389	16.92407	0.0009	15.47384	0.0009	36.64265	0.0025

1/16/2004	12:15	30	5	7	1.2	5.83	2.435932	16.9373	0.0007	15.4892	0.0007	36.69238	0.0025
1/16/2004	12:30	30	10	5.92	1.7	3.48	2.436826	16.93821	0.0007	15.49174	0.0007	36.69983	0.0015
1/16/2004	12:45	30	5	6.1	1	6.10	2.435133	16.93665	0.0006	15.48869	0.0006	36.6912	0.0016
1/16/2004	13:00	30	3.3	5.8	0.8	7.25	2.436877	16.93666	0.0025	15.48961	0.0025	36.69389	0.0062
1/16/2004	13:15	30	5	5.41	0.41	13.20	2.440755	16.91161	0.0011	15.45493	0.0013	36.58905	0.0046
1/20/2004	11:15	-	-	14.1	0.9	15.67	2.435648	16.91741	0.0006	15.46184	0.0006	36.60861	0.0024
1/20/2004	11:30	30	5	7.3	0.74	9.86	2.43271	16.93091	0.0006	15.48179	0.0007	36.6681	0.002
1/20/2004	11:57	30	5	6.45	0.33	19.55	2.434024	16.92081	0.0008	15.46764	0.0008	36.62215	0.0023
1/20/2004	12:12	30	5	6.25	0.4	15.63	2.435168	16.91234	0.0008	15.45594	0.0008	36.58676	0.0022
1/20/2004	12:47	-	-	14.66	1.04	14.10	2.43811	16.92143	0.0009	15.46541	0.0005	36.61826	0.0024
1/20/2004	13:04	30	5	7.39	0.58	12.74	2.438278	16.92494	0.0006	15.47282	0.0009	36.63845	0.0025
1/20/2004	13:26	30	5	6.6	0.4	16.50	2.437774	16.91029	0.0009	15.45343	0.0012	36.58043	0.0034
1/20/2004	13:54	30	3.3	6.21	0.2	31.05	2.440531	16.91092	0.0018	15.45447	0.0023	36.57848	0.006
1/26/2004	-	-	-	7.96	0.99	8.04	2.435563	16.93419	0.0006	15.48671	0.0006	36.68498	0.0017
1/26/2004	-	-	-	14.8	1.14	12.98	2.438093	16.92407	0.0005	15.4686	0.0005	36.62939	0.0014
1/26/2004	-	30	5	7.44	0.59	12.61	2.43752	16.91946	0.0012	15.4667	0.0013	36.62141	0.0036
1/26/2004	-	30	5	6.57	0.44	14.93	2.439954	16.91026	0.0009	15.45536	0.0014	36.58461	0.0039
1/26/2004	-	30	3.3	6.78	0.31	21.87	2.437076	16.92539	0.0016	15.47331	0.0016	36.64231	0.0048
2/5/2004	14:06	30	5	13.97	1.1	12.70	2.437465	16.92709	0.0007	15.4717	0.0008	36.63827	0.0019
2/5/2004	14:23	30	5	12.17	1.03	11.82	2.438611	16.92756	0.0003	15.47285	0.0003	36.64295	0.0009
2/10/2004	10:10	30	5	7.41	0.68	10.90	2.437107	16.92688	0.0005	15.47728	0.0007	36.65289	0.0019
2/10/2004	10:50	-	-	5.36	0.53	10.11	2.434553	16.92505	0.0007	15.47549	0.0006	36.64613	0.0019
2/10/2004	15:39	-	-	5.56	0.31	17.94	2.439537	16.91111	0.0011	15.45522	0.0013	36.58326	0.0039

APPENDIX B
LEAD EXTRACTION PROCEDURE (MODIFICATION OF THE TIMS HBR PB SEPARATION OF MANHES ET AL. (1978), SIMPLIFIED AND ADAPTED FOR MC-ICP-MS MEASUREMENTS OF PB ISOTOPES BY TL SPIKING.

1. Pack columns with a stem (resin bed) volume about 100 μl with 100-200 mesh Dowex 1X-8 resin;

2. Wash resin with 2 ml 6N HCl (optima grade);

3. Load sample dissolved in 100 μl -200 μl 1N HBr (seastar);

4. Wash 1 ml 1N HBr (seastar);

5. Wash 1 ml 1N HBr (seastar);

6. Wash 1 ml 1N HBr (seastar);

7. Collect Pb fraction in 1ml 20% HNO_3 (optima grade);

8. Evaporate the Pb solution to dryness on the hot plate;

9. Dissolve the Pb solution residue in 2% HNO_3 "optima" and spike it with Tl just before the analysis;

A fraction of the NBS 981 Pb isotopic standard was dried down and passed through the above column procedure to test for yield and for mass-dependant fractionation during the ion exchange chemistry. The yield was about 95%-97% and the measured isotopic values in NBS 981 after the column chemistry were: $^{206}Pb/^{204}Pb$=16.9367, $^{207}Pb/^{204}Pb$=15.4897, and $^{208}Pb/^{204}Pb$=36.6924. The ratios are indistinguishable from the wet and fresh dry plasma NBS 981 analyses (Appendix A), indicating that no detectable isotopic fractionation occurs during the ion exchange chromatography.

APPENDIX C
MIXING CALCULATIONS WITH 207PB/204PB BETWEEN SEDIMENTARY AND MAFIC SOURCES

Average values:

Othman et al. (1989) Pacific sediments			Pb(ppm)
206/204	207/204	208/204	8
18.707	15.626	38.702	
White et al. (1987) Pacific MORB			
18.586	15.511	38.085	1
Mafic Xenoliths			
18.702	15.520	38.208	1
Sedimentary xenoliths			
18.738	15.564	38.401	3

Results:

	Pacific MORB Sediment mix	Sedimentary and Mafic xenoliths mix
f	207/204	207/204
0	15.630	15.564
0.05	15.629	15.563
0.1	15.628	15.562
0.2	15.626	15.561
0.3	15.624	15.559
0.4	15.621	15.556
0.5	15.617	15.553
0.6	15.611	15.549
0.7	15.603	15.545
0.8	15.590	15.539
0.9	15.567	15.531
0.95	15.546	15.526
1	15.511	15.520

Mixing equation after Faure (1986):
*(207/204A*PbA*f+207/204B*PbB*(1-f)/(PA*f+PbB*(1-f)*

LIST OF REFERENCES

Abouchami, W., Galer, S.J.,G., and Hofman, A.W., 2000, High precision lead isotope systematics of lavas from the Hawaiian Scientific Drilling Project. Chem. Geol., 169, p. 187-209.

Bach, W., Alt, J.C., Niu, Y., Humphris, S.E., Erzinger, J., and Dick, H.J., 2001, The geochemical consequences of late-stage low-grade alteration of lower ocean crust at the SW Indian Ridge: Results from ODP hole 735B (Leg 176). Geochim. Cosmochim. Acta, 65, p. 3267-3287.

Baker, J., Waight, T., Meycen, C., 2004, Pb isotopic analysis of standards and samples using a ^{207}Pb-^{204}Pb double spike and thallium to correct for mass bias with a double focusing MC-ICP-MS. Chem. Geol., (submitted).

Bard, A.J., 1980, Photoelectrochemistry, Science, 207, p. 139-144.

Belshaw, N.S., Freedman, P.A., O'Nions, R.K., Frank, M., and Guo, Y., 1998, A new variable dispersion double-focusing plasma mass spectrometer with performance illustrated for Pb isotopes. Int. J. Mass Spectrometry, 181, p. 51-58.

Best, M.G., and Christiansen, E.H., 2001, Igneous Petrology, Blackwell Science, Malden, Massachusetts, 458 p.

Bodnar, R.J., 1995, Fluid-inclusion evidence for magmatic source for metals in porphyry copper deposits. In Thompson, J.F.H. ed. Magmas, Fluids, and Ore Deposits. Mineralogical Society of Canada Short Course Series, 23, p. 139-152.

Brenan, J.M., Shaw, H.F., Ryerson, F.J., Phinney, D.L, 1995, Mineral-aqueous fluid partitioning of trace elements at 900°C and 2.0 GPa: constraints on the trace element chemistry of mantle and deep crustal fluids. Geochim. Cosmochim. Acta, 59, p. 3332-3350.

Bureau, H., and Keppler, H., 1999, Complete miscibility between silicate melts and hydrous fluids in the upper mantle: experimental evidence and geochemical implications. Earth Planet. Sci. Lett., 165, p. 187-196.

Burgess, J., 1978, Metal Ions in Solution, Ellis Horwood, Chichester, 481 p.

Candela, P.A., 1989, Magmatic ore-forming fluids: thermodynamic and mass-transfer calculations of metal concentrations. In: Whitney, J.A., and Naldrett, A.J., (Eds.), Ore Deposition Associated with Magmas. Reviews in Economic Geology, 4, p. 203-221.

Candella, P.A., and Piccoli, P.M., 1995, Model of ore-metal partitioning from melts into vapor and vapor/brine mixtures. In: Thompson, J.F.H. (Ed.), Magmas, Fluids, and Ore Deposits, Mineralogical Society of Canada Short Course Series, 23, p. 101-127.

Carman, G.D., 2003, Geology, mineralization, and hydrothermal evolution of the Ladolam gold deposit, Lihir Island, Papua New Guinea. Society of Econ. Geol. Spec. Publication, 10, p. 247-284.

Carmichael, I.S.E., Lange, R.A., and Luhr, J.F., 1996, Quaternary minettes and associated volcanic rocks of Mascota, western Mexico: a consequence of plate extension above a subduction modified mantle wedge. Contrib. Mineral. Petrol., 124, p. 302-333.

Choppin, G. R., Liljenzin, J., and Rydberg, J., 2002, Radiochemistry and Nuclear Chemistry, Butterworth-Heinemann, Boston, 709 p.

Coleman, P.J., and Kroenke, L.,W., 1981, Subduction without volcanism in the Solomon Island arc. Geo-Mar. lett., 1, p. 129-134.

Collerson, K.D., Kamber, B.S., and Schoenberg, R., 2002, Application of accurate, high-precision Pb isotope ratio measurement by multi-collector ICP-MS. Chem. Geol., 188, p. 65-83.

Coogan, L.A., MacLeod, C.J., Dick, H.J., Edwards, S.J., Kvassnes, A., Natland, J.H., Robinson, P.T., Thompson, G., and O'Hara, M.J., 2001, Whole-rock geochemistry of gabbros from the Southwest Indian Ridge: constraints on geochemical fractionations between the upper and lower oceanic crust and magma chamber processes at (very) slow-spreading ridges. Chem. Geol., 178, p. 1-22.

Cotton, F.A., Wilkinson, G., Murillo, C.A., and Bochmann, M., 1999, Advanced Inorganic Chemistry, John Wiley & Sons, New York, 1355 p.

Davies, H.L., and Price, R.C., 1987, Basalts from the Solomon and Bismark Seas. Geo-Marine Letters, 6, p. 153-160.

Defant, M. J. and Kepezhinslas, P., 2001, Evidence suggests slab melting in arc magmas. Eos Transactions, 82, p. 65-69.

Doe, B.R., and Delevaux, M.H., 1972, Sources of lead in southeast Missouri galena ores. Econ. Geol., 67, p. 409-425.

Exon, N.F., Steward, W.D., Sandy, M.J., and Tiffin, D.L., 1986, Geology and offshore petroleum prospects of the eastern New Ireland Basin, northeastern Papua New Guinea. BMR Journal of Australian Geol. Geophys., 10, p. 39-51.

Ewart, A., and Hawkesworth, C.J., 1987, The Pleistocene-Recent Tonga-Kermadec lavas: interpretation of new isotopic and rare earth data in terms of a depleted mantle source model. J. Petrol., 28, p. 495-530.

Faure, G., 1986, Principles of Isotope Geology, John Wiley & Sons, New York, 464 p.

Franz, L., and Wirth, R., 2000, Spinel inclusion in olivine of peridotite xenoliths from Tubaf seamount (Bismarck Archipelago/Papua New Guinea): evidence for the thermal and tectonic evolution of the oceanic lithosphere. Contrib. Mineral. Petrol., 140, p. 283-295.

Franz, L., Becker, K.P., Kramer, W., and Herzing, P.M., 2002, Metasomatic mantle xenoliths from the Bismark microplate (Papua New Guinea) – thermal evolution, geochemistry, and extent of slab-induced metasomatism. J. Petrology, 43, p. 315-343.

German, C.R., Barreiro, B.A., Higgs, N.C., Ludford, E.M., and Palmer, M.R., 1995, Seawater-metasomatism in hydrothermal sediments (Escanaba Trough, northeast Pacific). Chem. Geol., 119, p. 175-190.

Gladney, E.S., Jones, E.A., Nickell, E.J., and Roealandts, I., 1990, 1988 compilation oe elemental concentration data for USGS basalt BCR-1. Geostandards Newsletter,14, p. 209-359.

Gregoire, M., McInnes, B.I.A., O'Reilly, S.Y., 2001, Hydrous metasomatism of oceanic sub-arc mantle, Lihir, Papua New Guinea Part 2. Trace element characteristics of slab-derived fluids. Lithos, 59, p. 91-108.

Hall, R., 2001, Cenozoic geological and plate tectonic evolution of SE Asia and the SW Pacific: computer-based reconstructions, model and animations. Journal of Asian Earth Sciences, 20, p. 353-431.

Harry, D.L., and Green, N.L., 1999, Slab dehydration and basalt petrogenesis in subduction systems involving very young oceanic lithosphere. Chem. Geol., 160, p. 309-333.

Heatherington, A.L., and Mueller, P.A., 1999, Lithospheric sources of North Florida, USA tholeiites and implications for the origin of the Suwannee Terrane. Lithos, 46, p. 215-233.

Hedenquist, J.W., and Lowenstern, J.B., 1994, The role of magmas in the formation of hydrothermal ore deposits. Nature, 370, p. 519-527.

Hermann, J., and Green, D.H., 2001, Experimental constraints on high pressure melting in subducted crust. Earth Planet. Sci. Lett., 188, p. 149-168.

Herzig, P.M., Hannington, M,. Stofers, P., Arribas, A., Becker, K.P., Binns, R., Browne, P., Gennerich, H.H., Hartman, M., Heesmam, B., and Scientific Party, 1994, Tectonics, petrology, and hydrothermal processes in areas of alkaline island-arc volcanoes in the Southwest Pacific: the Tabar-Lihir-Tanga-Feni island chain, Papua New Guinea. Cruise Report SONNE 94 Freiberg University of Mining and Technology, Freiberg, Germany.

Herzig, P. M., Hannington, M., Stoffers, P., Becker, K.P., Drischel, M., Franklin, J., Franz, L., Gemmel, J.B., Hoeppner, B., Horn, C., Horz, K., Jellineck, T., Jonasson, I.R., Kia, P., Nickelsen, S., Percival., J., Perfit, M.R., Petersen, S., Schmidt, M., Seifert, T., Thieben, O., Turkay, M., Tunnicliffe, V., and Winn, K., 1998, Volcanism, hydrothermal processes and biological communities at shallow submarine volcanoes of the New Ireland fore-arc (Papua New Guinea). Cruise Report SONNE-133 Freiberg University of Mining and Technology, Freiberg, Germany.

Herzig, P.M., Petersen, S., and Hannington, M.D., 1999, Epithermal-type gold mineralization at Conical Seamount: a shallow submarine volcano south of Lihir Island, Papua New Guinea. Proceedings SGA-IAGOD Meeting, Balkema, Rotterdam, p. 527-530.

Hickey-Vargas, R., Hergt, J.M., and Spaeda, P., 1995, The Indian Ocean-type isotopic signature in western Pacific marginal basins: origin and significance. In Taylor, B. and Natland, J. (Eds.) Active Margins and Marginal Basins of the Western Pacific. Geophysical Monograph, American Geophysical Union, 88, p. 175-197.

Johnson, R. W., Wallace, D.A., and Ellis, D. J., 1976, Feldspatoid-bearing potassic rocks and associated types from volcanic islands off the coast of New Ireland, Papua New Guinea: a preliminary account of geology and petrology, In: Johnson, R.W., (Ed.), Volcanism in Australia, Elsevier, Amsterdam, p. 297-316.

Johnson, R.W., 1979, Geotectonics and volcanism in Papua New Guinea: a review of the late Cenozoic. BMR, J. Aust. Geol. Geophys., 4, p. 181-207.

Johnson, R.W., Perfit, M.R., Chappell, B.W., Jaques, A.L., Shuster, R.D., and Ridley, W.I., 1988, Volcanism in the New Ireland basin and Manus island region: notes on the geochemistry and petrology of some dredged volcanic rocks from a rifted-arc region. In Circum-Pacific Council for Energy and Mineral Resources Earth Science Series, Houston, TX, 9, p. 113-131.

Kamenetsky, V.S., Binns, R.A., Gemmell, J.B., Crawford, A.J., Mernagh, T.P., Maas, R., and Steele, D., 2001, Parental basaltic melts and fluids in eastern Manus backarc basin: implications for hydrothermal mineralization. Earth Planet. Sci. Lett., 184, p. 685-702.

Kamenov, G. D., Macfarlane, A.W., and Riciputi, L., 2002, Sources of lead in the San Cristobal, Pulacayo, and Potosi mining districts, Bolivia, and reevaluation of regional ore lead isotope provinces. Econ. Geol., 97, p. 573-592.

Kamenov, G.D., Perfit, M.R., and Mueller, P.A., 2003, TIMS vs MC-ICP-MS Pb isotope analysis with application to ore deposit studies. GSA Annual Meet., 34, p. 518.

Kamenov, G.D., Mueller, P.A., and Perfit, M.R., 2004a, Optimization of mixed Pb-Tl solutions for high precision isotopic analyses by MC-ICP-MS. J. Analyt. At. Spectrom., 19, p. 1262-1267.

Kamenov, G.D., Perfit, M.R., Jonasson, I.R., and Mueller, P.A., 2004b, High-precision Pb isotope measurements reveal magma recharge as a mechanism for ore deposit formation: examples from Lihir Island and Conical Seamount, Papua New Guinea. Chem. Geol., (submitted).

Kelley, K.A., Plank, T., Ludden, J., and Staudigel, H., 2003, The composition of altered oceanic crust at ODP site 801 and 1149. Geochem. Geophys. Geosyst., 4 (6), doi:10.1029/2002GC000435.

Kennedy, A.K., Grove, T.L., and Johnson, R.W., 1990a, Experimental and major element constraints on the evolution of lavas from Lihir Island, Papua New Guinea. Contrib. Mineral. Petrol., 104, p. 722-734.

Kennedy, A.K., Hart, S.R., and Frey, F.A., 1990b, Composition and isotopic constraints on the petrogenesis of alkaline arc lavas: Lihir Island, Papua New Guinea. J. Geophys. Res., 95, p. 6926-6942.

LeMaitre, R.W., 1989, A classification of igneous rocks and glossary of terms. Recommendations of the International Union of Geological Sciences, subcommision on the systematics of igneous rocks. Blackwell, Oxford, 193 p.

Lackschewitz, K.S., Mertz, D.F., Devey C.W. and Garbe-Schönberg, C.D., 2003, Late Cenozoic volcanism in the western Woodlark Basin area, SW pacific: The sources of marine volcanic ash layers based on their elemental and Sr-Nd isotope compositions. Bulletin Volcanol., 65, p. 182-200.

Lin, T.S., and Nriagu, J.O., 1999, Thallium speciation in river waters with Chelex-100 resin. Anal. Chim. Acta, 395, p. 301-307.

Lloyd, F.E., Arima, M., and Edgar, A.D., 1985, Partial melting of a phlogopite-clinopyroxentie nodule from south-west Uganda: An experimental study bearing on the origin of highly potassic continental rift volcanics. Contr. Mineral. Petrol., 91, p. 321-329.

Macfarlane, A. W., Marcet, P., LeHuray, A. P. and Petersen, U., 1990, Lead isotope provinces of central Andes inferred from ores and crustal rocks. Econ. Geol., 85, p. 1857-1880.

Machado, N., Brroks, C., and Hart, S. R., 1986, Determination of initial 87Sr/86Sr and 143Nd/144Nf in primary minerals from mafic and ultramafic rocks: experimental procedure and implications for the isotopic character of the Archean mantle under the Abitibi greenstone belt, Canada. Geochim. Cosmochim. Acta, 50, p. 2335-2348.

Manhes, G., Minister, J.F., and Allegre, C.J., 1978, Comparative uranium-thorium-lead and rubidium-strontium study of the Sant Severing amphoterite: consequences for early solar system chronology. Earth Planet. Sci. Lett., 39, p. 14-24.

Mann, P., and Taira, A., 2004, Global tectonic significance of the Solomon Islands and Ontong Java Plateau convergent zone. Tectonophysics, 389, p. 137-190.

Martin, H., 1999, Adakitic magmas: modern analogues of Archaean granitoids. Lithos, 46, p. 411-429.

McInnes, B.I.A., 1992, A glimpse of ephemeral subduction processes from Simberi Island, Papua New Guinea. Ph.D. thesis, Univerisy of Ottawa, Canada, 235 p.

McInnes, B.I.A. and Cameron, E.M., 1994, Carbonated, alkaline hybridizing melts from a sub-arc environment: mantle wedge samples from Tabar-Lihir-Tanga-Feni arc, Papua New Guinea. Earth Planet. Sci. Lett., 122, p. 125-141.

McInnes, B. I. A., and Evans, N. J., 1996, Cu- and Pd- rich immiscible sulphide liquids in submarine shoshonitic lavas from the Tabar-Lihir-Tanga-Feni island arc, Papua New Guinea. Geological Society of Australia Abstracts, 41, p. 288.

McInnes, B.I.A., McBride, J.S., Evans, N.J., Lambert, D.D., and Andrew, A.S., 1999, Osmium isotope constraints on ore metal recycling in subduction zones. Science, 286, p. 512-516.

McInnes, B.I.A., Gregoire, M., Binns, R.A., Herzig, P.M., and Hannington, D., 2001, Hydrous metasomatism of oceanic sub-arc mantle, Lihir, Papua New Guinea: petrology and geochemistry of fluid-metasomatised mantle wedge xenoliths. Earth Planet. Sci. Lett., 191, p. 1-15.

Morin, D., and Corriveau, L., 1996, Fragmentation processes and xenolith transport in Proterozoic minette dyke, Grenville Province, Québec. Contrib. Mineral. Petrol., 125, p. 319-331.

Moyle, A.J., Doyle, B.J., Hoogvliet, H., and Ware, A.R., 1990, Ladolam gold deposit, Lihir Island. In Hughes, F.E. (Ed.), Geology of the Mineral Deposits of Australia and Papua New Guinea, 2, p. 1793-1805.

Mungall, J.E., 2002, Roasting the mantle: slab melting and the genesis of major Au and Au-rich Cu deposits. Geology, 30, p. 915-918.

Murphy, D.T., Kamber, B.S., and Collerson, K.D., 2002, A refined solution to the first terrestrial Pb-paradox. J. Petrol., 44, p. 39-53.

Müller, D., Frantz, L., Herzig, P.M., and Hunt, S., 2001, Potassic igneous rocks from the vicinity of epithermal gold mineralization, Lihir Island, Papua New Guinea. Lithos, p. 163-186.

Müller, D., Franz, L., Petersen, S., Herzig, P.M., and Hannington, M.D., 2003, Comparison between magmatic activity and gold mineralization at Conical Seamount and Lihir Island, Papua New Guinea. Mineralogy and Petrology, 79, p. 259-283.

Nielsen, S.G., Rehkamper, M., Baker, J., and Halliday, A., 2004, The precise and accurate determination of thallium isotope compositions and concentrations for water samples by MC-ICP-MS. Chem. Geol., (in press).

Othman. D.B., White, W.W., and Patchett, J., 1989, The geochemistry of marine sediments, island arc magma genesis and crust-mantle recycling. Earth. Planet. Sci. Lett., 94, p. 1-11.

Patino, L.C., Carr, M.J., and Feigenson, M.D., 2000, Local and regional variations in Central American arc lavas controlled by variations in subducted sediment input. Contrib. Mineral. Petrol., 138, p. 265-283.

Perez-Suarez, S.D., 2001, Petrology and geochemistry of the Mid-Cayman Rise: an end-member for the lower crust of a mid-ocean ridge. M.Sc. thesis, University of Florida, Gainesville, 115 p.

Poli, S., and Schmidt, M.W., 2002, Petrology of subducted slab. Annu. Rev. Earth Planet. Sci., 30, p. 207-235.

Perfit, M.R., Gust, D.A., Bence, A.E., Arculus, R.T., and Taylor, S.R., 1980, Chemical characteristics of island-arc basalts: implications for mantle sources. Chem. Geol., 30, p. 227-256.

Perfit, M.R., Langmuir, C.M., Baekisaoa, M., Chappell, B., Johnson, R.W., Staudigel, H., and Taylor, S.R., 1987, Geochemistry and petrology of rocks from the Woodlark basin: addressing questions of ridge subduction. In Circum-Pacific Council for Energy and Mineral Resources Earth Science Series, Houston, TX, 7, p. 113-154.

Petersen, S., Herzig, P.M., Hannington, M.D., Jonasson, I.R., and Arribas, A., 2002, Submarine gold mineralization near Lihir Island, New Ireland fore-arc, Papua New Guinea., Econ. Geol., 97, p. 1795-1813.

Petterson, M.G., Neal, C.R., Mahoney, J.J., Kroenke, L.W., Saunders, A.D., Babbs, T.L., Duncan, R.A., Tolia, D., McGrail, B., and Barron, M., 1997, Structure and deformation of north and central Malaita, Solomon Islands: tectonic implications for the Ontong Java Plateau-Solomon Arc collision, and for the fate of oceanic plateaus. Tectonophysics, 283, p. 1-33.

Rehkämper, M., and Halliday, A.N., 1998, Accuracy and long-term reproducibility of lead isotopic measurements by multiple-collector inductively coupled plasma mass spectrometry using an external for correction of mass discrimination. Int. J. Mass Spectrom., 181, p. 123-133.

Rehkämper, M., and Halliday, A.N., 1999, The precise measurement of Tl isotopic compositions by MC-ICPMS: Application to the analysis of geological materials and meteorites. Geochim. Cosmochim. Acta, 63, p. 935-944.

Rehkämper, M., and Mezger, K., 2000, Investigation of matrix effects for Pb isotope ratio measurements by multi-collector ICP-MS: verification and application of optimized analytical protocols. J. Analyt. At. Spectrom., 15, p. 1451-1460.

Rehkämper, M., Frank, M.J, Hein, R., Porcelli, D., Halliday, A.N., Ingri, J., and Liebetrau, V., 2002, Thallium isotope variations in seawater and hydrogenetic, diagenetic, and hydrothermal ferromanganese deposits. Earth Planet. Sci. Lett., 197, p. 65-81.

Reuer, M.K., Boyle, E.A., and Grant, B.C., 2003, Lead isotope analysis of marine carbonates and seawater by multiple collector ICP-MS. Chem. Geol., 200, p. 137-153.

Richards, J.P., McCulloch, M.T., Chappell, B.W., and Kerrich, R., 1991, Sources of metals in the Porgera gold deposit, Papua New Guinea: evidence from alteration, isotope, and noble metal geochemistry. Geochim. Cosmochim. Acta, 55, p. 565-580.

Rytuba, J., McKee, E.H., and Cox,D.P.,1993, Geochronology and geochemistry of the Ladolam gold deposit, Lihir Island, and gold deposits and volcanoes of Tabar and Tatau, Papua New Guinea. U.S. Geol. Surv. Bull., 2039, p. 119-126.

Schiano, P., Clochiatti, R., Shimizu, N., Maury, R., Jochum, K.P., and Hofman, A.W., 1995, Hydrous, silica-rich melts in the sub-arc mantle and their relationships with erupted arc lavas. Nature, 377, p. 595-600.

Schmidt, M.W., 1996, Experimental constraints on recycling of potassium from subducted oceanic crust. Science, 272, p. 1927-1930.

Sheppard, S.M.F., Nielsen, R.L., and Taylor, H.P., Jr., 1971, Hydrogen and oxygen isotope ratios in minerals from porphyry copper deposits. Econ. Geol., 66, p. 515-542.

Seewald, J.S., and Sefried, W.E., 1990, The effect of temperature on metal mobility in subseafloor hydrothermal systems: constraints from basalt alteration experiments. Earth Plnet. Sci. Lett., 101, p. 388-403.

Sillitoe, R.H., 1989, Gold deposits in western Pacific island arcs: the magmatic connection. Econ. Geol. Monograph, 6, p. 274-291.

Sillitoe, R.H., 1997, Characteristics and controls of the largest porphyry copper-gold and epithermal gold deposits in the circum-Pacific region. Austral. Jour. Earth Sci., 44, p. 373-388.

Sillitoe, R.H., 2002, Some metallogenic features of gold and copper deposits related to alkaline rocks and consequences for exploration. Mineral. Deposita, 37, p. 4-13.

Sinton, J.M., Ford, L.L., Chappell, B., and McCulloch, M.T., 2002, Magma genesis and mantle heterogeneity in the Manus back-arc basin, Papua New Guinea. J. Petrol., 44, p. 159-195.

Spera, F., J, 1984, Carbon dioxide in petrogenesis III: role of volatiles in the ascend of alkaline magma with special reference to xenolith-bearing mafic lavas. Contrib. Mineral. Petrol., 88, p. 217-232.

Stern, R.J., 2002, Subduction zones. Rev. Geophysics, 10.1029/2001RG000108.

Stracke, A., and Hegner, E., 1998, Rifting-related volcanism in a oceanic post-collisional setting: the Tabar-Lihir-Tanga-Feni (TLTF) island chain, Papua New Guinea. Lithos, 45, p. 545-560.

Stranks, D.R., and Yandell, J.K., 1969, Chemical effects of charge transfer absorption. I The photoinduced chain reaction between thallium (I) and thallium (III). J. Phys. Chem., 73, p. 840-849.

Sun, S., and McDonough, W.F., 1989, Chemical and isotopic systematics of oceanic basalts: implications for mantle composition and processes. In: Saunders, A.D., Norry, M.J. (Eds.), Magmatism in the Ocean Basins. Geol. Soc. Spec. Publ., 42, p. 313-345.

Switzer, J.A., Moorehead, E.L, and Dalesandro, D.M., 1982, Photoelectrochemistry of the thallic/thallous couple. J. Electrochem. Soc., 129, p. 2232-2237.

Tatsumi, Y., 1989, Migration of fluid phases and genesis of basalt magmas in subduction zones. J. Geophys. Res., 94, p. 4697-4707.

Taylor, B., 1979. Bismark sea: evolution of a back-arc basin. Geology, 7, p. 171-174.

Teagle, D., A., Alt, J.C., Chiba, H., Humphris, S.E., Halliday, A.,N., 1998, Strontium and oxygen isotopic constraints on fluid mixing, alteration and mineralization in the TAG hydrothermal deposit. Chem. Geol., 149, p. 1-24.

Thirwall, M.F., 2000, Inter-laboratory and other errors in Pb isotope analyses investigated using a ^{207}Pb-^{204}Pb double spike. Chem. Geol., 163, p. 299-322.

Thirwall, M.F., 2002, Multicollector ICP-MS analysis of Pb isotopes using a 207Pb-204Pb double spike demonstrates up to 400 ppm/amu systematic errors in Tl-normalization. Chem. Geol., 184, p. 255-279.

Tilton, G.R., Pollak, R.J., Clark, A.H., and Robertson, R.C., 1981, Isotopic composition of Pb in central Andean ore deposits. Geol. Soc. America Mem., 154, p. 791-816.

Todt, W., Cliff, R.A., Hanser,A., and Hofman, A.W., 1996, Evaluation of a 202Pb-205Pb double spike for high precision lead isotope analysis. Geophys. Monogr., 95, p. 429-437.

Trull, T.W., Perfit, M.R., and Kurz, M.D., 1990, He and Sr isotopic constraints on subduction contributions to Woodlark Basin volcanism, Solomon Islands. Geochim. Cosmochim. Acta, 54, p. 441-453.

Vroon, P.Z., van Bergen, M.J., White, W.M., and Varekamp, J.C., 1993, Sr-Nd-Pb isotope systematics of the Banda Arc, Indonesia: combined subduction and assimilation of continental material. J. Geophys. Res., 98, p. 22349-22366.

Wallace, D.A., Johnson, R.W., Chappell, B.W., Arculus, R.J., Perfit, M.R., Crick, I. H., 1983, Cainozoic volcanism of the Tabar, Lihir, Tanga, and Feni Islands, Papua New Guinea: geology, whole-rock analyses, and rock-forming minerals compositions. BMR Report, 243, 62p.

White, W.M., Hofmann, A.W., and Puchelt, H., 1987, Isotope geochemistry of Pacific Mid-Ocean ridge Basalt. J. Geophys. Res., 91, p. 4881-4893.

White, W.M., Albarède, F., and Tèlouk, P., 2000, High-precision analysis of Pb isotope ratios by multi-collector ICP-MS. Chem. Geol., 167, p. 257-270.

Winter, J.D., 2001, An Introduction to Igneous and Metamorphic Petrology, Prentice Hall, New Jersey, 697 p.

Woodhead, J.D., and Johnson, R.W., 1993, Isotopic and trace-element profiles across the New Britain island arc, Papua New Guinea. Contrib. Mineral. Petrol., 113, p. 479-491.

Woodhead, J.D., Volker, F, and McCulloch, M.T., 1995, Routine lead isotope determinations using a ^{207}Pb-^{204}Pb double spike: a long-term assessment of analytical precision and accuracy. The Analyst, 120, p. 35-39.

Woodhead, J.D., Eggins, S.M., and Johnson, R.W., 1998, Magma genesis in the New Britain island arc: further insights into melting and mass transfer processes. J. Petrol., 39, p. 1641-1668.

Woodhead, J.D., and Hergt, J.M., 2000. Pb-isotope analyses of USGS reference materials. Geostandards Newsletter, 24, p. 33-38.

Woodhead, J., 2002. A simple method for obtaining highly accurate Pb isotope data by MC-ICP-MS. J. Anal. At. Spectrom., 17, p. 1381-1385.

Yaxley, G.M., 2000, Experimental study of the phase and melting relations of homogeneous basalt+peridotite mixtures and implications for the petrogenesis of flood basalts. Contrib. Mineral. Petrol., 139, p. 326-338.

Zhang, M., Stephenson, P.J., O'Reilly, S.Y., McCulloch, M.T., and Norman, M., 2001, Petrogenesis and geodynamic implications of late Cenozoic basalts in North Queensland, Australia: trace-element and Sr-Nd-Pb isotope evidence. J. Petrol., 42, p. 685-719.

Zhu, X.K., Guo, Y., Williams, R.J.P., O'Nions, R.K., Matthews, A., Belshaw, N.S., Canters, G.W., de Wall, E.C., Weser, U., Burgess, B.K., and Salvado, B., 2002, Mass fractionation processes of transition metal isotopes. Earth Planet. Sci. Lett., 200, p. 47-62.

BIOGRAPHICAL SKETCH

George Kamenov was born on October 6, 1970, in Sofia, Bulgaria. He graduated from high school in 1988 and then served for 2 years in the Bulgarian Army as a border patrol. From 1991 to 1996 he completed a bachelor's/master's degree in geology from the Sofia University, Bulgaria, where he conducted research on metalliferous sediment samples from the Mid-Atlantic Ocean ridge. He worked as a research geologist in the Bulgarian Academy of Sciences from 1997 to 1998. In 1998, George arrived in Miami, Florida, where he completed a Master of Science degree in geology from the Florida International University in the fall of 2000. His master's research was focused on ore deposits in the Central Andes. In the fall of 2000, he began his Ph.D. at the University of Florida where his research is focused on deciphering the relationships between volcanism and ore deposit formation in SW Pacific island arcs. He will complete his Ph.D. at the University of Florida in the fall of 2004.